Catalytic conversion of biomass-derived sugars to renewable chemicals

（バイオマス由来糖から再生可能化学品への
触媒変換の研究）

Cheng Yang

（楊 程）

Hokkaido University

北海道大学

2022

Table of contents

Chapter 1

Introduction

1.1 Background

Since the Industrial Revolution in the 18th century, industrial societies have been growing rapidly by utilizing fossil resources such as coal and petroleum. However, the massive consumption of fossil resources leads to global warming due to the enormous amount of CO_2 emissions. The rising temperature may cause irreversible climate change, such as altered rainfall and sea-level rise.[1] Moreover, industrialized societies seriously concern about the depletion of fossil resources in terms of energy security. Fossil resources need millions of years for their regeneration, while they are extracted at a much quicker pace. Accordingly, the resource will naturally run out before too long.[2] Solving this problem is indispensable for the sustainable development of human civilization. For achieving this goal, we should use non-depleting and renewable resources that can regenerate quickly.

In recent years, biomass has been attracting significant attention as a renewable carbon resource. The first merit is that the resource is abundant. Cellulose, the most abundant terrestrial biomass, is generated 200 billion tons per year. Similarly, 100 billion tons of chitin, a representative marine biomass, is produced annually.[3] The total supply of these biomass resources is larger than the global energy demand (annually about 12 billion tons of oil equivalent).[4] Second, the use of biomass can be carbon neutral (Fig. 1.1). We utilize biomass to produce fuels and chemicals, and they are eventually released as CO_2 into the atmosphere. However, CO_2 is regenerated as biomass by photosynthesis in a short period. Therefore, efficient utilization of biomass resources may drastically change the modern civilization relying on fossil resources. Hopefully, the development of biomass utilization becomes a promising solution for alleviating current energy and environmental problems, thus catching significant notice in many countries.

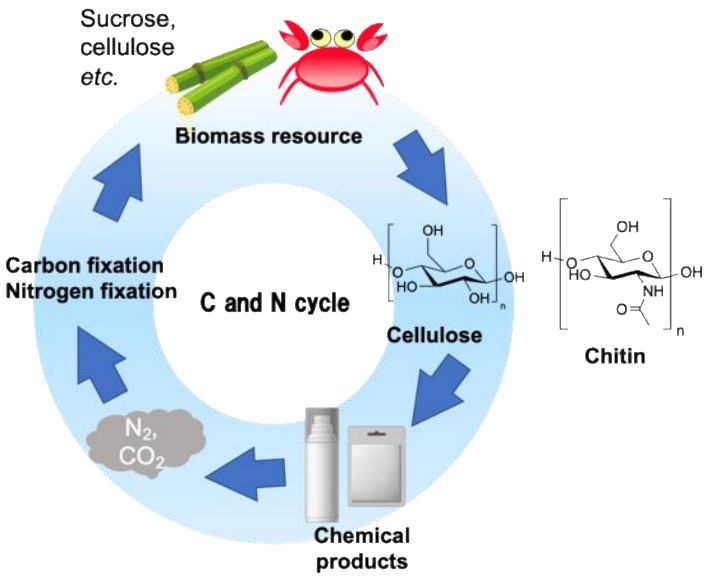

Figure 1.1 Prospect of cyclic utilization of biomass resources.

Promoted by the global policies for reducing carbon emissions, the biorefinery to produce functional chemicals has attracted much attention since the last decade. Currently, about 50 countries are planning to develop the bioeconomy, and fifteen of them, including many of the industrialized countries, have formulated dedicated bioeconomy policies.[5] Using suitable and abundant biomass-derived feedstock for biorefinery is necessary to achieve sustainable development. In this case, sugars derived from biomass are attractive feedstock because they are abundant, have specific stereochemistry, and can be converted to a wide range of chemicals. Among the biomasses in this category, inedible ones are especially attractive due to no competition with food production.

As the products that can be synthesized from biomass-derived sugars, the author is particularly interested in plastics. They are value-added and can be used for a long time different from fuels, and moreover, biomass-derived plastics often show superior characteristics to petroleum-based ones. An obvious example is isosorbide, a fused five-membered ring compound derived from glucose, which is a precursor to engineering plastics such as the polycarbonate with outstanding physicochemical properties named Durabio.

To achieve the efficient conversion of sugar compounds, the author aims for developing artificial catalytic reactions. A catalyst can enhance particular reactions to selectively convert the molecules. Properties of catalysts are tunable to meet the requirement. Hence, they may be useful to selectively convert sugar molecules having multiple functional groups. Notably, artificial catalysts can withstand a wide range of reaction conditions, and therefore they can complete reactions in a short time at a high temperature. This is a merit superior to biocatalysts, which work within narrow windows of reaction parameters.

Herein, the author aims for developing artificial catalytic reactions to convert inedible biomass-derived sugars to precursors to plastics. Scheme 1.1 shows the blueprint of this work, in which I pick up chitin and molasses as abundant inedible biomass released from food industry. Chitin consists of *N*-acetylglucosamine units, while molasses contains typical sugars such as sucrose. Using both typical and N-containing sugars increases the variety of the potential products. Within the scheme, the author first focuses on the conversion of sugar alcohol intermediates to fused five-membered ring products including isosorbide, because the step is highly demanded by industries. Afterwards, I also study the supply of the sugar alcohol from molasses to complete the scheme. In this chapter, to clarify the significance of this work, the author introduces the availability of biomass resources, mainly food-industry waste, and current research on the chemical transformation. Finally, I summarize the objective and significance of this work and outline of this dissertation.

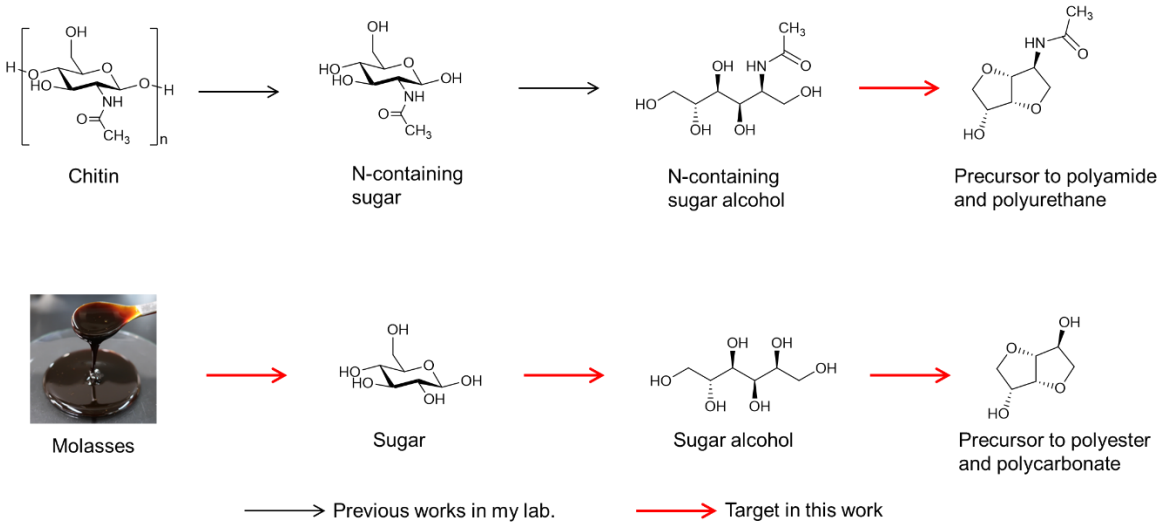

Scheme 1.1 Schematic of this work.

1.2 Sugar-containing biomass

1.2.1 Inedible biomass

Sugars can be obtained from both edible and inedible biomasses. For industrial applications, inedible biomasses are preferred as feedstock because they do not compete with food supply. This issue is more essential for the countries relying on food import to ensure food supply, such as Japan. The food self-sufficiency of Japan on a calorie basis was 37% in 2019, which was the lowest among the main industrialized countries.[6] In another viewpoint, the global population growth has been increasing the need of food corps. These factors emphasize the importance of inedible biomass utilization.

Inedible biomasses containing certain sugars or sugar units are suitable to synthesize particular products in large quantities.[7] Lignocellulose is the most abundant material in that category (200 billion tons per year). It is composed of cellulose (40–60%),[8] hemicellulose (20–35%),[9] and lignin (about 15–40%)[10] (Fig. 1.2). Cellulose consists of glucose units linked by glycosidic bonds and can be hydrolyzed to glucose, which is a versatile precursor to chemicals.[11,12] However, the purification and fractionation of lignocellulosic biomass is difficult and has contributed to the high cost of utilization.[13] Another potential resource is food-industry related wastes. A large amount of sugar-rich and relatively easily degradable wastes is available in particular places such as food factories, thus enabling their utilization in a shorter period than that of lignocellulose.

Therefore, the author uses the waste as a resource.

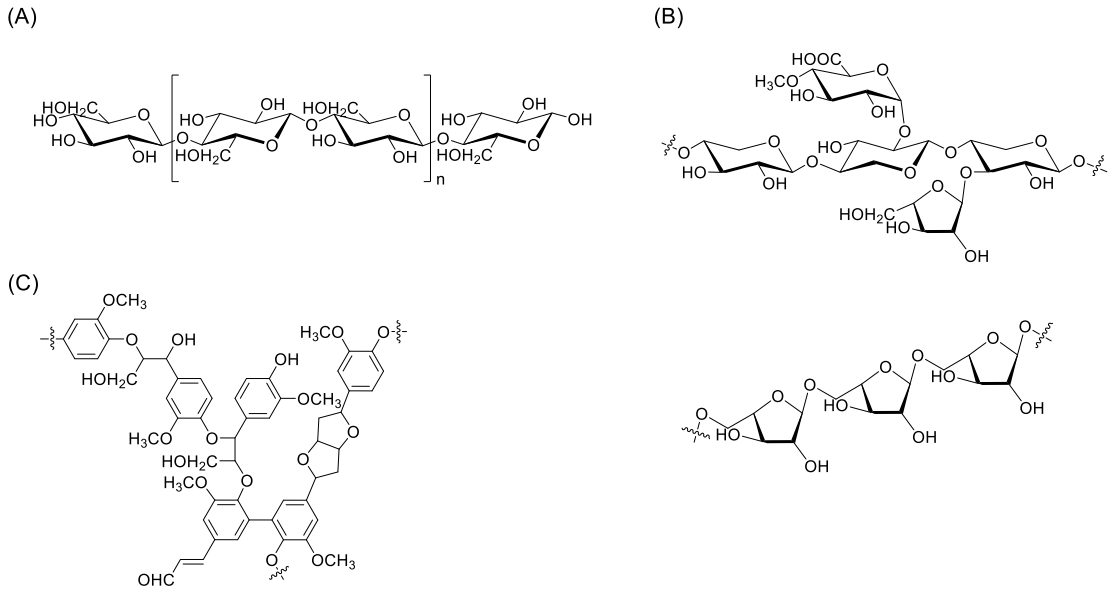

Figure 1.2 Composition of lignocellulosic cellulose. (A) Cellulose; (B) Hemicellulose (top: glucuronoarabinoxylan, bottom: arabinan); (C) Lignin. Adapted from the reference.[7]

1.2.2 Food loss and waste

Within the definition given by the Food and Agriculture Organizations of United Nations (FAO), 'food loss' is the decrease in the quantity or quality of food resulting from decisions and actions by food suppliers in the supply chain, excluding retailers, food service providers, and consumers, and 'food waste' is the complementary part in the chain (Fig. 1.3). However, the term 'loss' is ambiguous and misleading, and therefore, the author refers to all the wasted parts as food waste in this dissertation.

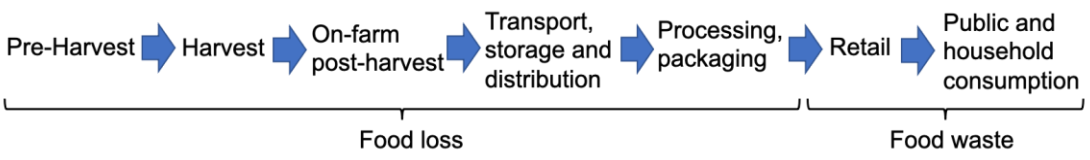

Figure 1.3 The food supply chain.[14]

The amount of food waste is very large, and for example, in Japan, approximately 20 million tons of food wastes occur annually. However, their quality varied in terms of purity and sugar content. If the waste is a mixture of many kinds of food, the utilization is difficult in the chemical industry and it is mainly used as fertilizers for cultivation or fodders.[15] The chemical industry requires a less-contaminated, abundant, cheap, and composition-stable food waste. As such a material, the author is interested in molasses, which is a viscous liquid generated in the sugar production from sugarcane. It still contains a large amount of sugars (40–50 wt%), it is abundant (global annual production: about 50 million tons), and the liquid form is suitable for chemical reactions. Another promising food waste is chitin, a polymer of a nitrogen-containing sugar, *N*-acetylglucosamine (NAG), found in crustacean shells. Except for proteins, which are structurally complicated, most food wastes consist of C, H, and O. However, chitin has N atoms in its monomer units and highly abundant (100 billion tons per year). Although the hydrolysis of chitin to NAG is as difficult as that of cellulose, the characteristic adds a further value in the products. Based on these reasons, the author focuses on molasses and chitin in this dissertation.

1.3 Molasses

1.3.1 Generation of molasses

Molasses is a food waste discharged in the sucrose production from both sugarcane and sugar beets.[16] The annual worldwide output of cane molasses is more than 40 million tons, which accounts about 80% of all molasses production (ca. 50 million tons).[17] Thus, I would like to mainly talk about sugarcane molasses. In the sugar production (Scheme 1.2), sugarcane is milled and mixed with water to make sugarcane juice. $Ca(OH)_2$ is added to adjust pH and precipitates the suspended materials. After this process, which is the so-called clarification, the sugarcane juice is concentrated by evaporation and the precipitated sucrose is separated from the syrup by centrifugation. The residual syrup is called molasses.

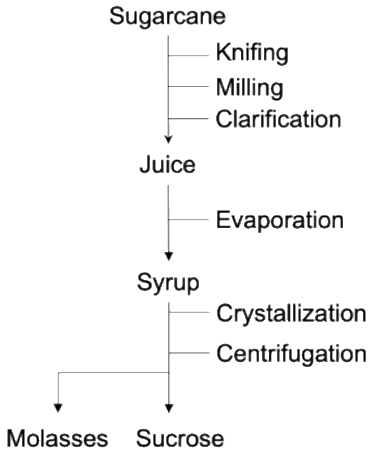

Scheme 1.2 Manufacturing process of sucrose from sugarcane.

1.3.2 Constituents of molasses

Molasses consists of sugars, inorganics, various organic compounds, and water (Table 1.1). Sugars are the predominant constituents in molasses (ca. 40%–60%), mainly consisting of sucrose, glucose, and fructose. The water content in molasses is only 12–17%. The high concentration of sugars makes molasses viscous. The variety and concentration of inorganic substances depends on producing areas of canes.[18] Those inorganic residuals accumulated to high concentrations in molasses due to the condensation process (Scheme 1.1), which is different from normal edible syrup. The high-concentration inorganic components are harmful for body health, thus making it barely available for food applications.[18] Additionally, the dark brown color of molasses (Fig. 1.4) is mainly caused by melanoidins, which are produced from the Maillard reaction of aldoses with amino acids and small peptides during the thermal treatment of sugarcane in the sugar manufacturing process.[19]

Figure 1.4 A sugarcane molasses produced in Okinawa Prefecture.

Table 1.1 Composition of sugarcane molasses.[20]

Component	Normal range /wt%
Water	12-17
Sucrose	30-40
Glucose	4-9
Fructose	4-12
Gums, starch, pentosans, traces of hexitols and uronic acids	2-5
Ash (Inorganic constituents)	7-15
Nitrogen compounds	2.5-4.5
Protein	0.5-4.5
Amino acids	0.3-0.5
Non-nitrogenous acids	1.5-6.0
Wax, sterols, and phosphatides	0.1-1.0
Vitamins	Varying amounts

1.3.3 Potential utilization of sugars found in molasses

1.3.3.1 Utilization of sugars

Molasses contains sucrose, glucose, and fructose, but their isolation for the sweetener application is not cost efficient. Instead, the author proposes that the sugars are potential feedstock for value-added chemicals. For the sugar-related chemistry, the current industry relies on sugars derived from starch. Yeast converts the food-derived sugars to ethanol, and the subsequent dehydration produces ethylene. Recently, we can find plastic bags made from the ethylene. Hydrogenation of the sugars gives sorbitol and mannitol, and sorbitol is a precursor to isosorbide, sorbitan, and vitamin C. In the laboratory research, various platform chemicals, such as 5-hydroxymethylfurfural[21] and ethylene glycol,[22–24] have been proposed as sugar derivatives. Among the potential

targets that can be synthesized from sugars, isosorbide is a remarkable platform molecule having important and practical applications (Fig. 1.5).[25] An outstanding example is the synthesis of the engineering plastic named Durabio. This material is the isosorbide-based commercial polycarbonate having superior properties over conventional polycarbonate.[26] Isosorbide has been converted to other plastics such as polyesters[27] and polyamides[28] in the laboratory study. The rigid framework and bifunctionality of isosorbide make it attractive in synthesis of polymers. In addition, isosorbide dinitrate has been used for a long time as a vasodilator,[29] and isosorbide diesters has been commercialized as surfactants[30] and PVC plasticizers.[31] Therefore, isosorbide is a good target in the biorefinery, and it is meaningful to replace the food biomass with inedible food waste as the feedstock. Accordingly, it is a challenge to convert sugars in molasses to isosorbide via sorbitol.

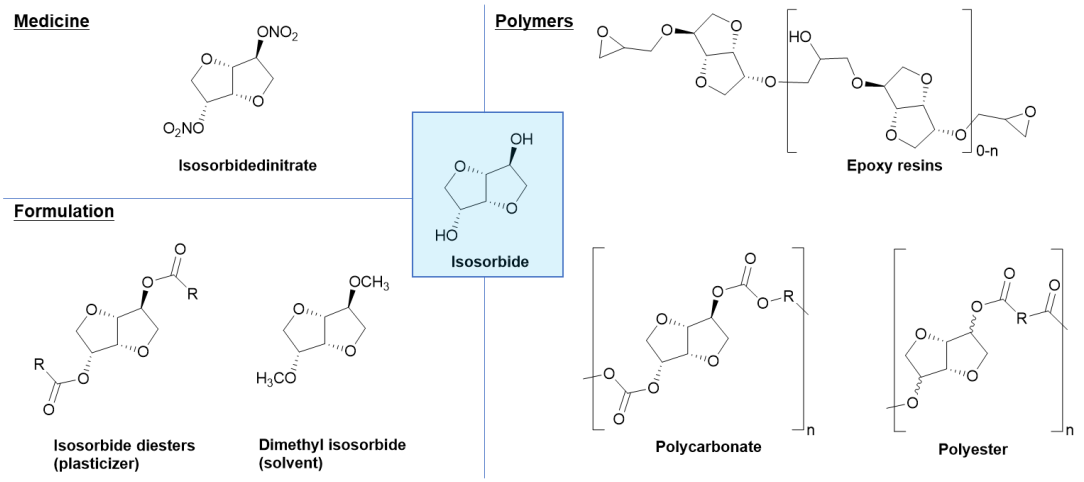

Figure 1.5 Isosorbide as a platform precursor to various chemicals. Adapted from the reference.[25]

1.3.3.2 Catalytic conversion of sugars to sugar alcohols

Related to the synthesis of sugar alcohols from molasses, the author introduces the industrial production of the sugar alcohols and related research. As mentioned above, starch is the most typical source for the production of sorbitol. First, an enzymatic hydrolysis converts starch to glucose, and the product is subsequently hydrogenated to sorbitol by Raney Ni catalyst under an H_2 pressure of 10–15 MPa.[32] Recently, supported

Ru catalysts are also employed for this reaction to decrease H_2 pressure.[11,33]

Laboratory research mainly focuses on the one-pot conversion of sugar dimers–polymers to sorbitol or mannitol to be more efficient. An easy source is sucrose, the hydrolysis of which produces glucose and fructose in the presence of mineral acid catalysts (Fig. 1.6A). Therefore, the hydrogenation reaction under acidic conditions readily converts sucrose to the sugars, and the sugars are converted to sorbitol and mannitol soon after the formation.[34] In this reaction, the hydrogenation of glucose mainly gives sorbitol (Fig. 1.6B), and that of fructose provides sorbitol and mannitol in 1:1 ratio in most cases (Fig. 1.6C).[35] In this research area, a significant target is the conversion of cellulose, for which Russian chemists combined mineral acids and supported Ru catalysts to produce sorbitol in 1950s.[36,37] After a long period of time, Fukuoka and Dhepe succeeded in the hydrolytic hydrogenation of cellulose to sorbitol and mannitol using only solid catalysts for the first time in 2006.[38] This work stimulated many researchers to participate in this research field.[39–47] They basically use supported Pt, Ru, and Ni catalysts, and it has been found that carbons are suitable supports due to the high water resistance.[11] These knowledges and insights are useful to design the catalytic conversion of molasses to sugar alcohols.

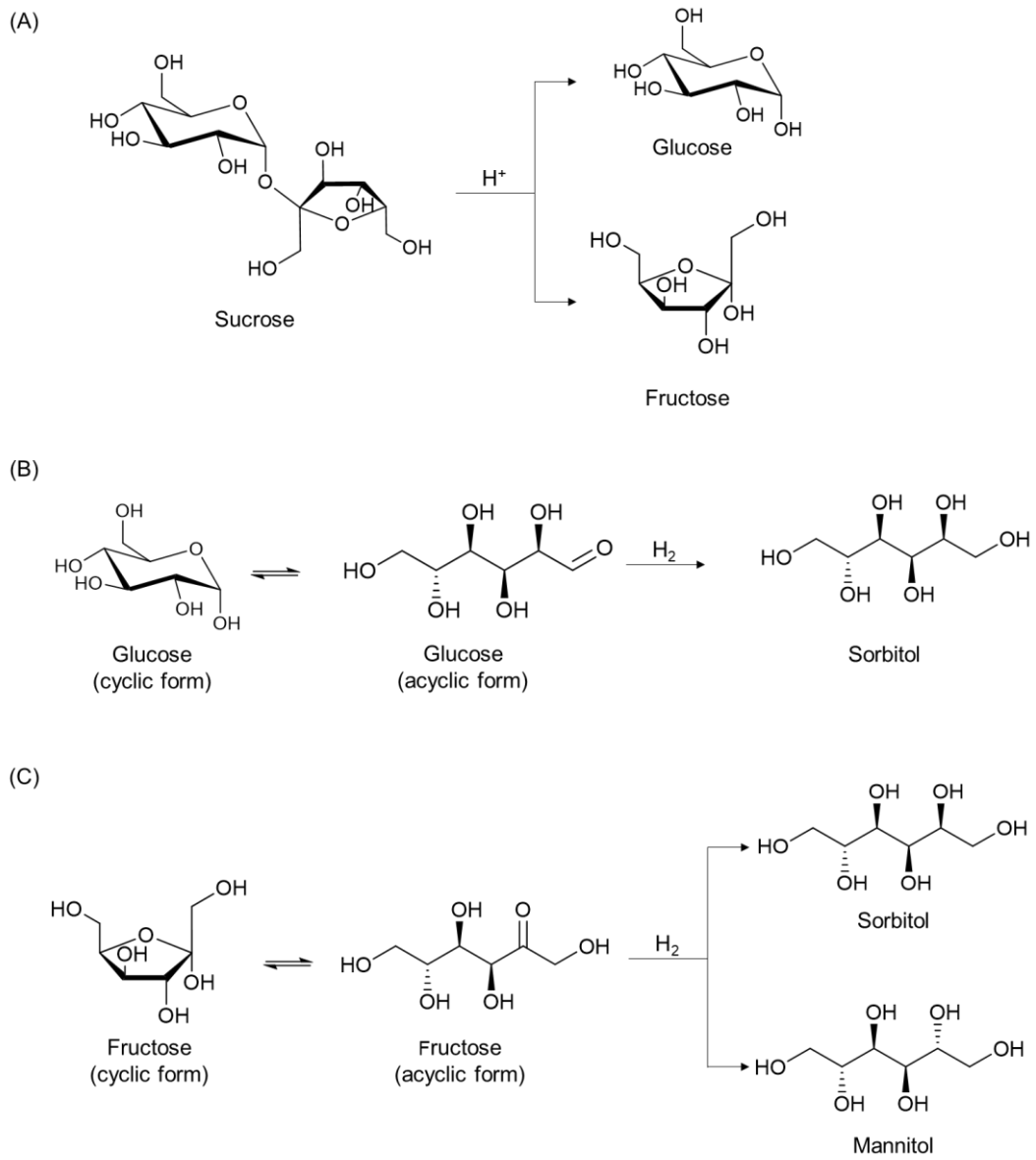

Figure 1.6 Reaction pathways of (A) hydrolysis of sucrose; (B) hydrogenation of glucose; (C) hydrogenation of fructose.

1.3.3.3 Dehydration of sorbitol to isosorbide

Isosorbide is an essential intermediate to produce polymers from sorbitol. The production of isosorbide passes through a two-step dehydration condensation (Fig. 1.7).[48,49] First, an -OH group is protonated, and then a secondary -OH group attacks the activated position with eliminating one molecule of water by an S_N2 reaction to form a cyclic compound. The products can be in three forms, depending upon the position of dehydration: 1,4-anhydrosorbitol (1,4-sorbitan), 3,6-anhydrosorbitol (3,6-sorbitan),

and 2,5-anhydromannitol (2,5-mannitan). The former two products are converted to isosorbide by the same type of reaction. 2,5-Mannitan is formed by the steric inversion due to the S_N2 reaction at the secondary position, and this compound is unavailable as a precursor to isosorbide.

The industrial synthesis of isosorbide uses H_2SO_4 with no solvent under vacuum conditions, but it produces a large amount of sulfuric acid pitch. Many works about the isosorbide synthesis from sorbitol have been reported. Conventional methods of isosorbide synthesis require strong acid catalyst. In 1987, Flèche et al. reported that use of 1% H_2SO_4 gives an isosorbide yield of 77% at 135 °C after 20 h.[50] Recently, Fukuoka et al. achieved 76% yield of isosorbide in the conversion of sorbitol over H-beta zeolite at 130 °C under decreased pressure for 2 h.[51] Instead of using strong acids, J. Robinson et al. used $NaHSO_4$, a weak acid, to convert sorbitol to isosorbide, giving 74% yield in the reaction at 210 °C under a microwave heating for 3 h.[52] Yamaguchi et al. have reported that water can convert sorbitol at a high temperature (300 °C) in the absence of catalyst, which gives 56% yield of isosorbide after a reaction for 3 h.[53] To summarize, strong acids or harsh conditions are needed to synthesize isosorbide so far. Moreover, the yield of isosorbide does not exceed 80%. Therefore, the efficient conversion of sorbitol to isosorbide has remained a challenge.

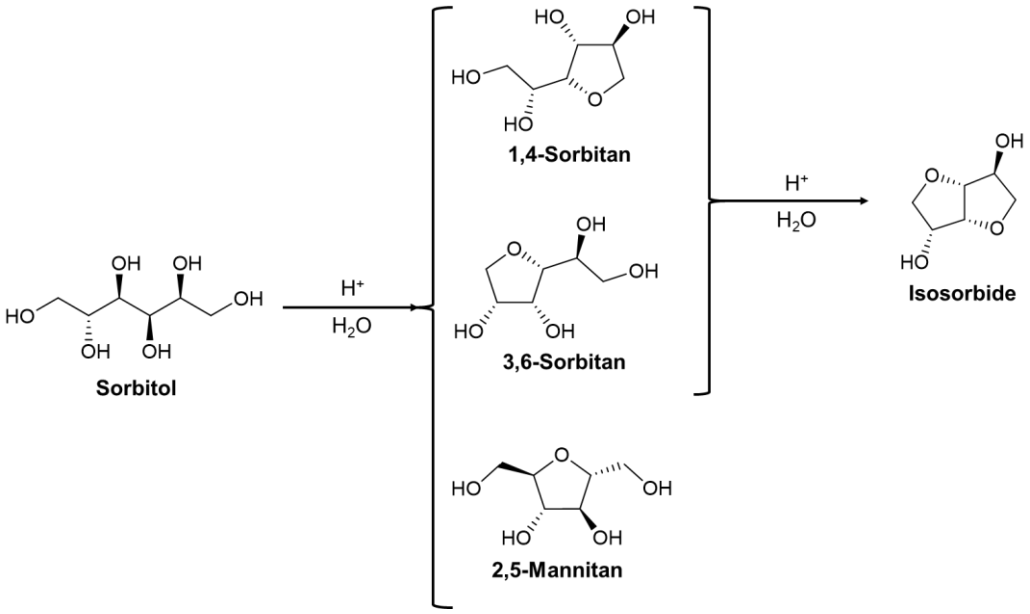

Figure 1.7 Synthesis of isosorbide from glucose.

1.4 Chitin

1.4.1 General introduction

Chitin is a marine biomass, widely found in fungi, plankton and exoskeletons of insects and crustaceans (Fig. 1.8). Industrial processes extract chitin from crustacean shell waste mainly. Most wastes contain less than 40% of chitin with impurities such as $CaCO_3$ and proteins (Table 1.2). Those impurities need to be removed in the process. Chitin is a natural polymer in which a large number of *N*-acetylglucosamine (NAG) units are connected by β-1,4-glycosidic bonds (Fig. 1.9). However, natural chitin contains both NAG and glucosamine units. Depending on the ratio of glucosamine units (deacetylation degree), the materials with deacetylation degrees of less than 40% are called chitin, and others are chitosan. The degree of polymerization is distributed from tens of thousands to millions.[54] Chitin has two crystal polymorphs named α- and β-forms.[55] The α-polymorph is more abundant in nature, in which the chitin molecules are oriented in antiparallel directions (Fig. 1.10). Chitin in shrimp shells and crab shells is mostly in the α-polymorph. Besides, the β-polymorph has a structure that chitin molecules are oriented in parallel. It is rare and found in squid pens as a mixture with proteins. The β-polymorph can be transformed into the α-polymorph by dissolution and recrystallization using HCl solution, but the reverse conversion does not occur. The α-polymorph is more thermodynamically stable due to a larger number of hydrogen bonds.[56] The a-polymorph has four intramolecular and two intermolecular hydrogen bonds for each NAG unit, while the β-polymorph has only four intramolecular hydrogen bonds.[57]

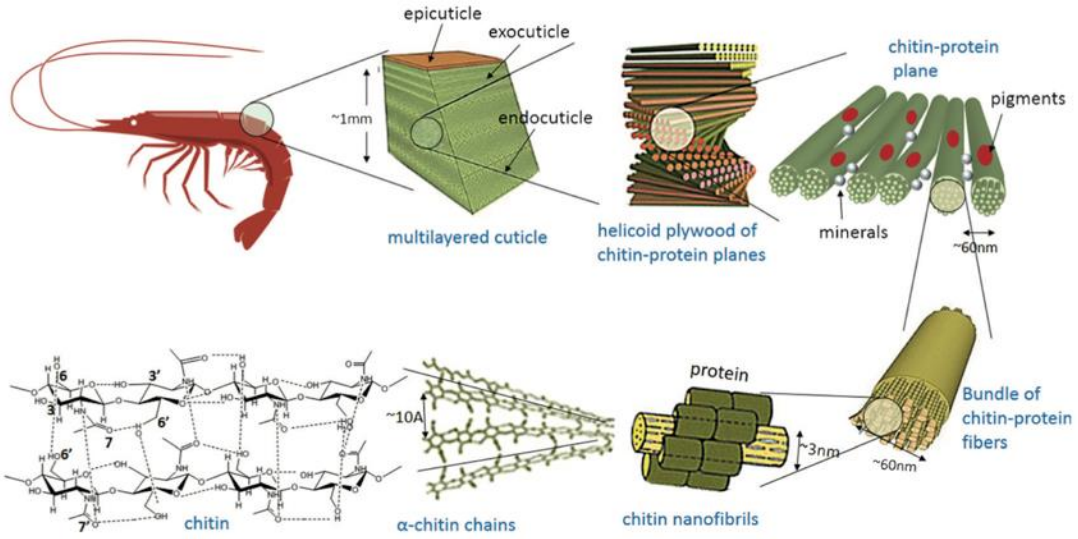

Figure 1.8 The composition of shell, illustrating the structure and spatial arrangement of chitin, protein, and minerals in the crustacean shells. Adapted from the reference.[58]

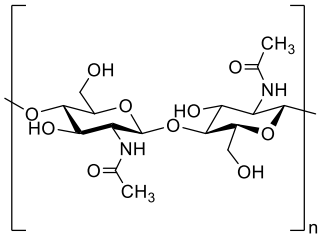

Figure 1.9 Molecular structure of chitin.

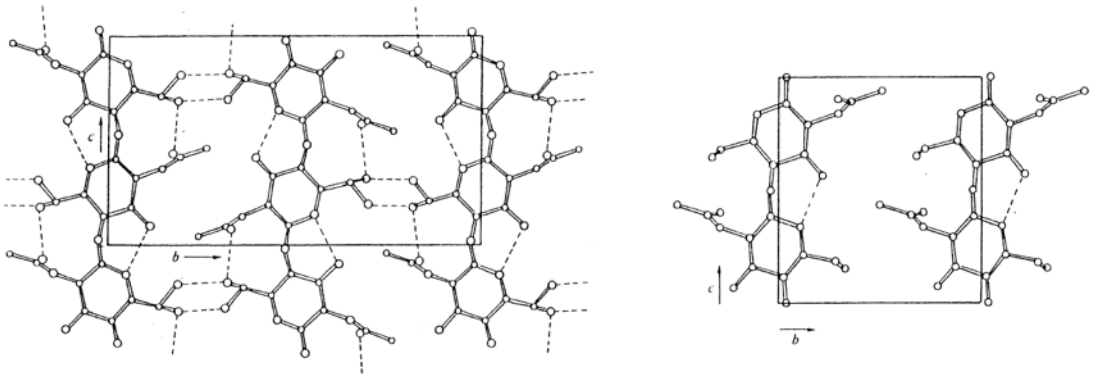

Figure 1.10 Structure of α-polymorph (left) and β-polymorph of chitin (right). Adapted from the reference.[59]

Table 1.2 Contents of chitin and Calcium carbonate.[54]

Source	Chitin /%	$CaCO_3$ /%
Crab cuticle	15-30	40-50
Shrimp cuticle	30-40	20-30
Krill cuticle	20-30	20-25
Squid pen	20-40	Negligible
Clam/oyster shell	3-6	85-90
Insect cuticle	5-25	Negligible
Fungi cell wall	10-25	Negligible

1.4.2 Extraction of chitin from crude marine biomass

The conventional extraction process of chitin from raw shell waste combines pigments extraction, demineralization, deproteinization, and decolorization steps (Fig. 1.11). Pigment extraction with a bean oil removes astaxanthin and lipids from shell waste. The following demineralization processes are generally performed in strong acid solutions (typically HCl), which remove mineral impurities such as calcium and magnesium compounds. Then, deproteinization is conducted with NaOH. For convenience, the purified chitin is bleached by H_2O_2.[58]

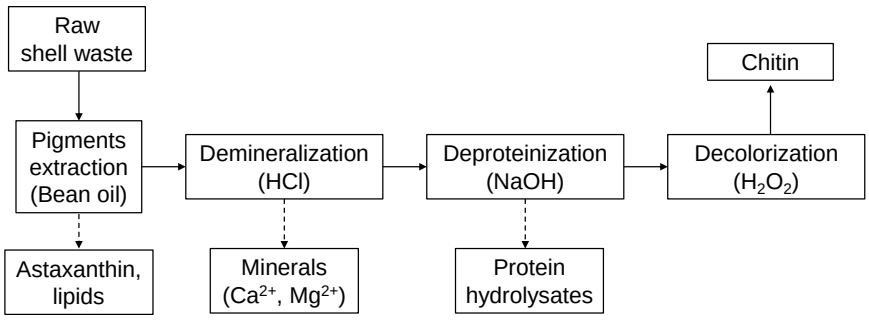

Figure 1.11 Flow chart of industrial fractionation methods for shells. Adapted from the reference.[58]

As the conventional method of chitin purification exhausts a large amount of waste and is expensive, several alternative techniques have been proposed. The representative

ways are bioprocessing[60–64] and solvent extraction.[65–68] However, the application of these methods are limited at laboratory scale so far due to low efficiency. Nowadays, the produced chitin are mainly used as functional materials such as tissue wound healing material,[69] membrane[70] and nanofiber.[71,72]

1.4.3 Depolymerization of chitin to sugar monomers

Other than the use of chitin in the polymer form, chitin is also a promising source for organonitrogen compound since a nitrogen atom is contained in every monomer unit. N-containing molecules play important roles in pharmaceutical industry, as more than 90% of commercial drugs bear amino groups or azaheterocyclic moieties as pharmacophores.[73] Other than the pharmaceutical use, nitrogen-containing molecules participate in the synthesis of food additives, detergents, polymer materials and agrochemicals.[74,75] Currently, N atoms in artificial organic compounds come from the ammonia produced by the Haber-Bosch process. However, the process consumes a large amount of energy corresponding to 1% of the world's total energy production and 1.4% of global CO_2 emissions.[76] The application of chitin as nitrogen source is expected to substitute N atoms derived from the energy-consuming ammonia process.

To use chitin as a chemical source, the depolymerization to NAG is needed. Due to the rigid structure of chitin owing to intermolecular hydrogen bonds,[77] the conversion of chitin to monomers has remained a challenge. Chitin depolymerization has been achieved by enzymatic reactions[78] and supercritical water treatment.[79] Limitations of these methods are long reaction time and high cost. The traditional HCl treatment is used for the industrial hydrolysis of chitin. However, it generates a large amount of wastewater and cannot avoid deacetylation.[80] To overcome the unpleasant issues of the HCl treatment, Fukuoka and his co-workers developed a mechanocatalytic method for chitin depolymerization,[81] which can selectively produce oligomers and NAG with no deacetylation. Chitin was first impregnated with a catalytic amount of H_2SO_4 and then ball-milled at 500 rpm for 6 h without any solvent. The ball-milling firstly decreases the crystallinity of chitin, which increases the accessibility of acid to chitin. Both tensile and compressive forces effectively promote the cleavage of glycosidic bonds, in which

compressive forces less strongly activate the chemical bonds but are similarly important to or more important than tensile forces due to its better availability (Fig. 1.12).[82] The acetamide group is well-preserved as the tensile stress does not accelerate its hydrolysis, which is a particular advantage of this method and difficult to achieve in classical acidic hydrolysis by HCl. In 2018, G. Margoutidis et al. developed a heterogeneous mechanocatalytic depolymerization method of chitin, using a natural clay, kaolinite, as catalyst.[83] This method achieved 5.1% yield of NAG by a 6-hour ball milling, and enhanced the solubility of products (up to 75.8% water-soluble products in 6 h, cf. 35.0% without kaolinite). Kaolinite is an aluminosilicate consisting of SiO_4 tetrahedra sheets bound to Al_2O_6 octahedra sheets as in a 1:1 ratio. H^+ ions were released from Al-OH groups on the octahedral sheets of kaolinite, to promote the hydrolysis of chitin. As a natural, economical clay material, kaolinite is applied in the mechanocatalytic depolymerization of woody biomass,[84] and the application of kaolinite on marine biomass depolymerization may provide advanced prospect for the utilization of chitin.

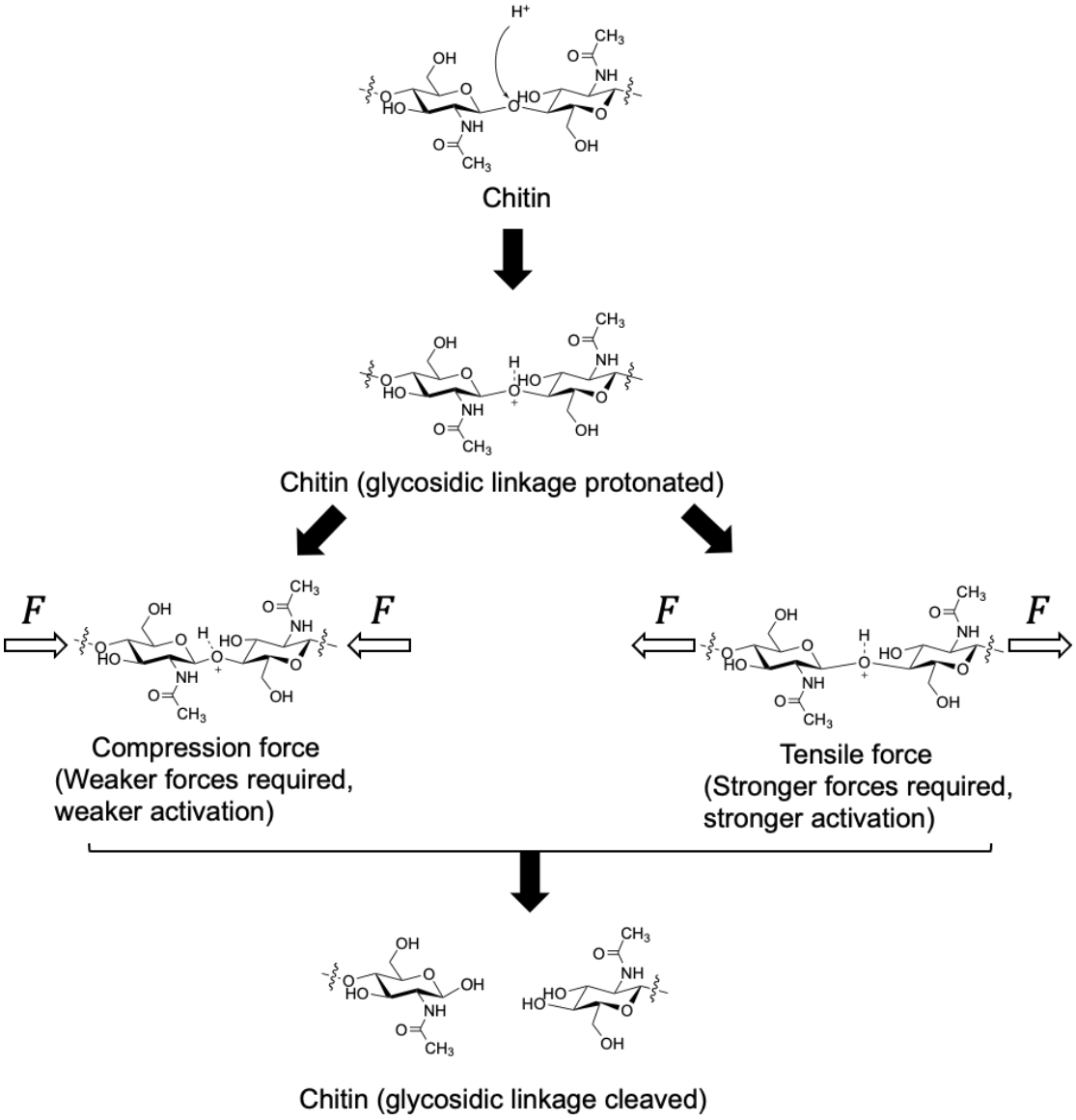

Figure 1.12 Proposed schematic of chitin depolymerization by ball-milling.[81,82]

1.4.4 Conversion of NAG

Due to the structural similarity, NAG can likely perform reactions as the case of glucose such as dehydration and hydrogenation. The dehydration of NAG can give a nitrogen-containing furan derivative named 3-Acetamido-5-acetylfuran (3A5AF), which is an important building block for N-containing aromatic compounds.[85–88] Besides, the hydrogenation of NAG gives the sugar alcohol called 2-acetamido-2-deoxysorbitol (ADS, Fig. 1.13), which is a promising platform chemical for its structural similarity with sorbitol and nitrogen-containing property.

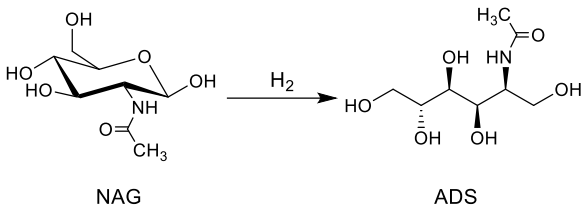

Figure 1.13 Hydrogenation of NAG to ADS.

1.4.4.1 Catalytic conversion of NAG to sugar alcohol

In 2014, Bobbink et al. found a nitrogen-containing polyol, 2-acetamido-2-deoxysorbitol (ADS) could be synthesized for a high yield (98%) using Ru/C (5wt%) catalyst at a mild condition (80 °C, 4 MPa H_2) by hydrogenation of NAG.[89] The yield of ADS strongly relied on the reaction temperature because high temperature facilitated other side reactions such as hydrogenolysis and dehydration. In 2016, Kobayashi et al. reported a one-pot and two-step catalytic conversion method of ADS from chitin using mechanocatalysis in the presence of H_2SO_4 and subsequent hydrolytic hydrogenation by H_2SO_4 and Ru/TiO_2 without any purification process.[90] The yield of ADS is strongly relative to the reaction temperature and pH, as the hydrolysis favorably proceeds at high temperature and low pH (2.0), but the hydrogenation prefers a low temperature and a specific pH of 3–4. Thus, pH of the solution was adjusted to 3.0 by adding $NaHCO_3$ after the hydrolysis reaction for high selectivity. The yield of ADS increased to 52% (Fig. 1.14).

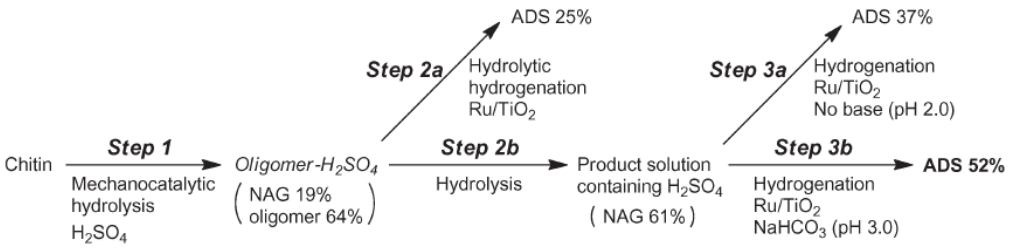

Figure 1.14 Catalytic conversion of chitin to ADS. Steps 2b and 3a, 3b were performed in one pot. Adapted from the reference.[90]

1.4.4.2 Dehydration of ADS to ADI

Analogous to the dehydration condensation of sorbitol to isosorbide, Sagawa et al. has reported the catalytic conversion from ADS to 2-acetamide-2-deoxyisosorbide (ADI, Fig. 1.15).[91] By induction of nitrogen-containing group, ADI is expected to be a new potential precursor to nitrogen-containing polymers to improve the thermal stability of polymers. Dehydration of ADS mainly produces three kinds of monoanhydrate intermediates, in which 1,5-anhydro-ADS is a dead-end product and the other two are available to give ADI by once more dehydration cyclization (Fig. 1.15). To achieve the conversion from ADS to ADI, superstrong acid is found to be pivotal, because the Lewis basic carbonyl O at the acetamide group traps an acid proton, thus leading to high activation energies in the dehydration reactions (Fig. 1.16A). To compensate for this effect, a large amount of superstrong acid is needed for the conversion of ADS to ADI. CF_3SO_3H (pK_a = −15, S/C = 2.0) under decreased pressure of less than <0.1 kPa and 150 °C provides ADI at 33% yield.

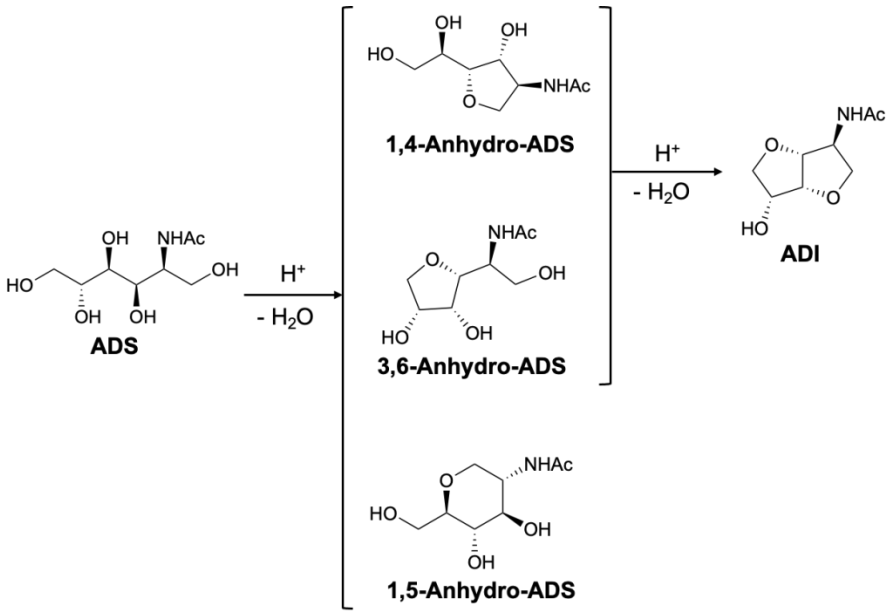

Figure 1.15 Conversion of ADS to ADI (acetamido group is denoted -NHAc for convenience).

In 2020, Sagawa et al., upgraded the method of ADI production using superstrong

acid.[92] The addition of a Lewis acid, $Yb(OTf)_3$, as a co-catalyst in the ADS dehydration by traditional CF_3SO_3H catalyst effectively accelerates the reaction and increases the yield of ADI by changing regio-selectivity of the reaction. $Yb(OTf)_3$ functions as two roles in the new reaction system: (1) $Yb(OTf)_3$ coordinates the carbonyl O, to prevent the neutralization of protons by the amide groups (Fig. 1.16B). (2) $Yb(OTf)_3$ selectively promotes the dehydration at C-6 position (3,6-dehydration) over that at C-1 position (1,4- and 1,5-dehydration), to reduce the formation of 1,5-anhydro-ADS, a major by-product, and leads to a slight improvement of ADI yield. The enhancement of selectivity is proposed to be caused by coordination of the bulky Yb complex at amide position, which increases the steric hindrance for the dehydration reactions at C-1. The combination achieved 40% yield of ADI at a 150 °C reaction for 1 h under < 0.1 kPa, using CF_3SO_3H at S/C = 2.0 combined with $Yb(OTf)_3$ at S/C = 10.

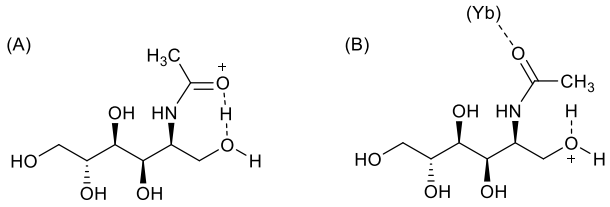

Figure 1.16 (A) Proton neutralization by carbonyl O at acetamido group;[91] (B) Shielding of neutralization by $Yb(OTf)_3$.[92]

1.5 Objective of this dissertation

In this dissertation, the author focuses on developing artificial catalytic reactions to synthesize precursors to plastics from inedible biomass-derived sugars. Chitin and molasses were chosen as inedible biomass feedstock released from food industry. The author firstly aims for the conversion of sugar alcohol intermediates to fused five-membered ring products including ADS and isosorbide. Those attractive precursor to plastics potentially provides a wide range of polymers. I also try to establish an efficient supply method of sugar alcohol from molasses, which hopefully enhances the utilization of such food-industry wastes for chemical production and contributes to ensure food supply. I hope this dissertation can assist in developing sugars-based

biorefinery and support the sustainable construction of our civilization.

1.6 Outline of the dissertation

Chapter 1 *General Introduction*

This chapter introduced the background and significance of this work.

Chapter 2 *Dehydration condensation of a chitin-derived sugar alcohol using a weak acid catalyst*

The author studies the catalytic conversion of a N-containing sugar alcohol synthesized by the hydrogenation of NAG to an amide alcohol having condensed five-membered rings. The main finding is that H_3PO_3, a weak acid catalyst, can drive the reaction, which is largely different from the previous systems relying on superstrong acids.

Chapter 3 *Application of H_3PO_3 catalyst in the dehydration condensation of sorbitol*

This chapter shows that H_3PO_3 is applicable for the conversion of sorbitol to isosorbide.

Chapter 4 *Hydrolytic hydrogenation of molasses to sugar alcohols*

The author developed an efficient pre-treatment and catalytic conversion of molasses to synthesize sugar alcohols. Montmorillonite K10 removes a part of catalyst poisons, which is S-containing organic compounds, contained in molasses, and Raney Ni can produce sorbitol and mannitol from the pre-treated molasses.

Chapter 5 *General conclusion*

This chapter summarizes the conclusions of each chapter and gives a general conclusion of this dissertation.

1.7 References

1 S. Solomon, G. K. Plattner, R. Knutti and P. Friedlingstein, *Proc. Natl. Acad.*

Sci. U. S. A., 2009, **106**, 1704–1709.

2 M. Höök and X. Tang, *Energy Policy*, 2013, **52**, 797–809.

3 J. Robertson, *Am. Math. Mon.*, 2004, **111**, 915.

4 N. Abas, A. Kalair and N. Khan, *Futures*, 2015, **69**, 31–49.

5 C. Boldt, *Bioeconomy Policy (Part III): Update Report of National Strategies around the World*, 2020.

6 農林水産省, 日本の食料自給率, https://www.maff.go.jp/j/zyukyu/zikyu_ritu/012.html, (accessed 6 September 2021).

7 H. Kobayashi, H. Ohta and A. Fukuoka, *Catal. Sci. Technol.*, 2012, **2**, 869–883.

8 H. K. Sharma, C. Xu and W. Qin, *Waste and Biomass Valorization*, 2019, **10**, 235–251.

9 A. K. Chandel, V. K. Garlapati, A. K. Singh, F. A. F. Antunes and S. S. da Silva, *Bioresour. Technol.*, 2018, **264**, 370–381.

10 A. J. Ragauskas, G. T. Beckham, M. J. Biddy, R. Chandra, F. Chen, M. F. Davis, B. H. Davison, R. A. Dixon, P. Gilna, M. Keller, P. Langan, A. K. Naskar, J. N. Saddler, T. J. Tschaplinski, G. A. Tuskan and C. E. Wyman, *Science*, 2014, **344**, 6185.

11 H. Kobayashi, T. Komanoya, K. Hara and A. Fukuoka, *ChemSusChem*, 2010, **3**, 440–443.

12 H. Kobayashi, M. Yabushita, T. Komanoya, K. Hara, I. Fujita and A. Fukuoka, *ACS Catal.*, 2013, **3**, 581–587.

13 D. M. Alonso, J. Q. Bond and J. A. Dumesic, *Green Chem.*, 2010, **12**, 1493–1513.

14 FAO, *The State of Food and Agriculture 2019. Moving forward on food loss and waste reduction. Rome.*, 2019.

15 農林水産省, 生ごみ等の飼料化・たい肥化の現状及び課題等について, 東京都, 2005.

16 FAO, *OECD-FAO Agric. outlook 2019-2028*, 2019, 154–165.

17 H. Olbrich, *The Molasses*, Biotechnologie-Kempe GmbH, Berlin, 2006.

18 W. W. Binkley and M. L. Wolfrom, *Sci. reports Ser. Sugar Res. Found.*, 1953, **8**, 291–314.

19 R. Chandra, R. N. Bharagava and V. Rai, *Bioresour. Technol.*, 2008, **99**, 4648–4660.

20 M. Paterson-Beedle, J. F. Kennedy, F. A. D. Melo, L. L. Lloyd and V. Medeiros, *Carbohydr. Polym.*, 2000, **42**, 375–383.

21 T. Wang, M. W. Nolte and B. H. Shanks, *Green Chem.*, 2014, **16**, 548–572.

22 I. T. Clark, *Ind. Eng. Chem.*, 1958, **50**, 1125–1126.

23 L. Ye, X. Duan, H. Lin and Y. Yuan, *Catal. Today*, 2012, **183**, 65–71.

24 Y. Jia and H. Liu, *Catal. Sci. Technol.*, 2016, **6**, 7042–7052.

25 C. Dussenne, T. Delaunay, V. Wiatz, H. Wyart, I. Suisse and M. Sauthier, *Green Chem.*, 2017, **19**, 5332–5344.

26 S. Chatti, G. Schwarz and H. R. Kricheldorf, *Macromolecules*, 2006, **39**, 9064–9070.

27 B. A. J. Noordover, V. G. van Staalduinen, R. Duchateau, C. E. Koning, R. A. T. M. van Benthem, M. Mak, A. Heise, A. E. Frissen and J. van Haveren, *Biomacromolecules*, 2006, **7**, 3406–3416.

28 A. A. Caouthar, A. Loupy, M. Bortolussi, J. C. Blais, L. Dubreucq and A. Meddour, *J. Polym. Sci. Part A Polym. Chem.*, 2005, **43**, 2480–2491.

29 G. K. Jett, S. K. Dengle, M. R. Platt, R. C. Eberhart, J. T. Willerson and J. T. Watson, *Cardiovasc. Res.*, 1978, **12**, 497–506.

30 L. Moity, Y. Shi, V. Molinier, W. Dayoub, M. Lemaire and J. M. Aubry, *J. Phys. Chem. B*, 2013, **117**, 9262–9272.

31 B. Yin and M. Hakkarainen, *J. Appl. Polym. Sci.*, 2010, **119**, 2400–2407.

32 H. Kobayashi and A. Fukuoka, *Green Chem.*, 2013, **15**, 1740–1763.

33 T. Komanoya, H. Kobayashi, K. Hara, W. J. Chun and A. Fukuoka, *Appl. Catal. A Gen.*, 2011, **407**, 188–194.

34 L. C. A. Maranhão and C. A. M. Abreu, *Ind. Eng. Chem. Res.*, 2005, **44**, 9642–9645.

35 A. W. Heinen, J. A. Peters and H. Van Bekkum, *Carbohydr. Res.*, 2000, **328**, 449–457.

36 A. A. Balandin, N. A. Vasyunina, S. V. Chepigo and G. S. Barysheva, *Dokl. Akad. Nauk SSSR*, 1959, **128**, 941–944.

37 A.A. Balandin, N. A. Vasyunina, G. S. Barysheva and S. V. Chepigo, *Bull. Acad. Sci. USSR, Div. Chem. Sci. (Engl. Transl.)*, 1957, **6**, 403.

38 A. Fukuoka and P. L. Dhepe, *Angew. Chemie - Int. Ed.*, 2006, **45**, 5161–5163.

39 H. Kobayashi, Y. Ito, T. Komanoya, Y. Hosaka, P. L. Dhepe, K. Kasai, K. Hara and A. Fukuoka, *Green Chem.*, 2011, **13**, 326–333.

40 N. Yan, C. Zhao, C. Luo, P. J. Dyson, H. Liu and Y. Kou, *J. Am. Chem. Soc.*, 2006, **128**, 8714–8715.

41 R. Palkovits, K. Tajvidi, J. Procelewska, R. Rinaldi and A. Ruppert, *Green Chem.*, 2010, **12**, 972–97.

42 S. Van de Vyver, J. Geboers, M. Dusselier, H. Schepers, T. Vosch, L. Zhang, G. Van Tendeloo, P. A. Jacobs and B. F. Sels, *ChemSusChem*, 2010, **3**, 698–701.

43 M. Y. Zheng, A. Q. Wang, N. Ji, J. F. Pang, X. D. Wang and T. Zhang, *ChemSusChem*, 2010, **3**, 63–66.

44 J. Geboers, S. Van De Vyver, K. Carpentier, K. De Blochouse, P. Jacobs and B. Sels, *Chem. Commun.*, 2010, **46**, 3577–3579.

45 W. Deng, X. Tan, W. Fang, Q. Zhang and Y. Wang, *Catal. Letters*, 2009, **133**, 167–174.

46 N. Ji, T. Zhang, M. Zheng, A. Wang, H. Wang, X. Wang and J. G. Chen, *Angew. Chemie*, 2008, **120**, 8638–8641.

47 C. Luo, S. Wang and H. Liu, *Angew. Chemie - Int. Ed.*, 2007, **46**, 7636–7639.

48 J.C Goodwin, J.E Hodge, D Weisleder, *Carbohydrate research*, 1980, **79**, 133-141.

49 K. Bock, C. Pedersen and H. Thøgersen, 1981, 441–449.

50 G. Flèche and M. Huchette, *Starch - Stärke*, 1986, **38**, 26–30.

51 H. Kobayashi, H. Yokoyama, B. Feng and A. Fukuoka, *Green Chem.*, 2015,

17, 2732–2735.

52 J. M. Robinson, A. M. Wadle, M. D. Reno, R. Kidd, S. R. Barrett Hinsz and J. Urquieta, *Energy and Fuels*, 2015, **29**, 6529–6535.

53 A. Yamaguchi, N. Hiyoshi, O. Sato and M. Shirai, *Green Chem.*, 2011, **13**, 873–881.

54 S.-K. Kim, *Chitin, Chitosan, Oligosaccharides and Their Derivatives*, 2011, vol. 15.

55 F. Khoushab and M. Yamabhai, *Mar. Drugs*, 2010, **8**, 1988–2012.

56 G. Cárdenas, G. Cabrera, E. Taboada and S. P. Miranda, *J. Appl. Polym. Sci.*, 2004, **93**, 1876–1885.

57 I. A. Hoell, G. Vaaje-Kolstad and V. G. H. Eijsink, *Biotechnol. Genet. Eng. Rev.*, 2010, **27**, 331–366.

58 X. Chen, H. Yang and N. Yan, *Chem. - A Eur. J.*, 2016, **22**, 13402–13421.

59 S. K. Kim, *Chitin, Chitosan, Oligosaccharides and Their Derivatives*, 2011, vol. 15.

60 N. Gagné and B. K. Simpson, *Food Biotechnol.*, 1993, **7**, 253–263.

61 Z. Zakaria, G. M. Hall and G. Shama, *Process Biochem.*, 1998, **33**, 1–6.

62 W. L. Teng, E. Khor, T. K. Tan, L. Y. Lim and S. C. Tan, *Carbohydr. Res.*, 2001, **332**, 305–316.

63 S. Duan, L. Li, Z. Zhuang, W. Wu, S. Hong and J. Zhou, *Carbohydr. Polym.*, 2012, **89**, 1283–1288.

64 F. Sedaghat, M. Yousefzadi, H. Toiserkani and S. Najafipour, *Int. J. Biol. Macromol.*, 2016, **82**, 279–283.

65 H. Xie, S. Zhang and S. Li, *Green Chem.*, 2006, **8**, 630–633.

66 S. Yamazaki, A. Takegawa, Y. Kaneko, J. Kadokawa, M. Yamagata and M. Ishikawa, *Electrochem. commun.*, 2009, **11**, 68–70.

67 Y. Wu, T. Sasaki, S. Irie and K. Sakurai, *Polymer (Guildf).*, 2008, **49**, 2321–2327.

68 M. Shimo, M. Abe and H. Ohno, *ACS Sustain. Chem. Eng.*, 2016, **4**, 3722–3727.

69 N. L. B. M. Yusof, A. Wee, L. Y. Lim and E. Khor, *J. Biomed. Mater. Res. - Part A*, 2003, **66**, 224–232.

70 K. Madhumathi, N. S. Binulal, H. Nagahama, H. Tamura, K. T. Shalumon, N. Selvamurugan, S. V. Nair and R. Jayakumar, *Int. J. Biol. Macromol.*, 2009, **44**, 1–5.

71 S. Ifuku, M. Nogi, K. Abe, M. Yoshioka, M. Morimoto, H. Saimoto and H. Yano, *Biomacromolecules*, 2009, **10**, 1584–1588.

72 Y. Fan, T. Saito and A. Isogai, *Biomacromolecules*, 2008, **9**, 1919–1923.

73 H. Kim and S. Chang, *Acc. Chem. Res.*, 2017, **50**, 482–486.

74 F. De Schouwer, S. Adriaansen, L. Claes and D. E. De Vos, *Green Chem.*, 2017, **19**, 4919–4929.

75 X. Li, J. Ma, X. Jia, F. Xia, Y. Huang, Y. Xu and J. Xu, *ACS Sustain. Chem. Eng.*, 2018, **6**, 8048–8054.

76 V. Kyriakou, I. Garagounis, A. Vourros, E. Vasileiou and M. Stoukides, *Joule*, 2020, **4**, 142–158.

77 V. L. Deringer, U. Englert and R. Dronskowski, *Biomacromolecules*, 2016, **17**, 996–1003.

78 H. Sashiwa, S. Fujishima, N. Yamano, N. Kawasaki, A. Nakayama, E. Muraki, K. Hiraga, K. Oda and S. I. Aiba, *Carbohydr. Res.*, 2002, **337**, 761–763.

79 M. Osada, C. Miura, Y. S. Nakagawa, M. Kaihara, M. Nikaido and K. Totani, *Carbohydr. Polym.*, 2013, **92**, 1573–1578.

80 A. Einbu and K. M. Vårum, *Biomacromolecules*, 2007, **8**, 309–314.

81 M. Yabushita, H. Kobayashi, K. Kuroki, S. Ito and A. Fukuoka, *ChemSusChem*, 2015, **8**, 3760–3763.

82 H. Kobayashi, Y. Suzuki, T. Sagawa, K. Kuroki, J. Hasegawa and A. Fukuoka, *Phys. Chem. Chem. Phys.*, 2021, **23**, 15908–15916.

83 G. Margoutidis, V. H. Parsons, C. S. Bottaro, N. Yan and F. M. Kerton, *ACS Sustain. Chem. Eng.*, 2018, **6**, 1662–1669.

84 S. M. Hick, C. Griebel, D. T. Restrepo, J. H. Truitt, E. J. Buker, C. Bylda and R. G. Blair, *Green Chem.*, 2010, **12**, 468–47.

85 K. W. Omari, L. Dodot and F. M. Kerton, *ChemSusChem*, 2012, **5**, 1767–1772.

86 X. Chen, Y. Gao, L. Wang, H. Chen and N. Yan, *Chempluschem*, 2015, **80**, 1565–1572.

87 Y. Liu, C. N. Rowley and F. M. Kerton, *ChemPhysChem*, 2014, **15**, 4087–4094.

88 D. Padovan, H. Kobayashi and A. Fukuoka, *ChemSusChem*, 2020, **13**, 3594–3598.

89 F. D. Bobbink, J. Zhang, Y. Pierson, X. Chen and N. Yan, *Green Chem.*, 2015, **17**, 1024–1031.

90 H. Kobayashi, K. Techikawara and A. Fukuoka, *Green Chem.*, 2017, **19**, 3350–3356.

91 T. Sagawa, H. Kobayashi, C. Murata, Y. Shichibu, K. Konishi and A. Fukuoka, *ACS Sustain. Chem. Eng.*, 2019, **7**, 14883–14888.

92 T. Sagawa, H. Kobayashi and A. Fukuoka, *Mol. Catal.*, 2020, **498**, 111282.

Chapter 2

Dehydration condensation of a chitin-derived sugar alcohol using a weak acid catalyst

2.1 Introduction

Chitin is one of the most plentiful biomass that can be obtained from marine food waste, such as the shell of oysters, crabs and lobsters.[1] It is a polymer of *N*-acetylglucosamine (NAG), which contains naturally fixed nitrogen. Therefore, chitin is a promising resource to produce nitrogen compounds without ammonia synthesized by the energy-consuming Haber-Bosch process.[2] The hydrolysis and the subsequent hydrogenation of chitin produces 2-acetamido-2-deoxysorbitol (ADS). A potential useful derivative of ADS is 2-acetamido-2-deoxyisosorbide (ADI), which is obtained via the dehydration condensation.[3] ADI has a rigid framework with one hydroxy group and one acetamido group, and therefore this compound would be a monomer for producing nitrogen-containing polymers. Moreover, the structure is similar to that of isosorbide, which has the same condensed five-membered rings with two hydroxy groups. Isosorbide is a monomer for an engineering plastic named Durabio, which shows excellent properties such as good scratch resistance, high impact resistance and outstanding transparency. Thus, I expect that ADI is a promising monomer for synthesizing nitrogen-containing polymers with outstanding properties.

The attractive prospect of ADI motivated the author to focus on its efficient production. Previous reports showed that CF_3SO_3H catalyst afforded 33% yield of ADI at a high S/C ratio (2.0). ADS and ADI both have acetamide groups, and the functional group has high basicity. Therefore, the acid-dehydration reaction needs to overcome the leveling effect, which is the reason why a large amount of CF_3SO_3H is needed regardless of the very high acid strength. However, a more economical and less corrosive catalyst is necessary for the low-cost and environmental-friendly synthesis of

ADI. Herein, I explored weak acid catalysts that can convert ADS to ADI.

2.2 Experimental section

2.2.1 Reagents

The reagents used in this work are shown at the following table.

Table 2.1 Information about reagents.

Name	Supplier
N-acetylglucosamine ($C_8H_{15}NO_6$; NAG)	Fujifilm Wako Pure Chemical Industries
Methanol (CH_3OH)	Fujifilm Wako Pure Chemical Industries
Sulfuric acid (H_2SO_4)	Fujifilm Wako Pure Chemical Industries
Hydrochloric acid (HCl)	Fujifilm Wako Pure Chemical Industries
Oxalic acid ($H_2C_2O_4$)	Fujifilm Wako Pure Chemical Industries
Phosphorous acid (H_3PO_3)	Sigma-Aldrich
2,4-Dinitrobenzonic acid (DNBA; $C_7H_4N_2O_6$)	Alfa Aesar
Phosphorus acid (H_3PO_4)	Fujifilm Wako Pure Chemical Industries
Acetic acid (CH_3COOH)	Fujifilm Wako Pure Chemical Industries
DL-Malic acid ($C_4H_6O_5$)	Fujifilm Wako Pure Chemical Industries
Dimethyl phosphite ($C_2H_7O_3P$)	Tokyo Chemical Industry
Diethyl phosphite ($C_4H_{11}O_3P$)	Tokyo Chemical Industry
Diisopropyl phosphite ($C_6H_{15}O_3P$)	Tokyo Chemical Industry
Ru/C (Ru 5 wt%)	Sigma-Aldrich
Hydrogen gas (H_2)	Air Liquide Kogyo Gas

2.2.2 Synthesis of ADS from NAG

NAG (1.6 g) and 5 wt% Ru/C (1.0 g) were added in water (40 mL), and the mixture was filled in a crucible-type autoclave provided by Nitto Koatsu and pressurized with H_2 (4 MPa). The autoclave was kept at 80 °C for 1 h, and then the mixture was filtered using a mixed cellulose ester membrane (Advantec, 25AS045AN, 0.45 μm pores). The mixture was condensed under a reduced pressure till almost dried, followed by

dissolution with methanol (40 mL) and kept at −30 °C for recrystallisation. Finally, ADS was obtained as a white solid (isolated yield 64%).[4]

2.2.3 Conversion of ADS by acid catalysts

An aqueous mixture of ADS (112 mg, 0.5 mmol) and an acid catalyst (at a determined ratio) in H_2O (0.2 mL) were added into a Schlenk tube (Kanto Chemical, 20 mL). The reactor was connected to a rotary pump via a liquid N_2 trap for drying at a reduced pressure (< 0.1 kPa) overnight at a room temperature. The apparatus was immersed in an oil bath and kept for a certain time at a determined temperature under the atmospheric pressure or reduced pressure (Fig. 2.1). After reaction, the apparatus was cooled down till ambient temperature.

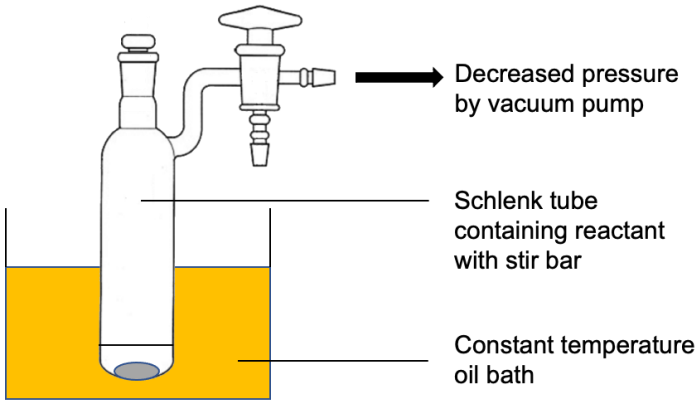

Figure 2.1 Experimental setup for the ADS dehydration.

2.2.4 Liquid chromatography analysis

2.2.4.1 High pressure liquid chromatography (HPLC) analysis

Soluble products of the reaction were analyzed using a HPLC (Shimadzu LC-20AD) equipped with a Rezex RPM-Monosacharide Pb++ column (Phenomenex, 300 × ø 7.8 mm, 70 °C) with a refractive index detector (RID). Water at a flow rate of 0.6 mL min^{-1} was applied as a mobile phase.

Calculations of yield of each product used the following equation:

$$\text{Yield (\%)} = \frac{f \times A \times V}{m/M} \times 100 \qquad (2.1)$$

where f is calibration factor (mol/L), A is area from HPLC chart, V is volume of water (L), m is the mass of ADS (g), M is the molecular weight (g/mol).

2.2.4.2 Size exclusion chromatography (SEC) analysis

Size exclusion chromatography (SEC) analysis of product mixtures was conducted using an HPLC (Shimadzu, LC-20AR) equipped with two GF-210 HQ columns in a row (Shodex, 300 mm × ø 7.5 mm, 50 °C) with an RID detector. A 0.02 mol L^{-1} acetic acid aqueous solution was used as an eluent (0.5 mL min^{-1}).

2.2.4.3 Liquid chromatography-mass spectroscopy (LC/MS) analysis

LC/MS analysis was performed using an HPLC system (Shimadzu LC-20AR) equipped with a SH-1011 column (Shodex Sugar 300 mm × ø 8.0 mm) and a mass spectrometer (MS, LCMS-2020). The MS was composed of an electrospray ionizer (ESI) and a quadrupole mass analyzer.

2.2.5 Nucleic magnetic resonance (NMR) analysis

Proton decoupled phosphorus nuclear magnetic resonance (NMR; ^{31}P 243 MHz) was measured with a JEOL ECX-600 spectrometer. H_3PO_4 at 85% concentration was applied as an external standard.

2.2.6 Ultraviolet-visible spectroscopy analysis

For the ultraviolet-visible (UV-Vis) spectroscopy, all samples were diluted 10 times using distilled water before the measurements. Then those samples were measured in quartz cells with 1 cm optical path length on a JASCO V-650 at a scan rate of 400 nm min^{-1}.

2.2.7 DFT calculations

2.2.7.1 DFT calculations of reaction pathways

Gaussian 16[5] software program was used for the DFT calculations at the B3LYP/6-31+G(d, p) level to determine energy profiles of the conversion of ADS in different

reaction pathways.[6–9] The solvation effect was involved by the solvation model based on density (SMD)[10] with using *N,N*-dimethylformamide to reproduce the effect of acetamido groups. Each found transition state had only one imaginary number vibration frequency, and connected the reactant and the expected product by the intrinsic reaction coordinate (IRC).[11]

2.2.7.2 DFT calculations for NMR chemical shift prediction

Chemical shift values (δ) in ^{31}P NMR were predicted by eq. 2.2, in which the coefficients *a* and *b* were determined by the least-squares fitting method using the chemical shift values obtained by actual NMR measurements and the σ_{calc} values of the commercially available phosphite esters (dimethyl phosphite, diethyl phosphite and diisopropyl phosphite).

$$\delta_{pred} = a\sigma_{calc} + b \qquad (2.2)$$

where σ_{calc} is a computed isotropic shielding constant.

To determine σ_{calc} of a compound, based on the thermodynamic distribution, the influence of multiple conformations was included. I used the molclus[12] with Gaussian 16 to systematically make the possible conformations of the compounds. After optimizing their geometric structures at the level of B3LYP/6-31+G(d,p), those unstable conformations which do not contribute to σ_{calc} were excluded. To be more accurate, the energy and isotropic shielding constant of each structure are determined using the Gauge-Independent Atomic Orbit (GIAO) method at the B3LYP/6-311+G(d,p) level for the single-point calculation,[13,14] which could be used for an accurate predict of the shielding constant of phosphorus.[15] The equation used for summarizing the influences of different conformations on σ_{calc} is shown below (eq. 2.3, 2.4). Assuming *n* conformations should be considered, the ratio of the existence of a specific conformation (number *k* within *n*) to the most stable conformation (the first) could be estimated (K_k, obtained by eq. 2.3) using an energy difference between the two conformations. At the end, σ_{calc} was defined as their existence ratio-weighted average

of the shielding constants (eq. 2.4).

$$K_k = e^{-\frac{E_k - E_1}{RT}} \qquad (2.3)$$

where *e* is the Napier's constant, *R* is the gas constant, and *T* is the ambient temperature (298 K).

$$\sigma_{calc} = \frac{\sum_1^n K_k \sigma_k}{\sum_1^n K_k} \qquad (2.4)$$

where σ_k is the calculated shielding tensor of each conformation.

2.3 Results and discussion

2.3.1 Typical reaction pathway of ADS dehydration

The typical reaction pathway from ADS to ADI includes a two-step dehydration reaction (Scheme 2.1).[3] The first dehydration converts ADS to 1,4-anhydro-ADS, 3,6-anhydro-ADS and 1,5-anhydro-ADS. For convenience, anhydro-ADS is denoted AHADS hereafter. 1,4-AHADS and 3,6-AHADS produce ADI by the second dehydration, and 1,5-AHADS is a by-product. Additionally, the acetylation of ADI gives 6-*O*-acetyl-ADI (denoted ADIAc). The second-step dehydration, namely 1,4- and 3,6-AHADS to ADI, is the rate-determining step.[3]

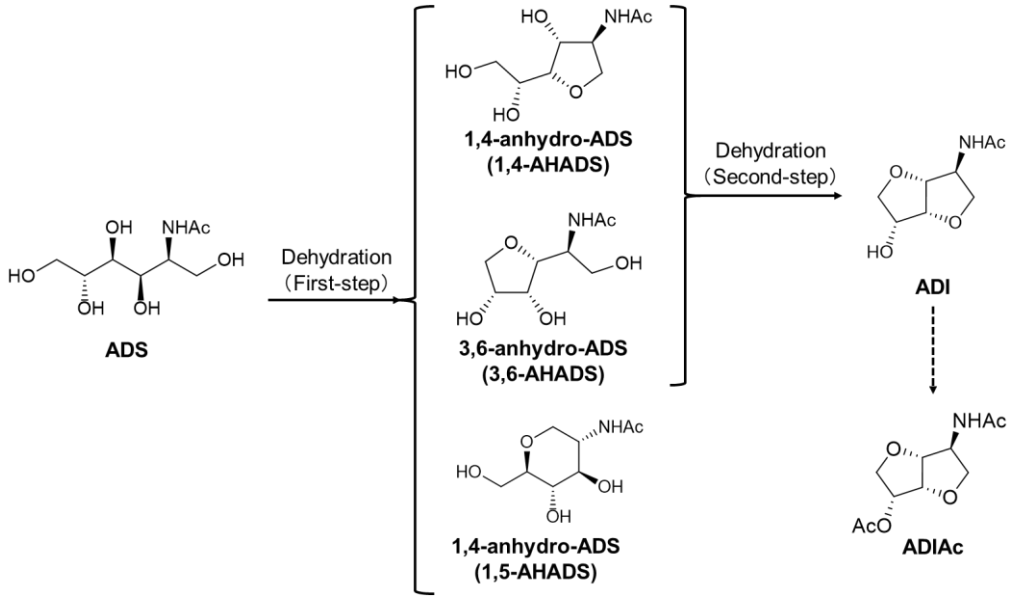

Scheme 2.1 Reaction pathway from ADS to ADI.

2.3.2 Screening test of weak acids

To evaluate the influence of acidity on activity of ADS dehydration, I tested several acids with pH values varied from −15 to 2.8 (specifically, CF_3SO_3H, HCl, H_2SO_4, $H_2C_2O_4$, H_3PO_3, 2,4-Dinitrobenzonic acid (denoted DNBA), H_3PO_4, and malic acid; the pK_a of each acid is shown in Fig. 2.2) at S/C = 2.0 at 150 °C under the atmospheric pressure for 3 h. A reaction with no catalyst converted ADS to AHADSs in 28% yield in total (entry 1) but did not produce ADI at all. Thus, the reaction needs a catalyst. CF_3SO_3H, HCl and H_2SO_4, namely strong acids, gave ADI in 11–19% yield, AHADS and ADIAc (entries 2–4). Plenty of unidentified by-products were also formed (49–67%), which are supposed to be deacetylated compounds and humins.

Then, various weak acids with pK_a values of 1.2–2.8 ($H_2C_2O_4$, H_3PO_3, DNBA, H_3PO_4 and malic acid) (entries 5–9) were tested. Among these acids, H_3PO_3 gave the highest yield of ADI (19%, entry 6), and notably this yield was as high as that given by CF_3SO_3H (19%, entry 2).

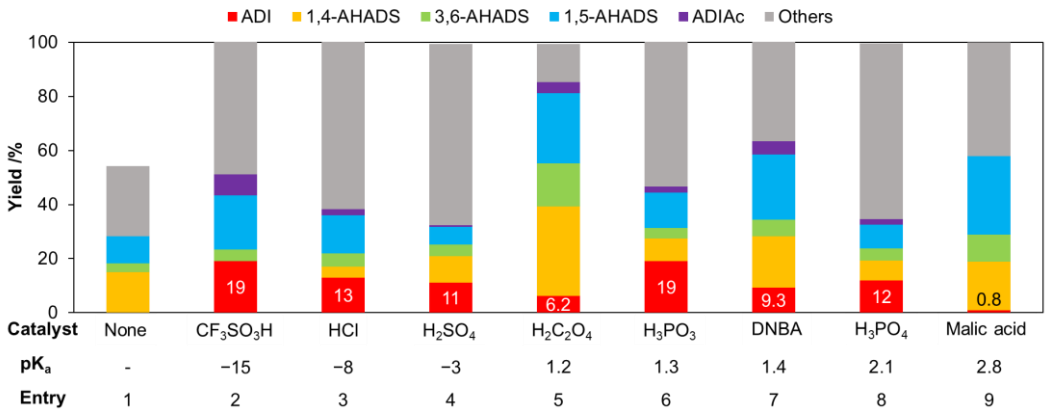

Figure 2.2 Dehydration of ADS by acid catalysts with different pKa values. Reaction conditions: NAG 0.05 mol; S/C = 2.0; p = 1 atm; 150 °C; 3 h.

2.3.3 Optimization of reaction conditions to maximum the yield of ADI

The reaction conditions were optimized to maximize the yield of ADI using H_3PO_3 (Fig. 2.3). First, I attempted to depressurize the reaction system to remove the H_2O produced

from dehydration for promoting the reaction. The decrease in pressure from 100 kPa to less than 0.1 kPa increased the yield of ADI from 19% (entry 6) to 24% (entry 12). Second, the influence of temperature was studied under the vacuum condition. By decreasing the reaction temperature from 150 °C, the reaction at 130 °C gave a similar yield of ADI (24%, entry 11) but that at 110 °C decreased the yield to 18% (entry 10). The high-activation-energy characteristic[3] of this reaction suggests that a higher reaction temperature is favorable; however, high temperature also promotes side reactions to give more by-products such as humins. Thus, I chose 130 °C as the temperature for the following experiments to alleviate the influence from side reactions. Then, the S/C ratio was varied from 2.0 to 8.0 at 130 °C. The increase in the S/C ratio from 2.0 to 4.0 increased the yield of ADI within the range of error, and slightly increased AHADS (entry 13). The reaction at the S/C ratio of 8.0 drastically decreased ADI yield to 10% due to the slow dehydration of 1,4- and 3,6-AHADS to ADI (entry 14). I conclude that pressure, temperature, and S/C ratio are all influential on the yield of ADI. The best reaction conditions for H_3PO_3 are p < 0.1 kPa, 130 °C, S/C = 4.0, 3 h, which gives the highest yield of ADI (25%).

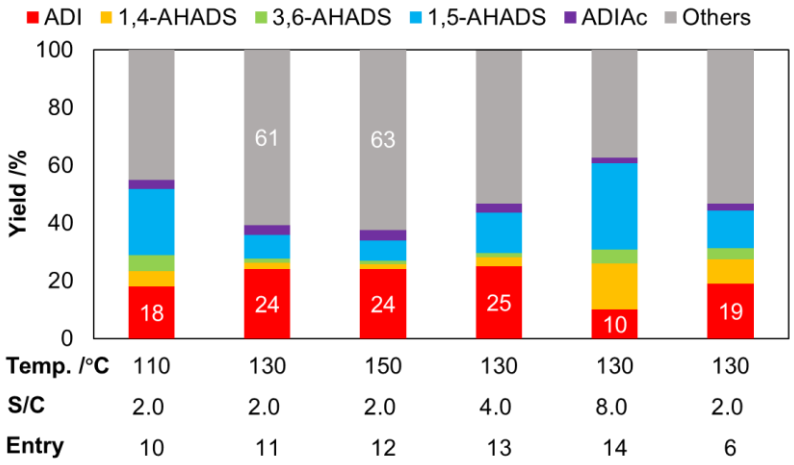

Figure 2.3 Optimization of reaction conditions for the dehydration of ADS by H_3PO_3. Reaction conditions: NAG 0.05 mol; p < 0.1 kPa; 3 h.

Reactions using different weak acids were also conducted under the optimized

condition for H_3PO_3 (Fig. 2.4). $H_2C_2O_4$ and DNBA gave 12–13% yield of ADI (entries 16, 17), and H_3PO_4 gave only 8.9% yield (entry 18). I conclude that H_3PO_3 is the most active catalyst for ADS dehydration condensation among all the tested weak acids.

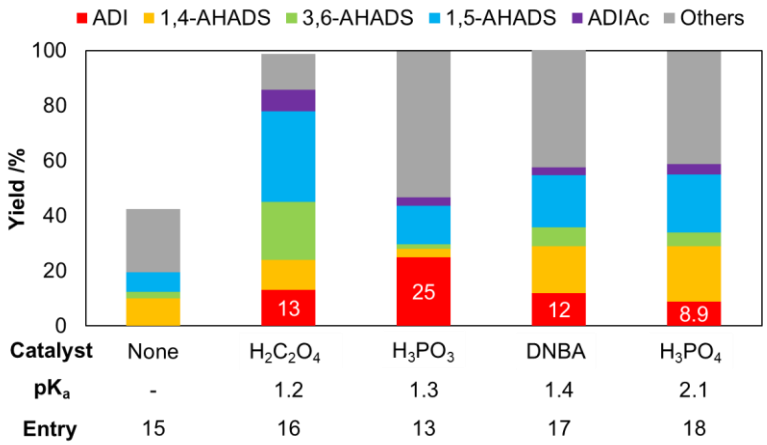

Figure 2.4 Dehydration of ADS by various catalysts under the optimized condition for H_3PO_3. Reaction conditions: NAG 0.05 mol; S/C = 4.0; p = 0.1 kPa; 130 °C; 3 h.

2.3.4 UV analysis of product solutions

In the screening test of acids, the color of each product mixture was yellowish to brown (Fig. 2.5A). The product mixture given by CF_3SO_3H and H_3PO_4 showed especially dark colors (Fig. 2.5A), which implies a large amount of by-products. The color may be derived from humins, which contain large amounts of chromophoric conjugated structures. In my reaction system, 3,6-AHADS is one of the potential precursors to humins, because it can be dehydrated to a furfural alcohol, and furans is well known to polymerize in the presence of an acid catalyst (Fig. 2.6).[16–20] In contrast, H_3PO_3 and $H_2C_2O_4$ provided pale yellow solutions (Fig. 2.5A).

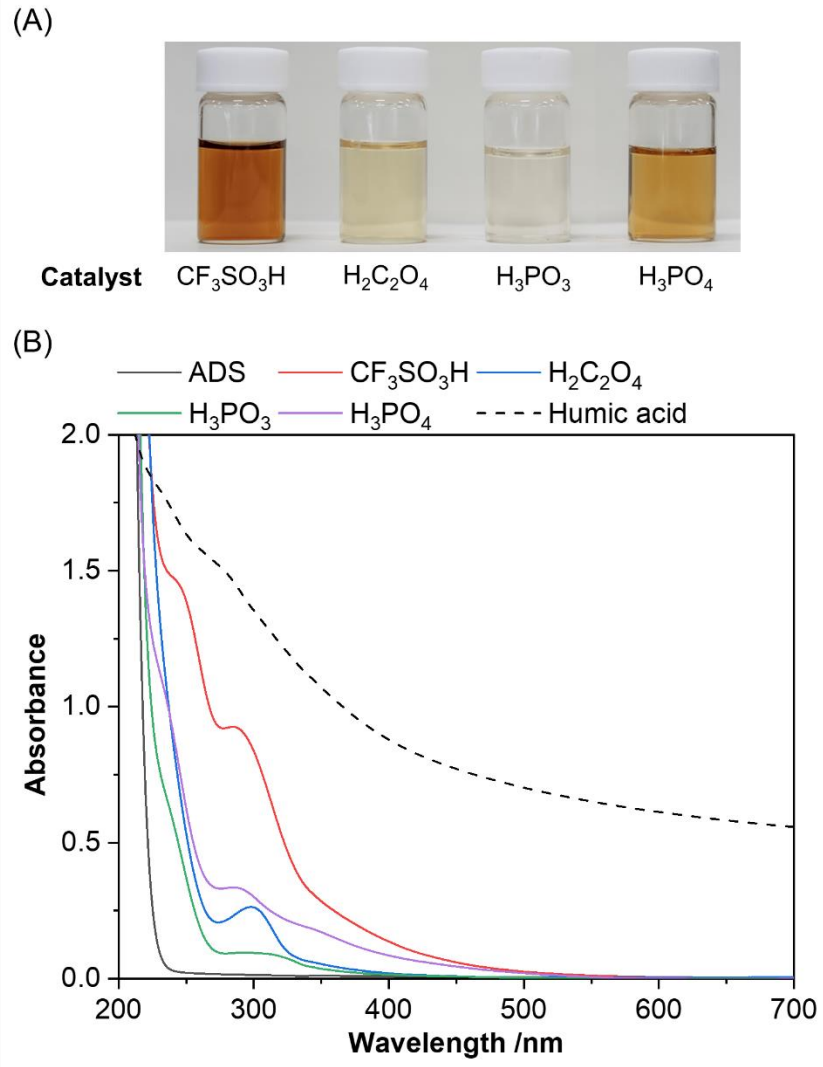

Figure 2.5 (A) Photographs of aqueous solutions of products after the dehydration of ADS catalyzed by CF_3SO_3H, $H_2C_2O_4$, H_3PO_3 and H_3PO_4. (B) UV-Vis spectra of the solutions above, ADS, and humic acid.

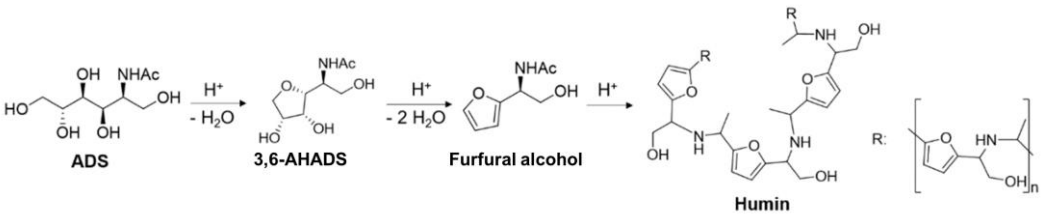

Figure 2.6 Possible example for production of furan derivatives and humins from ADS.

The phenomenon inspired me conducting UV analysis of the product mixtures to understand the difference in colors (Fig. 2.5B). Those acids had no absorption peaks

at >230 nm, except for $H_2C_2O_4$, which has an absorption for C=O π–π* transition (240 nm). A pure ADS solution was measured as a controlled experiment, giving a peak at < 220 nm mainly derived from C=O π–π* transition. AHADS and ADI may have similar peak position and absorbance because of no structural change around the unsaturated bond. For the reaction mixtures, those given by CF_3SO_3H and H_3PO_4 provided additional peaks at 230–320 nm. The peaks are assignable to unsaturated bonds or conjugated systems such as furanics.[21] The absorption peaks are extended to visible region (>380 nm), suggesting the existence of large conjugated structures in humins.[22] I have confirmed that a soluble humin material showed a broad absorption in visible region (Humic acid in Fig. 2.5B). Compared to the two acids discussed above, H_3PO_3 and $H_2C_2O_4$ gave smaller peaks for conjugated structures. It is notable that they showed almost no absorption in the visible region (>380 nm). I realized that the two acids have reducing ability (eqs. 3.5, 3.6), while other acids do not. Possibly, H_3PO_3 and $H_2C_2O_4$ convert the unsaturated chemical bonds in by-products to saturated ones, and therefore they provide the pale color for the product solutions.

$$H_3PO_4 + 2H^+ + 2e^- \rightleftarrows H_3PO_3 + H_2O \quad E° = -0.276 \text{ V vs SHE} \quad (3.5)$$

$$2CO_2 + 2H^+ + 2e^- \rightleftarrows H_2C_2O_4 \quad E° = -0.475 \text{ V vs SHE} \quad (3.6)$$

2.3.5 Size exclusion chromatography analysis

In the previous section, the UV analysis implied that the product mixtures contained humins. Humins are produced by intermolecular condensation, thus having large molecular weights (M_w) in the range of 300–10^6.[23] Therefore, they can be distinguished by the molecular size with monomeric compounds such as ADS and ADI (M_w < 300). Based on this fact, an SEC analysis of the production mixtures were performed to quantitatively analyze condensation products including humins (Fig. 2.7). The SEC analysis separates molecules according to their size and elutes them in order of decreasing M_w. The peak area ratio of the products with M_w below and above 300 were calculated (Table 2.2). H_3PO_3 and $H_2C_2O_4$ produced condensation products (M_w > 300) in peak area ratios of 36% and 10%, respectively. These ratios were lower than those

given by CF_3SO_3H (62%) and H_3PO_4 (53%). This is because H_3PO_3 and $H_2C_2O_4$ possibly alleviates the side-reactions, by reducing the unsaturated structures which are able to form humins.[24] For summary, the reducing activity of H_3PO_3 and $H_2C_2O_4$ is effective for keeping the production mixture pale color and for decreasing the condensation by-products. However, as shown in Fig. 2.2, H_3PO_3 produces unidentified by-products as much as non-reducing acids. I speculate that this is due to the formation of their H_3PO_3 monoesters (phosphite esters), which have molecular weight at 287 (Sorbitol ester) and 269 (1,4-AHADS ester) and considered as non-condensation products ($300 \geq M_w$).

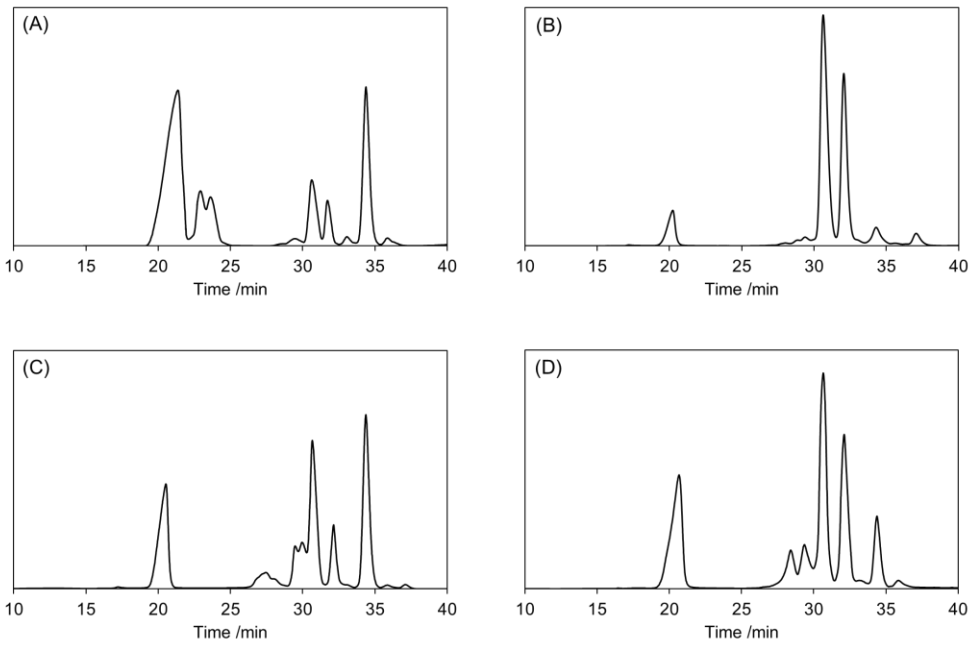

Figure 2.7 SEC charts refer of ADS dehydration product using various acid catalysts: (A) CF_3SO_3H; (B) $H_2C_2O_4$; (C) H_3PO_3; (D) H_3PO_4.

Table 2.2 Result of SEC analysis of product mixtures.

Catalyst	Ratio of peak area /%	
	$M_w > 300$	$300 \geq M_w$
None	0	100
CF_3SO_3H	62	38

$H_2C_2O_4$	10	90
H_3PO_3	37	63
H_3PO_4	53	47

2.3.6 Kinetic analysis of ADS dehydration by H_3PO_3

For a better understanding of the high activity of H_3PO_3 for ADI production (25%), the time course of ADS dehydration by H_3PO_3 was studied (Fig. 2.8A), and that by H_3PO_4 was also employed as comparison (Fig. 2.8C). In the case of H_3PO_3, yields of 1,4- and 3,6-AHADS were maximized at 0.5 h, and then gradually decreased due to consecutive reactions. 1,5-AHADS was similarly produced, but it decreased very slowly after 1 h. ADI increased in a sigmoidal curve, and the yield reached 25% at 3 h. This profile demonstrates that ADI forms by successive reactions via 1,4- and 3,6-AHADS. In case of H_3PO_4, 1,4- and 3,6-AHADS showed similar trend with H_3PO_3; 1,5-AHADS reached the maximum at 1 h, then slowly decline. However, yield of ADI increases slowly, then stopped after 2 h. To reveal the difference in kinetic parameters of the two reactions, the author applied a pseudo first-order approximation which is often employed for the dehydration of sugar alcohols[25–27] (solid lines in Figs. 2.8A and C). In both cases, the approximation nicely followed the experimental data, giving reliable rate constants. As summarized in Figs. 2.8B and D, H_3PO_3 produced 1,4- (k = 0.79 h^{-1}), 3,6- (0.82 h^{-1}) and 1,5-AHADS (0.95 h^{-1}) at similar rate constants (ratio 31:32:37), which resembled those of H_3PO_4 (30:33:37). However, H_3PO_3 gave larger rate constants for the dehydration of 1,4- and 3,6-AHADS to ADI (1.0 and 1.1 h^{-1}) than those for the first step. The values were five-fold greater than those for H_3PO_4 (0.18 h^{-1} and 0.22 h^{-1}). This is an outstanding characteristic of H_3PO_3 compared to other weak acids, because the second dehydration is the rate-determining step of other acid systems.

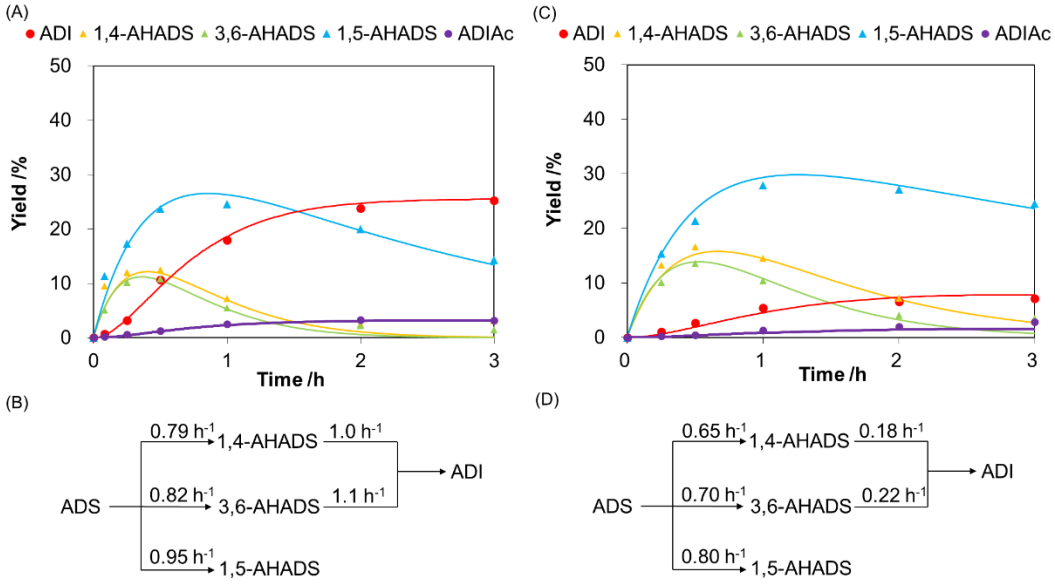

Figure 2.8 (A) Time course of ADS dehydration by H_3PO_3 and (B) pseudo first-order rate constants obtained by the curve fitting; (C) Time course of ADS dehydration by H_3PO_4 and (D) pseudo first-order rate constants obtained by the curve fitting. In (A) (C), the plots indicate actual experimental results, and the lines show theoretical yield curves based on the kinetic analysis.

2.3.7 LC-MS analysis and ^{31}P-NMR analysis

I focused on why H_3PO_3 specifically shows high activity among weak acids. Possible causes would be particular acid strength suitable for the reaction or different reaction mechanism. For the former, oxalic acid (pK_a = 1.2) and DNBA (pK_a = 1.4) were much less active than H_3PO_3 (pKa = 1.3) regardless of the similar acidity (Fig. 2.2). Therefore, the high activity of H_3PO_3 cannot be explained by acid strength. Instead, I speculate that the reaction mechanism is different. Thus, the product mixture made with H_3PO_3 was analyzed with an LC/MS to clarify whether unexpected intermediates are present. After performing a short-time ADS dehydration by H_3PO_3 (1 h, S/C = 4.0, 130 °C, pressure < 0.1 kPa), the product gave three major peaks at 10, 22, and 34 min in the chromatogram (Fig. 2.9A). The peak at 10 min indicated *m*/*z* = 250 and 268 (Fig. 2.9B), and the mass numbers are ascribed to phosphite esters of AHADS ($[M-H_2O-H]^-$, *m*/*z* = 250; $[M-H]^-$, *m*/*z* = 268) and possibly that of ADI ($[M-H]^-$, *m*/*z* = 250). The second peak (22 min) showed *m*/*z* = 286 (Fig. 2.9C), which is assignable to the ester of ADS

([M−H]⁻). The third peak (34 min) is supposed to be ADI (Fig. 2.9D; [M-H]⁻, *m*/*z* = 186).

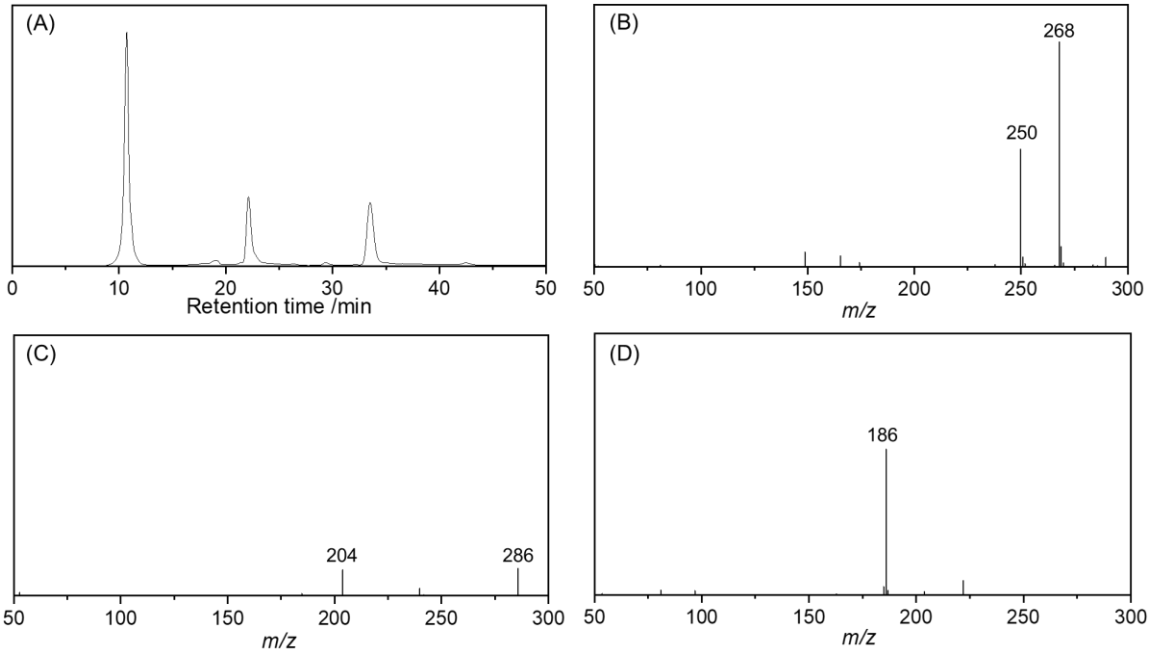

Figure 2.9 (A) LC chart given by RID detector of the product solution after the dehydration of ADS by H_3PO_3 (S/C = 4.0) at 130 °C under < 0.1 kPa of pressure for 1 h. The mass spectra are recorded using a negative ion mode at (B) 10 min, (C) 22 min and (D) 34 min.

The appearance of those H_3PO_3 esters motivated the author to conduct ^{31}P NMR analysis of each fraction (Fig. 2.10). For the fraction at 10 min, other than the peak of H_3PO_3 at 4.6 ppm, several peaks appeared in the range of 6.0–8.0 ppm. In contrast the fraction at 22 min gave no peak, though the fraction collection was continued for three days. Concentration of the product may be very low, or the compound does not contain phosphorus.

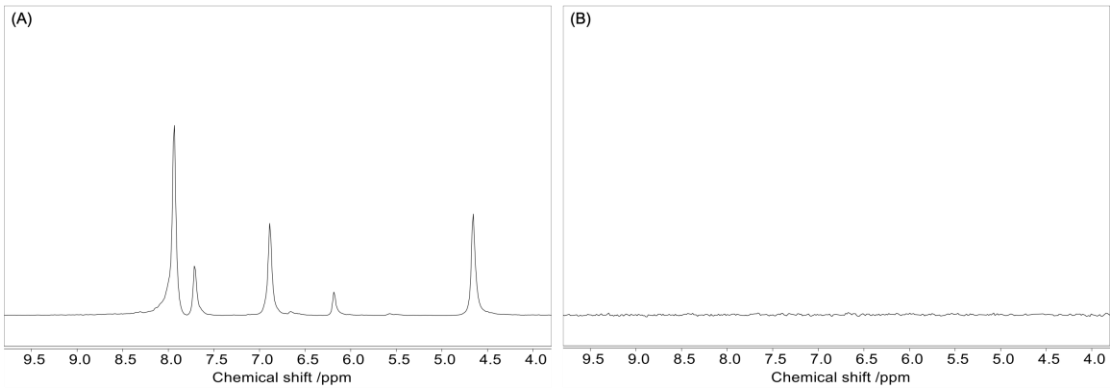

Figure 2.10 ^{31}P NMR spectra of the HPLC fractions shown in Fig. 2.9. (A) Retention time: 10 min. (B) Retention time: 22 min.

2.3.8 ^{31}P NMR prediction by DFT calculation

For the 10-min fraction, the analytical assignment of the peaks in NMR spectra was difficult. Instead, the ^{31}P NMR chemical shifts of phosphite esters were predicted using a quantum chemical calculation method. After determining the coefficients a and b as −0.457 and 141.2 by using the three commercial phosphite esters (Fig. 2.11), eq. 2.2 was applied to estimate the ^{31}P chemical shifts for phosphorous acid esters of 1,4-AHADS and 3,6-AHADS (Table 2.3). For convenience, those compounds are denoted 1,4- and 3,6-AHADS-*n*P, where *n* indicates the ester position. The peaks predicted by calculation are in the range of 6–8 ppm, which was approximately the same as those observed in the actual experiment (6–8 ppm, Fig. 2.11). Among the compounds listed in Table 2.3, 1,4-AHADS-6P, 1,4-AHADS-3P, 3,6-AHADS-1P and 3,6-AHADS-4P are the possible intermediates to give ADI by hydrolysis followed by ring closure. The others are by-products, because their dehydration condensation does not produce five-membered ring structures.

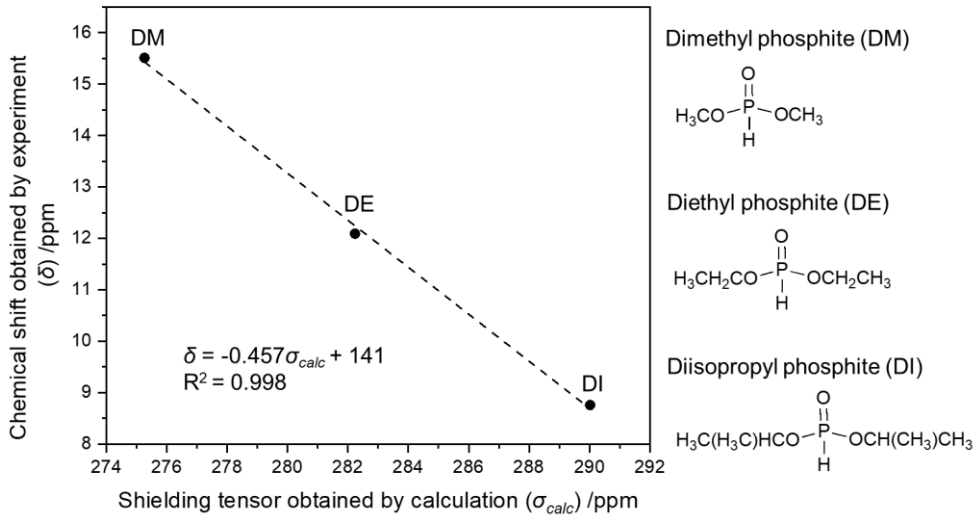

Figure 2.11 Determination of the coefficients *a* and *b* using the least-squares method using standard compounds.

Table 2.3 Computed shielding constants and predicted chemical shifts of phosphites.

Compound	σ_{calc} /ppm	δ_{pred} /ppm	Compound	σ_{calc} /ppm	δ_{pred} /ppm
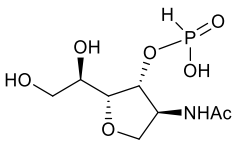 1,4-AHADS-3P	293.1	7.3	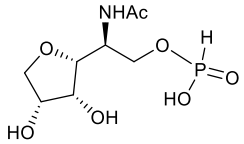 3,6-AHADS-1P	295.6	6.2
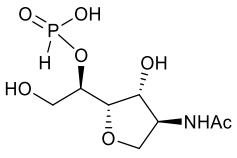 1,4-AHADS-5P	291.2	8.2	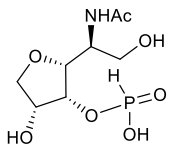 3,6-AHADS-4P	295.6	6.1
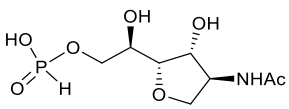 1,4-AHADS-6P	293.4	7.2	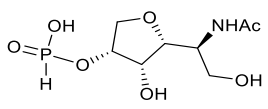 3,6-AHADS-5P	291.5	8.0

The results of LC-MS and ^{31}P-NMR analysis imply that the dehydration condensation of ADS with H_3PO_3 possibly takes place via AHADS phosphites. This is a new reaction pathway (denoted as phosphite mechanism) that differs from the typical acid mechanism.

2.3.9 DFT calculations of post-reaction solutions

For a better understanding of the reaction mechanism, DFT calculations were conducted to determine the energy profiles of different reaction pathways. Both the typical acidic mechanism and phosphite mechanism were considered in the DFT calculations. For the simple acid-catalyzed reaction (Scheme 2.2A), the primary hydroxy group should be protonated; however, the carbonyl O in the acetamido group initially trapped the proton (E = −8 kJ mol^{-1}) due to the strong basicity. This quenching effect led to a high activation energy (TS1, E_a = 107 kJ mol^{-1}) for the cyclization reaction to produce 1,4-AHADS. Similarly, the product produced a stable adduct with a proton at the carbonyl O (E = −19 kJ mol^{-1}). This resulted in a higher activation energy (TS2, E_a = 118 kJ mol^{-1}) for the second dehydration to form ADI. Accordingly, the high activation energy due to proton trapping by the acetamido group accounts for the low reaction rate to obtain ADI.

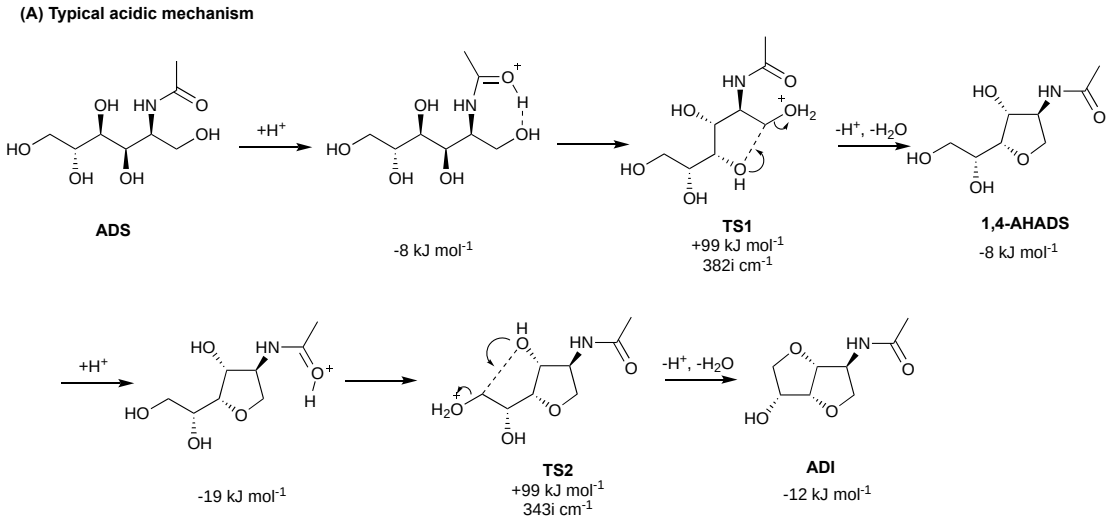

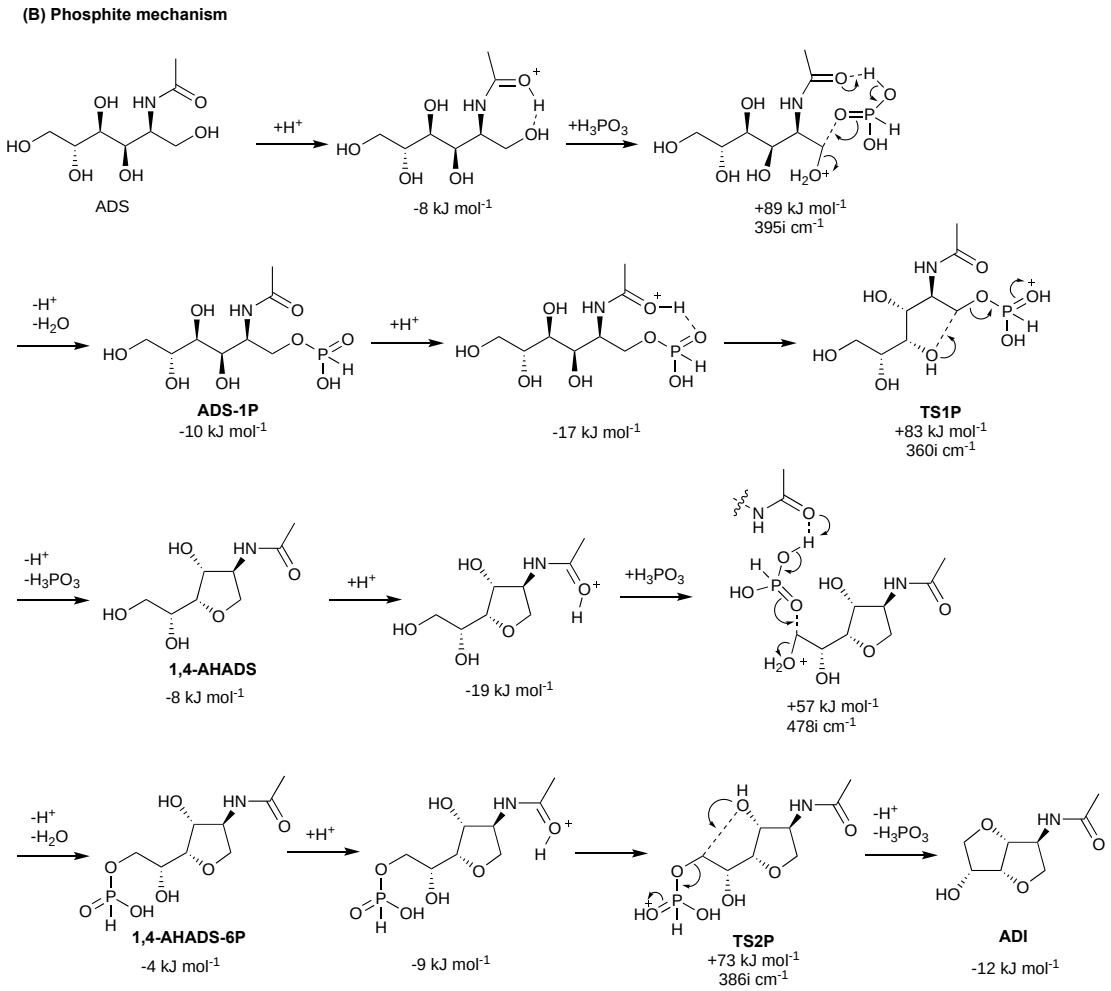

Scheme 2.2 Proposed reaction mechanisms for conversion of ADS to ADI using (A) typical acid catalysts and (B) H_3PO_3. Proton formation is assumed as $2H_3PO_3 \rightarrow H^+ + [H_2PO_3 \cdots H_3PO_3]^-$.

In the case of the phosphite mechanism (Scheme 2.2B), the esterification of ADS with H_3PO_3 produced ADS-1P with an E_a of 96 kJ mol^{-1}. The esterification can also occur at the secondary OH groups. However, the product, ADS-1P, was 10–30 kJ mol^{-1} more stable than those esters produced at the secondary hydroxy groups. Thus, ADS-1P is expected to be the main product of the esterification. The ester captured a proton between P=O and carbonyl O of acetamido group, followed by an S_N2 reaction in which H_3PO_3 worked as leaving group. This reaction generated 1,4-AHADS with an E_a of 100 kJ mol^{-1} (TS1P). This value was slightly lower than E_a of the typical acid mechanism (107 kJ mol^{-1}). The esterification and dehydration of 1,4-AHADS to ADI resembled those of ADS. First, 1,4-AHADS produced 1,4-AHADS-6P with an E_a of 76 kJ mol^{-1},

and then it was similarly converted to ADI with an E_a of only 82 kJ mol^{-1} (TS2P). Accordingly, the phosphite mechanism provides remarkably lower activation energy for the second cyclization, compared to the typical acid mechanism (118 kJ mol^{-1}). This is likely due to the easy protonation of P=O group than that of OH. The DFT calculations have indicated that the P=O in 1,4-AHADS-6P has a proton affinity of 1066 kJ mol^{-1}, which is 42 kJ mol^{-1} higher than that of the primary OH group in 1,4-AHADS (1024 kJ mol^{-1}). I conclude that H_3PO_3 can create a new reaction pathway via esters with low activation energies, which significantly accelerates the step of converting 1,4-AHADS to ADI.

2.4 Conclusions

In this chapter, I studied the dehydration condensation of a polyol (ADS) derived from chitin. I found that H_3PO_3 shows exceptionally high catalytic activity among the weak acids catalysts tested. Additionally, the reducing ability of H_3PO_3 decreases the coloring of the product likely by converting unsaturated bonds to saturated ones. It may decrease the formation of humins as indicated by the SEC analysis, because the unsaturated structures induce intermolecular condensation. For the kinetics of the H_3PO_3-catalyzed reaction, rate constants for the dehydration of AHADS to ADI are larger than those of ADS to AHADS. This kinetics is specific to H_3PO_3, as other weak acids give much lower rate constants to the conversion of AHADS, compared to that of ADS. LC-MS and ^{31}P NMR analyses have shown that the reaction pathway using H_3PO_3 contains phosphite esters of ADS and AHADS. DFT calculations of the reaction mechanism supported the hypothesis, in which ADS first produces phosphite esters and the esters convert to AHADS by S_N2 reactions, then AHADS are transformed into ADI by the same mechanism. Importantly, in this mechanism the activation energy is significantly lower than that of conventional acid-catalyzed mechanism. P=O groups in the esters can easily capture proton due to high basicity, which leads to the quick cyclization reaction. In contrast, the conventional acid systems need protonation of less basic hydroxy groups of the substrates, but protons are rather caught by amide groups. Thus, the new pathway opened by H_3PO_3 overcomes the inhibition effect and provides the

low activation energy. My reaction decreases the cost and environmental load of ADI synthesis.

2.5 References

1 M. Yadav, P. Goswami, K. Paritosh, M. Kumar, N. Pareek and V. Vivekanand, *Bioresour. Bioprocess.*, 2019, **6**, 8.

2 V. Kyriakou, I. Garagounis, A. Vourros, E. Vasileiou and M. Stoukides, *Joule*, 2020, **4**, 142–158.

3 T. Sagawa, H. Kobayashi, C. Murata, Y. Shichibu, K. Konishi and A. Fukuoka, *ACS Sustain. Chem. Eng.*, 2019, **7**, 14883–14888.

4 T. Sagawa, H. Kobayashi, C. Murata, Y. Shichibu, K. Konishi and A. Fukuoka, *ACS Sustain. Chem. Eng.*, 2019, **7**, 14883–14888.

5 H. B. Schlegel, *Adv. Chem. Phys.*, 2007, **67**, 249–286.

6 A. D. Becke, *J. Chem. Phys.*, 1993, **98**, 5648–5652.

7 D. E. Woon and T. H. Dunning, *J. Chem. Phys.*, 1993, **98**, 1358–1371.

8 T. H. Dunning, *J. Chem. Phys.*, 1989, **90**, 1007–1023.

9 P. J. Hay and W. R. Wadt, *J. Chem. Phys.*, 1985, **82**, 270–283.

10 A. V. Marenich, C. J. Cramer and D. G. Truhlar, *J. Phys. Chem. B*, 2009, **113**, 6378–6396.

11 K. Fukui, *J. Phys. Chem.*, 1970, **74**, 4161.

12 T. Lu, *Molclus program, Version 1.9.9.3*, http://www.keinsci.com/research/molclus.html (accessed Feb. 12, 2021).

13 K. Wolinski, J. F. Hinton and P. Pulay, *J. Am. Chem. Soc.*, 1990, **112**, 8251–8260.

14 M. P. Andersson and P. Uvdal, *J. Phys. Chem. A*, 2005, **109**, 2937–2941.

15 M. Tafazzoli and H. P. Ebrahimi, *Phosphorus, Sulfur Silicon Relat. Elem.*, 2011, **186**, 1491–1500.

16 S. Bertarione, F. Bonino, F. Cesano, S. Jain, M. Zanetti, D. Scarano and A. Zecchina, *J. Phys. Chem. B*, 2009, **113**, 10571–10574.

17 X. Gao, L. Peng, H. Li and K. Chen, *BioResources*, 2015, **10**, 6548–6564.

18 T. Kim, R. S. Assary, H. Kim, C. L. Marshall, D. J. Gosztola, L. A. Curtiss and P. C. Stair, *Catal. Today*, 2013, **205**, 60–66.

19 G. M. González Maldonado, R. S. Assary, J. A. Dumesic and L. A. Curtiss, *Energy Environ. Sci.*, 2012, **5**, 8990–8997.

20 Z. Zhang, K. Dong and Z. Zhao, *ChemSusChem*, 2011, **4**, 112–118.

21 C. S. Uyguner and M. Bekbolet, *Catal. Today*, 2005, **101**, 267–274.

22 Z. Cheng, J. L. Everhart, G. Tsilomelekis, V. Nikolakis, B. Saha and D. G. Vlachos, *Green Chem.*, 2018, **20**, 997–1006.

23 Q. Chang, *Colloid and Interface Chemistry for Water Quality Control, Chapter 7 - Electrical Properties*, Academic Press, London, 2016, vol. 104.

24 N. Shi, Q. Liu, H. Cen, R. Ju, X. He and L. Ma, *Biomass Convers. Biorefinery*, 2020, **10**, 277–287.

25 H. Yokoyama, H. Kobayashi, J. Hasegawa and A. Fukuoka, *ACS Catal.*, 2017, **7**, 4828–4834.

26 A. Yamaguchi, N. Muramatsu, N. Mimura, M. Shirai and O. Sato, *Phys. Chem. Chem. Phys.*, 2017, **19**, 2714–2722.

27 M. Yabushita, H. Kobayashi, A. Shrotri, K. Hara, S. Ito and A. Fukuoka, *Bull. Chem. Soc. Jpn.*, 2015, **88**, 996–1002.

Chapter 3

Application of H_3PO_3 in the dehydration condensation of sorbitol

3.1 Introduction

Isosorbide has shown versatile applicability such as building block of engineering plastics.[1] Current synthesis of isosorbide uses concentrated H_2SO_4 as catalyst, which is not environmental-friendly due to the discharge of sulfuric acid pitch.[2] Many efforts has been paid to develop a new production method to apply a weak acid catalyst for isosorbide production.[3–6] However, application of weak acid needs harsh reaction condition such as microwave heating[4], high temperature,[5] or use of oxidizing acid,[7] which are not favorable for industrial application due to cost and corrosion issues. Previously, I found H_3PO_3 (pK_a = 1.3) showed characteristic activity for dehydration condensation of ADS to ADI.[8] Since sorbitol is an analog of ADS, I speculate H_3PO_3 may also be useful for the dehydration of sorbitol. In this chapter, I applied H_3PO_3 for the conversion of sorbitol to isosorbide.

3.2 Experimental

3.2.1 Reagents

The reagents used in this work are shown at the following table.

Table 3.1 Information about reagents.

Name	Supplier
D-Sorbitol ($C_6H_{14}O_6$)	Tokyo Chemical Industry
1,4-anhydro-glucitol ($C_6H_{12}O_5$;1,4-Sorbitan)	Santa Cruz Biotechnology
Isosorbide ($C_6H_{10}O_4$)	Tokyo Chemical Industry
Oxalic acid ($H_2C_2O_4$)	Fujifilm Wako Pure Chemical Industries
Phosphorous acid (H_3PO_3)	Sigma-Aldrich
2,4-Dinitrobenzonic acid ($C_7H_4N_2O_6$; DNBA)	Alfa Aesar

3.2.2 Dehydration of sorbitol by acid catalysts

First, a substrate mixture was prepared, in which sorbitol (182 mg, 1.0 mmol) and acid catalyst (at a determined ratio) were dissolved in H_2O (0.2 mL). Then, the product mixture was filled in a Schlenk tube (Kanto Chemical, 20 mL), which was depressurized (< 0.1 kPa) using a rotary pump via a liquid N_2 trap and kept overnight at room temperature. For performing reaction, the apparatus was heated using an oil bath for a certain time at 130 °C, under reduced pressure (< 0.1 kPa, Fig. 3.1).

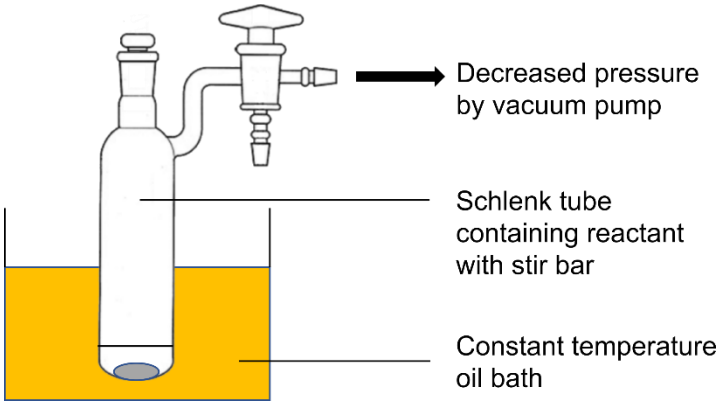

Figure 3.1 Experimental equipment of sorbitol dehydration.

3.2.3 Reflux experiment

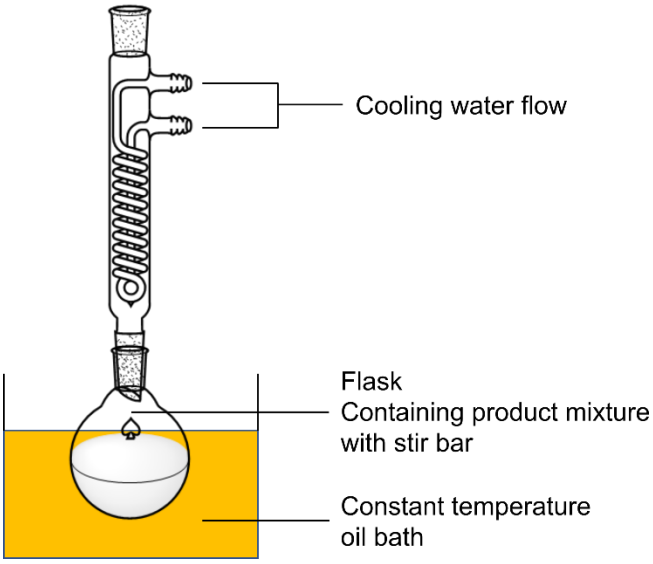

Figure 3.2 Experimental equipment used for reflux of product mixture.

Reflux of product mixture solution was conducted to hydrolyze phosphite esters. After the dehydration condensation of sorbitol, the product was dissolved using 20 mL water and moved to a 100 mL flask. A Dimroth-type condenser tube was inserted into flask and connected with a condenser pump for flowing cooling water at 5 °C (Fig. 3.2). The whole apparatus was immersed into an oil bath and kept at 90 °C for 3 h.

3.2.4 Liquid chromatography analysis

3.2.4.1 High pressure liquid chromatography (HPLC) analysis

After reaction, the product mixture was dissolved with 20 mL water, then analyzed by a HPLC (Shimadzu LC-20AD) equipped with a Rezex RPM-Monosacharide Pb++ column (Phenomenex, 300 × ø 7.8 mm, 70 °C) with a refractive index detector (RID). Water at a flow rate of 0.6 mL min^{-1} was used as the mobile phase.

The calculation of product yield uses the following formula:

$$\text{Yield}\ (\%) = \frac{f \times A \times V}{m/M} \times 100 \qquad (3.1)$$

where f is calibration factor (mol/L), A is area from HPLC chart, V is volume of water (L), m is the mass of sorbitol (g), M is the molecular weight (g/mol).

3.2.4.2 Liquid chromatography-mass spectroscopy (LC/MS) analysis

LC/MS analysis of soluble products were conducted, using a HPLC system (Shimadzu LC-20AR) equipped with an SH-1011 column (Shodex Sugar 300 mm × ø 8.0 mm) and a mass spectrometer (MS, LCMS-2020). The MS consists of an electrospray ionizer (ESI) and a quadrupole mass analyzer.

3.2.5 NMR analysis

Proton decoupled phosphorus nuclear magnetic resonance (NMR; ^{31}P 243 MHz) was recorded using a JEOL ECX-600 spectrometer. H_3PO_4 (85%) was used as an external standard.

3.3 Results and discussion

3.3.1 Typical reaction pathway of sorbitol dehydration

The conversion of sorbitol to isosorbide passes through a two-step dehydration reaction (Fig. 3.1).[9] The first-step dehydration converts ADS to 1,4-Sorbitan, 3,6-Sorbitan and 2,5-Mannitan. Among them, 1,4-Sorbitan and 3,6-Sorbitan produce isosorbide by the second dehydration, and 2,5-Mannitan is a dead-end product. Previous reports have shown that 3,6-Sorbitan is produced at a very slow rate and consumed at a quicker rate, thus it is hard to be detected in this reaction system.[10] 1,4-Sorbitan is the predominant intermediate to give isosorbide. The second-step dehydration is the rate-determining step of this reaction.

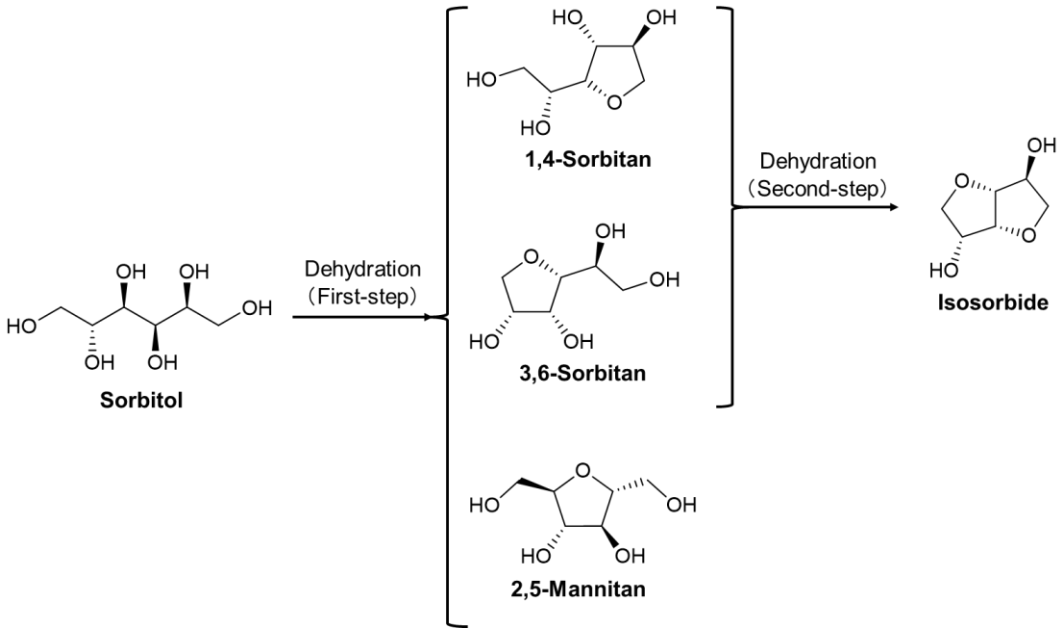

Scheme 3.1 Reaction pathway of sorbitol conversion to isosorbide.

3.3.2 Influence of acidity on isosorbide yield

In Chapter 3, I successfully converted ADS to ADI using H_3PO_3 at a reaction condition at S/C = 4.0, p < 0.1 kPa, 130 °C for 3 h.[8] For conversion of sorbitol to isosorbide, firstly I conducted the reaction using weak acids with different pKa values under a similar condition with a shorter reaction time (S/C = 4.0, p < 0.1 kPa, 130 °C, 1 h) to

observe the influence of acidity on isosorbide yield (Fig. 3.3). Among the weak acids tested, H_3PO_3 gave a high yield of isosorbide (46%), which is a similar phenomenon as the case of ADS dehydration;[8] on the other hand, $H_2C_2O_4$, DNBA and H_3PO_4 showed low activity (yield of isosorbide: 6.4%, 4.1%, 3.1%, respectively). Those reactions also gave 1,4-sorbitan to some extent (7.0–22%), but no trace of 3,6-Sorbitan was recorded. The characteristic activity of H_3PO_3 inspired me to conduct a further optimization of reaction condition to increase the yield of isosorbide using H_3PO_3.

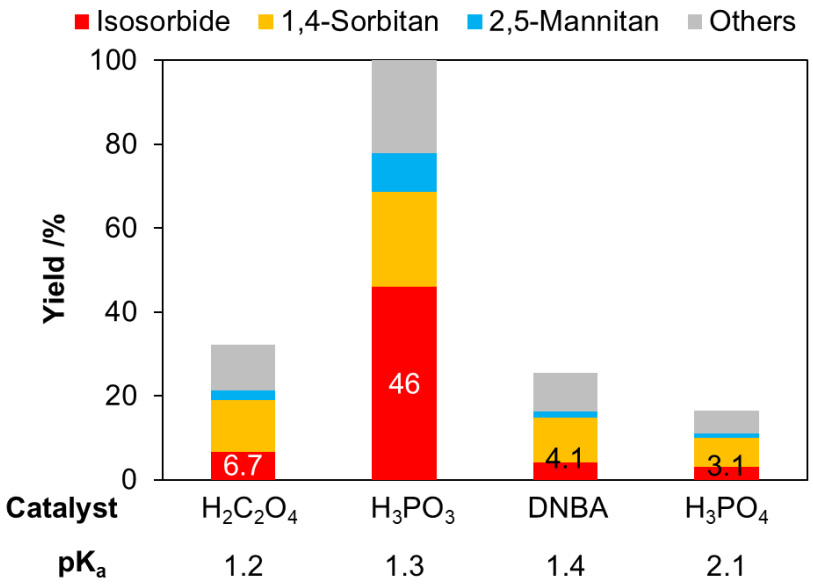

Figure 3.3 Dehydration of sorbitol by weak acid catalysts with different pKa values. Reaction condition: Sorbitol 1.0 mmol; S/C = 4.0; p < 0.1 kPa; 130 °C; 1 h.

3.3.3 Influences of S/C ratio on isosorbide yield

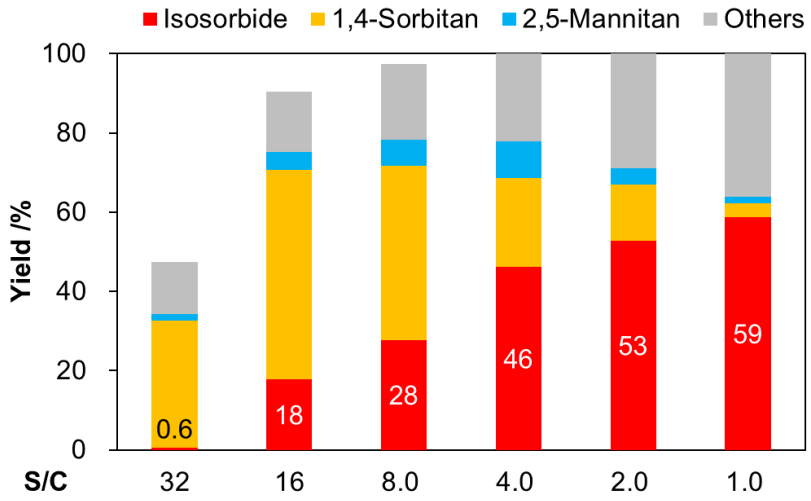

Figure 3.4 Dehydration of sorbitol by H_3PO_3 for 1 h. Reaction condition: Sorbitol 1.0 mmol; p < 0.1 kPa; 130 °C; 1 h.

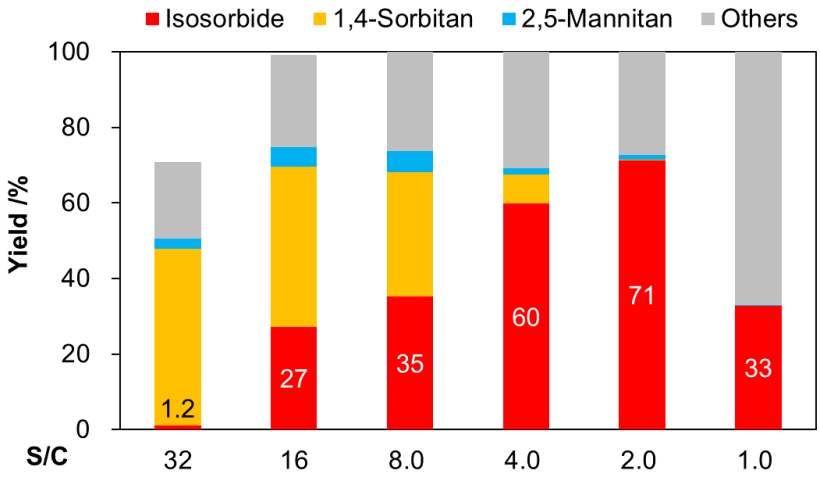

Figure 3.5 Dehydration of sorbitol by H_3PO_3 for 3 h. Reaction condition: Sorbitol 1.0 mmol; p < 0.1 kPa; 130 °C; 3 h.

In Chapter 3, H_3PO_3 at S/C = 4.0 gave ADI at 25% yield, and a large amount of humin was produced as by-products. Actually, humin can be readily produced from sugar at acidic environment.[11–15] Thus, I attempted to conduct a screening test of S/C ratio from 32 to 1.0 to find a suitable H_3PO_3 concentration to give high yield of isosorbide with less by-products (Fig. 3.4). At S/C = 32 (entry 5), only a small amount of isosorbide

was obtained (0.6%). This implies the activity of H_3PO_3 is very low when used at a low concentration. H_3PO_3 at a ratio of S/C = 16 (entry 6) successfully catalyzed the reaction and gave isosorbide at 18% yield. As the S/C ratio changed from 8.0 to 1.0 (entry 7, entry 2, and entries 8–9), the yield of isosorbide gradually increased (28%–59%), and the amount of 1,4-sorbitan declined, which indicates the activity of H_3PO_3 is enhanced as its concentration increases; on the other hand, side reactions were also promoted to give more by-products. Since 1,4-sorbitan is the intermediate of sorbitol conversion to isosorbide,[16] the remained 1,4-sorbitan possibly produce more isosorbide if reaction time is extended. Thus, I conducted those reactions at a longer time of 3 h (Fig. 3.5).

At S/C = 32, the yield of isosorbide hardly increased (entry 10, 1.2%) compared with the case of 1 h (entry 5, 0.6%). The extension of reaction time gave slight improvement of isosorbide yield for S/C = 16 (from 18% to 27%) and 8.0 (from 28% to 35%), with a large amount of 1,4-sorbitan remained. This phenomenon implies that the second-step dehydration condensation of sorbitol didn't proceed well when a lower concentration of H_3PO_3 (S/C $\geq$ 8) was used. At S/C = 4.0, the yield of isosorbide significantly improved to 60%. At S/C = 2.0, 71% yield of isosorbide was achieved, which was the highest among those entries. At S/C = 1.0, the reaction gave isosorbide at 33% yield and a large amount of by-product, which is possibly caused by the promotion of side-reactions such as humin production at a high acid concentration. I conclude that a higher concentration of H_3PO_3 (S/C = 4.0 and 2.0, specifically) is favorable for isosorbide production from sorbitol; the highest yield of isosorbide (71%) was obtained at S/C = 2.0. A time course analysis of products yield (Fig. 3.6) was performed at the optimized reaction condition (S/C = 2.0; 130 °C). From the start of the reaction, sorbitol continuously decreased and reached less than 2.0% at 30 min. As the dehydration product of sorbitol, 1,4-sorbitan initially increased and reached the highest at 15 min, then gradually decreased. As 1,4-sorbitan declines, yield of isosorbide continuously increases from the initial stage, and finally reached 71% at 3 h. Additionally, 2,5-Mannitan as a by-product was produced and kept at a minor amount during the reaction process.

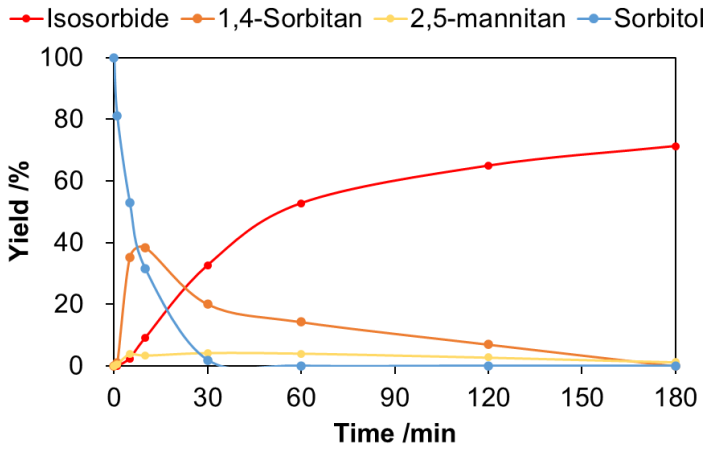

Figure 3.6 Product yield time course of sorbitol dehydration condensation. Reaction condition: Sorbitol 1.0 mmol; S/C ratio = 2.0; p < 0.1 kPa; 130 °C.

3.3.4 LC-MS analysis and ^{31}P-NMR analysis

In the last section, with the optimization of reaction condition, a high yield of isosorbide (71%) was achieved. However, the high activity of H_3PO_3 cannot be explained only by acid strength (H_3PO_3: pK_a = 1.3), because $H_2C_2O_4$ (pK_a = 1.2) and 2,4-DNBA (pK_a = 1.4) showed obviously low activity than H_3PO_3, even though they have similar acidity (Fig. 3.3). For clarification of the reaction mechanism, I conducted a LC/MS analysis of the production mixture given by H_3PO_3 to detect the fractions of reaction intermediates.

The product mixture of 10 min in the time course analysis was applied for LC-MS analysis. The MS chart showed large peaks at m/z = 227 and 245 at 10 min of retention time (Fig. 3.7B), which are ascribed to H_3PO_3 monoesters of 1,4-sorbitan ($[M-H]^-$, m/z = 227) and sorbitol ($[M-H]^-$, m/z = 245), respectively. This result suggests H_3PO_3 monoesters are proposed to exist in the reaction system. In Chapter 3, the dehydration condensation of ADS using H_3PO_3 was found to pass through a specific reaction mechanism via phosphite esters. Since sorbitol is an analog of ADS, I speculate the dehydration of sorbitol may pass through a similar phosphite mechanism (Scheme 3.2B). Initially, the esterification of sorbitol with H_3PO_3 produces sorbitol ester, then the ester captures a proton between P=O group of H_3PO_3 and C=O of acetamido group,

followed by an S_N2 reaction in which H_3PO_3 functions as leaving group to generate 1,4-sorbitan. The esterification and dehydration of 1,4-sorbitan mirrors that of sorbitol. First, 1,4-sorbitan produces 1,4-sorbitan ester, then it likely converts to isosorbide via an S_N2 reaction. In this reaction mechanism, H_3PO_3 functions in both protonation and esterification of each substrate and intermediate.

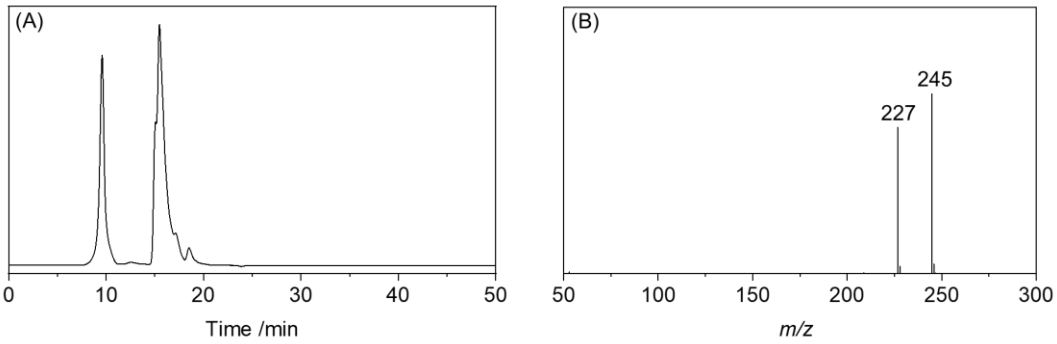

Figure 3.7 (A) LC chart of the product solution after the dehydration of sorbitol by H_3PO_3 (S/C = 2.0) at 130 °C under < 0.1 kPa of pressure for 10 min. The mass spectra were obtained using a negative ion mode at (B) 10 min.

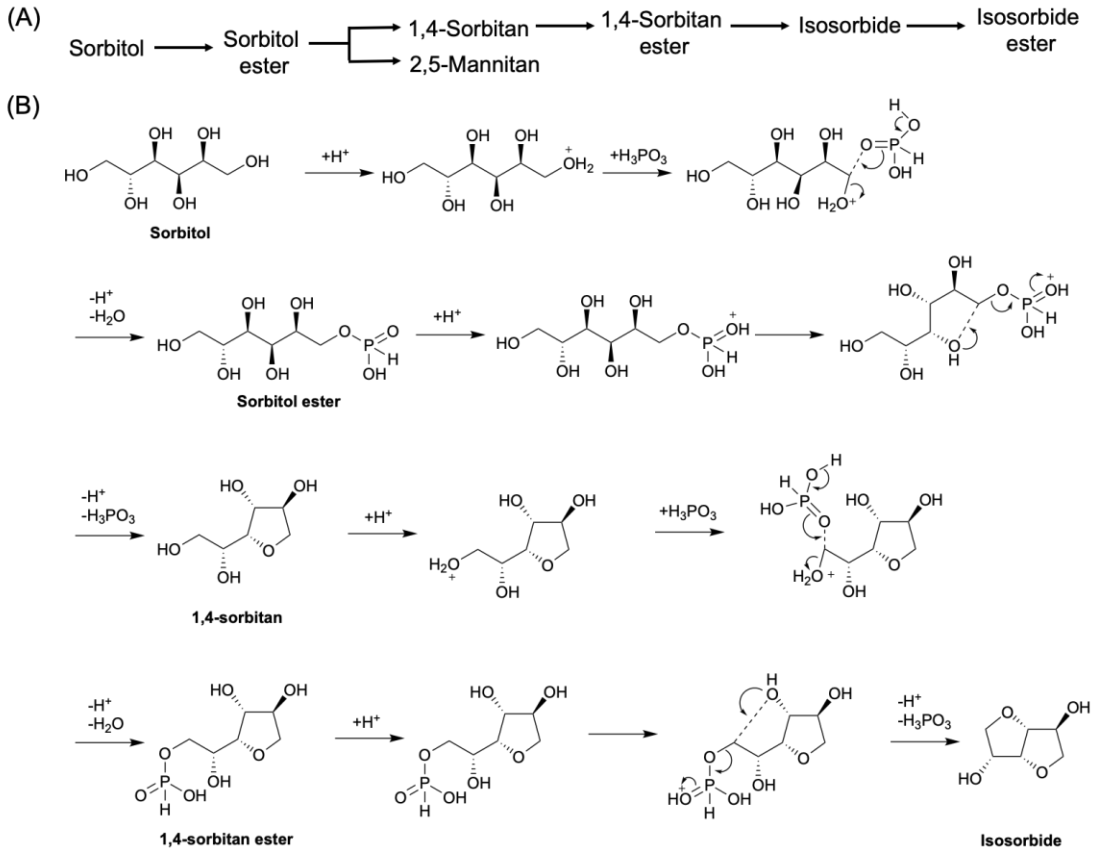

Scheme 3.2 (A) Product sequence of sorbitol dehydration using H_3PO_3; (B) A detailed reaction mechanisms for conversion of sorbitol to isosorbide using H_3PO_3.

The appearance of those phosphite esters motivated me to conduct a ^{31}P NMR time course analysis to track the phosphite ester fractions during the reaction process. The ^{31}P NMR spectrum from 0–3 h were shown in Fig. 3.8. Other than the peak of H_3PO_3 at 4.63 ppm, several peaks appeared in 5.0–8.4 ppm range. Those peaks were supposed to be monoesters derived from polyols (sorbitol, 1,4-sorbitan and isosorbide) in this reaction system. Since those compounds are commercially available, I used those reagents to conduct short-time reactions using H_3PO_3 at the same reaction condition for 1–10 min and analyzed the product mixtures by ^{31}P NMR. The peaks given by each spectrum were considered as the phosphite esters derived from each sugar alcohol respectively, and their chemical shift values were recorded (Table 3.2). Referring to those chemical shift values, the assigned peaks in the ^{31}P NMR time course analysis (Fig. 3.9) were categorized into three types: sorbitol ester, 1,4-sorbitan ester, and isosorbide ester. The normalized peak area of categorized esters derived from each

sugar alcohol were merged to reveal their change during the reaction process (Fig. 3.9). The other non-assigned peaks in the spectra were considered as esters derived from other by-products such as 2,5-mannitan.

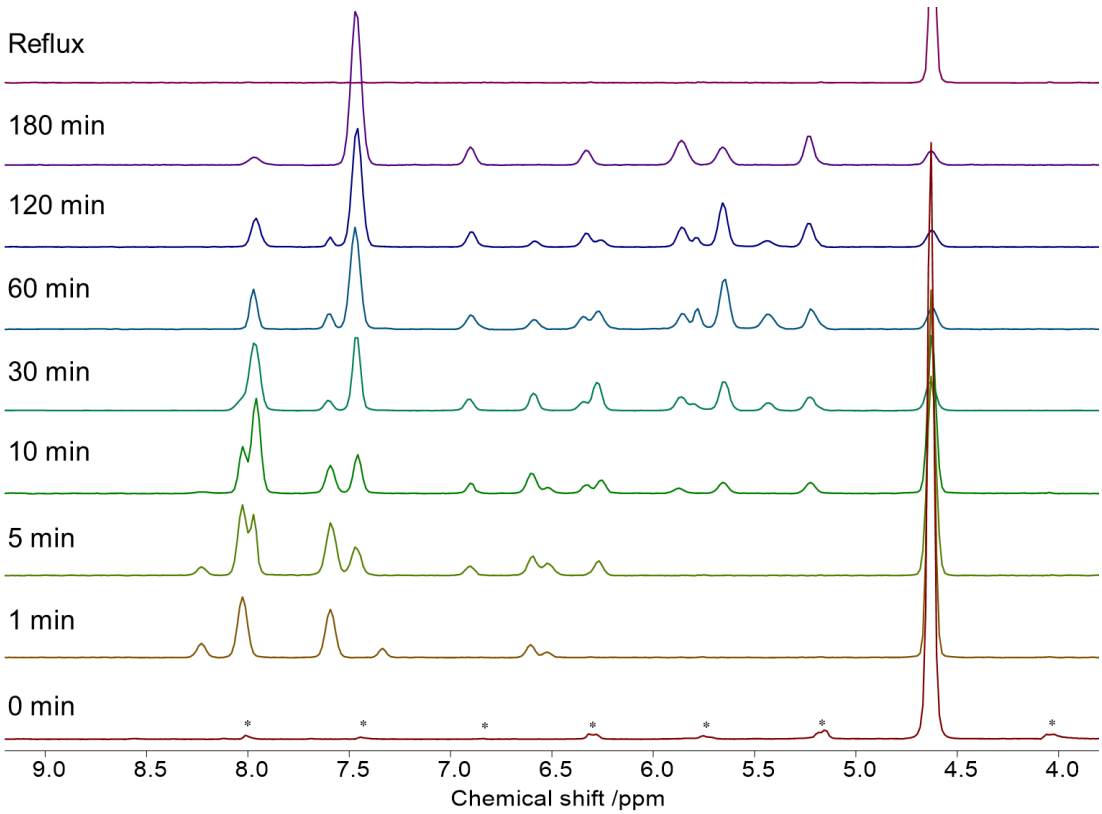

Figure 3.8 ^{31}P NMR time course of sorbitol dehydration condensation (*spinning side bands). Reaction condition: Sorbitol 1.0 mmol; S/C ratio = 2.0; p < 0.1 kPa; 130 °C.

Table 3.2 Assignment of peaks in ^{31}P NMR spectra

Corresponding compound	**Chemical shift /ppm**
Sorbitol	8.23, 8.03, 7.60, 7.34, 6.60, 6.51
1,4-Sorbitan	7.97, 7.47, 6.33, 5.66
Isosorbide	5.23
H_3PO_3	4.63

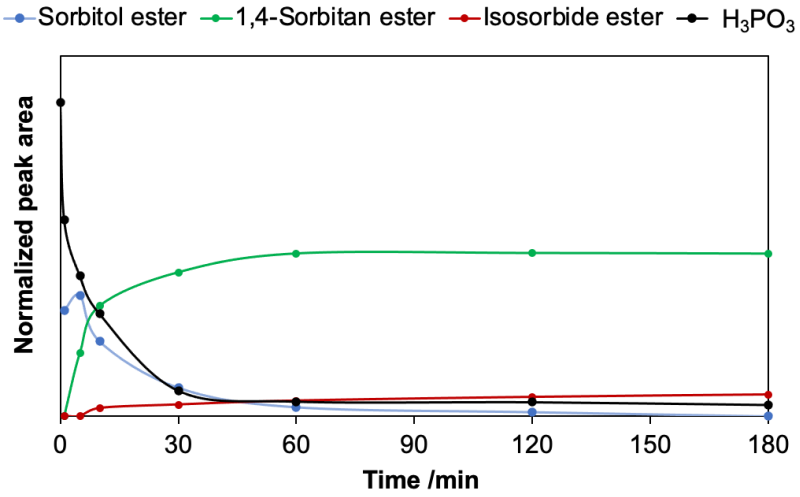

Figure 3.9 Normalized ^{31}P NMR peak area of phosphite esters during sorbitol dehydration. Reaction condition: Sorbitol 1.0 mmol; S/C ratio = 2.0; p < 0.1 kPa; 130 °C.

During the reaction process, H_3PO_3 decreased from the start and reached a low amount at 30 min. This trend is similar with that of sorbitol in product yield time course (Fig. 3.6), which implies that those two compounds react with each other at the initial stage, and possibly produce sorbitol esters. The amount of H_3PO_3 leveled off after 1 h, suggesting that the consumption and production rate of H_3PO_3 were similar. As a large fraction of H_3PO_3 converted to esters, the concentration of free H_3PO_3 became low after 1 h. However, the reaction continuously proceeded, possibly because some phosphite ester can function as acid catalyst to provide protons.[17] Sorbitol ester increases from the start, and reached the maximum at 10 min, then declines and leveled off at 60 min. Sorbitol ester can give 1,4-sorbitan via an S_N2 reaction. As 1,4-sorbitan increases from 0−15 min, 1,4-sorbitan ester showed a similar trend to increase during that period. Then, as 1,4-sorbitan declined from 15 min, 1,4-sorbitan ester continuously increased and leveled off at 30 min. A possible explanation for this phenomenon is the production and accumulation of unreactive phosphite esters of 1,4-sorbitan. To give isosorbide, a 1,4-sorbitan molecule needs a condensation occurs between C-3 and C-6, thus requires a phosphite monoester formed at one of those positions. The other esters formed with C-2 and C-5 are unreactive to give isosorbide thus regarded as dead-end products, which

accumulated during the reaction process and probably cause the leveling off. Additionally, isosorbide ester was also produced and kept at a minor amount. The sequence of products in the figure is consistent with that revealed by the time course. The product sequence revealed by product yield time course (Fig. 3.6) and ^{31}P NMR time course (Fig. 3.9) basically matches that at the proposed reaction pathway (Scheme 3.2A), which implies that the conversion of sorbitol to isosorbide by H_3PO_3 possibly passes through a similar ester mechanism as the case of ADS conversion to ADI.[8]

3.3.5 Reflux of product mixture

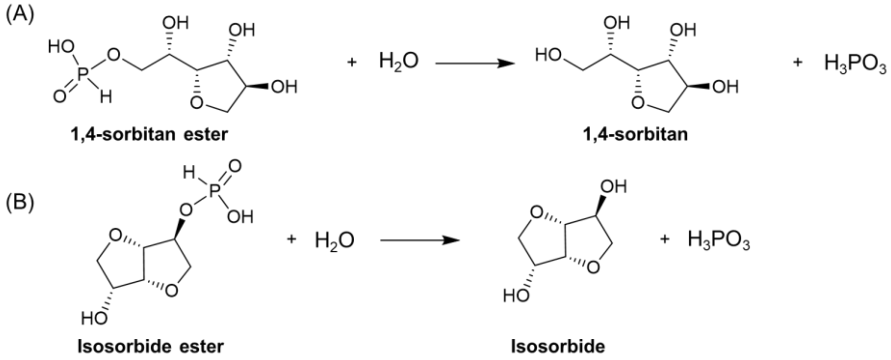

Figure 3.10 Proposed hydrolysis reaction pathway of (A) 1,4-sorbitan ester and (B) isosorbide ester.

From the time course of phosphite esters, I noticed that 1,4-sorbitan ester and isosorbide ester remained after a 3-hour reaction. Possibly, those esters can be hydrolyzed to give 1,4-sorbitan, isosorbide and H_3PO_3 (Fig. 3.10), which motivated me to conduct a hydrolysis experiment. A conventional method of converting a phosphite ester into the corresponding alcohol and H_3PO_3 uses refluxing in acid aqueous solution.[18,19] In my experiment, since H_3PO_3 was remained in the product mixture, I simply dissolved the product mixture of a 3-hour reaction by water and reflux. After the reflux, all the peaks assigned as phosphite esters disappeared in the ^{31}P NMR analysis, and H_3PO_3 increased. Meanwhile, the yield of isosorbide slightly increased from 71% to 74%, and 1,4-sorbitan was also recovered (Fig. 3.11). This implies that the esters of 1,4-sorbitan and isosorbide were hydrolyzed to give sugar alcohols and H_3PO_3 as expected. I conclude

that the phosphite esters formed in this reaction can be readily hydrolyzed under aqueous acidic environment.

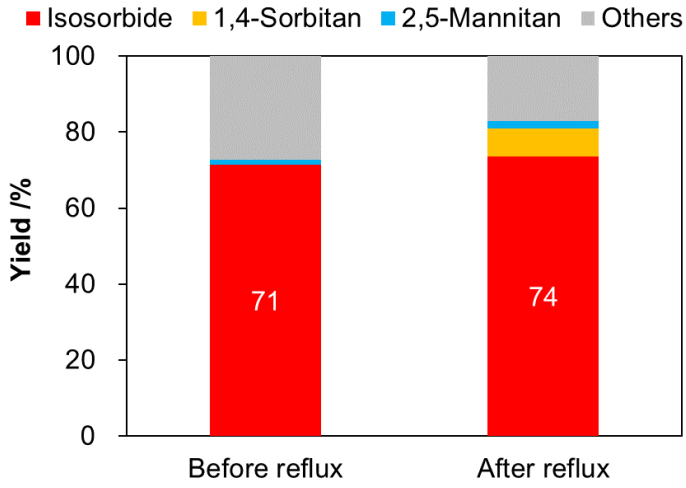

Figure 3.11 Comparison of product yield. The production mixture was obtained after a 3-hour reaction (Reaction condition: Sorbitol 1.0 mmol; S/C = 2.0; p < 0.1 kPa; 130 °C; 3 h).

3.4 Conclusion

I studied the conversion of sorbitol to isosorbide using weak acids. H_3PO_3 showed high activity among the weak acids tested. Similar to the case of ADS dehydration, the presence of phosphite ester is confirmed by LC-MS and ^{31}P NMR analysis, which implies the reaction may pass through a special reaction mechanism via phosphite esters, in which H_3PO_3 forms ester with substrate, then functions as leaving group to generate dehydration product by S_N2 reaction. The esterification also gives some unreactive phosphite esters of 1,4-sorbitan and isosorbide, which can be hydrolyzed by reflux to improve the product yield.

3.5 References

1 J. C. Goodwin, J. E. Hodge and D. Weisleder, *Carbohydr. Res.*, 1980, **79**, 133–141.

2 T. Bito, J. Hoshi, S. Amano, H. Kamataki, Y. Sasaki, T. Urabe, F. Sano and O.

Shouji, *Annu. Rep. Tokyo Metrop. Res. Inst. Environ. Prot.*, 2003, **2003**, 137–141.

3 K. Bock, C. Pedersen and H. Thøgersen, *Acta Chem. Scand.*, 1981, **35**, 441–449.

4 J. M. Robinson, A. M. Wadle, M. D. Reno, R. Kidd, S. R. Barrett Hinsz and J. Urquieta, *Energy and Fuels*, 2015, **29**, 6529–6535.

5 A. Yamaguchi, N. Hiyoshi, O. Sato and M. Shirai, *Green Chem.*, 2011, **13**, 873–881.

6 M. Yabushita, H. Kobayashi, A. Shrotri, K. Hara, S. Ito and A. Fukuoka, *Bull. Chem. Soc. Jpn.*, 2015, **88**, 996–1002.

7 J. Defaye, A. Gadelle and C. Pedersen, *Carbohydr. Res.*, 1990, **205**, 191–202.

8 C. Yang, T. Sagawa, A. Fukuoka and H. Kobayashi, *Green Chem.*, 2021, **23**, 7228–7234.

9 T. Sagawa, H. Kobayashi, C. Murata, Y. Shichibu, K. Konishi and A. Fukuoka, *ACS Sustain. Chem. Eng.*, 2019, **7**, 14883–14888.

10 F. Delbecq, M. R. Khodadadi, D. Rodriguez Padron, R. Varma and C. Len, *Isosorbide: Recent advances in catalytic production*, 2020, vol. 482.

11 S. Bertarione, F. Bonino, F. Cesano, S. Jain, M. Zanetti, D. Scarano and A. Zecchina, *J. Phys. Chem. B*, 2009, **113**, 10571–10574.

12 X. Gao, L. Peng, H. Li and K. Chen, *BioResources*, 2015, **10**, 6548–6564.

13 T. Kim, R. S. Assary, H. Kim, C. L. Marshall, D. J. Gosztola, L. A. Curtiss and P. C. Stair, *Catal. Today*, 2013, **205**, 60–66.

14 G. M. González Maldonado, R. S. Assary, J. A. Dumesic and L. A. Curtiss, *Energy Environ. Sci.*, 2012, **5**, 8990–8997.

15 Z. Zhang, K. Dong and Z. Zhao, *ChemSusChem*, 2011, **4**, 112–118.

16 P. Che, F. Lu, X. Si, H. Ma, X. Nie and J. Xu, *Green Chem.*, 2018, **20**, 634–640.

17 W. D. Kumler and J. J. Eiler, *J. Am. Chem. Soc.*, 1943, **65**, 2355–2361.

18 R. Rabinowitz, *J. Org. Chem.*, 1963, **28**, 2975–2978.

19 W. Mabey and T. Mill, *J. Phys. Ref. Data*, 1978, **7**, 383–415.

Chapter 4

Hydrolytic hydrogenation of molasses to sugar alcohols

4.1 Introduction

Molasses is a waste generated in the production of sucrose from crops such as sugarcane. It is a dark brown viscous liquid that contains 40–50 wt% of sugars, specifically sucrose, glucose, and fructose.[1] In Japan, Okinawa Prefecture produced 28,252 tons of molasses in 2016.[2] Worldwide, the amount reaches 50 million tons annually.[1] Although molasses contains a large amount of sugars, it is not very suitable as food due to significant amounts of impurities. Therefore, molasses has been applied as livestock feed, food additive, and feedstock for ethanol fermentation.

Herein, the author proposes using molasses as the feedstock for conversion to sorbitol and mannitol (Scheme 4.1). The sugar alcohols are versatile platform chemicals for producing various functional chemicals.[3-4] Currently, sorbitol is mainly produced from starch, and mannitol is co-produced with sorbitol by the hydrogenation of fructose. The two feedstocks compete with food supply, which is not favorable from the perspective of food security. Hence, molasses is advantageous over the current raw materials in this sense. However, the catalytic conversion of molasses to sugar alcohols has not been studied so far. Molasses contains various impurities such as organosulfur compounds. They may strongly affect the catalytic process of converting sugars in molasses into sugar alcohols. Hydrogenation catalysts are commonly sensitive to impurities.[5] Therefore, in this chapter, I aimed for developing a pretreatment method and clarifying decisive factors to achieve selective production of sugar alcohols from molasses.[6]

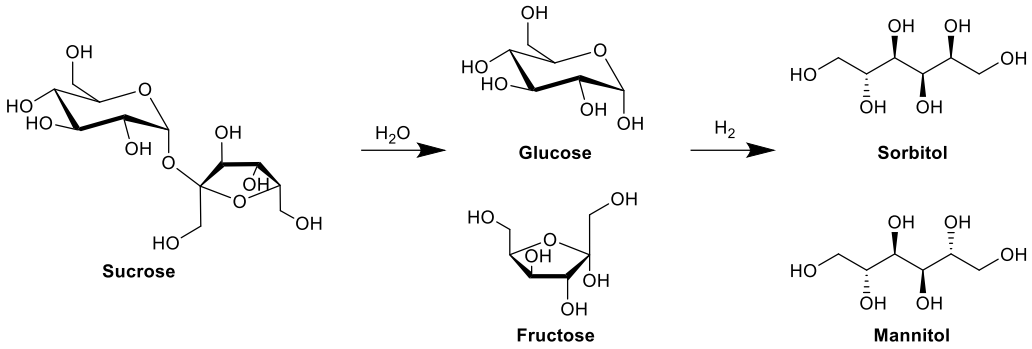

Scheme 4.1 Conversion of sugars in molasses to sugar alcohols.

4.2 Experimental section

4.2.1 Reagents

The reagents used in this work are shown at the following table.

Table 4.1 Information about reagents.

Name	Supplier
Molasses	Mitsubishi Gas Chemical Company
D-Glucose ($C_6H_{12}O_6$)	Kanto Chemical
D-Fructose ($C_6H_{12}O_6$)	Fujifilm Wako Pure Chemical Industries
Sucrose ($C_{12}H_{22}O_{11}$)	Fujifilm Wako Pure Chemical Industries
L-Cysteine ($C_3H_7NO_2S$)	Fujifilm Wako Pure Chemical Industries
L-Aspartic acid ($C_4H_7NO_4$)	Fujifilm Wako Pure Chemical Industries
Sulfuric acid (H_2SO_4)	Fujifilm Wako Pure Chemical Industries
Hydrochloric acid (HCl)	Fujifilm Wako Pure Chemical Industries
Formic acid (HCOOH)	Fujifilm Wako Pure Chemical Industries
Hydrogen peroxide (H_2O_2)	Kanto Chemical
Montmorillonite K 10	Sigma-Aldrich
Activated carbon Norit SX Ultra	Sigma-Aldrich
Raney Ni	Sigma-Aldrich
Ru powder	Sigma-Aldrich
Pt black	Sigma-Aldrich

H_2	Air Liquide Kogyo Gas
N_2	Air Liquide Kogyo Gas

4.2.2 Pretreatment of molasses samples

Molasses was pretreated by filtration and adsorption to remove catalyst poisons as shown in Scheme 4.2. The pristine molasses (4.2 g) was diluted with 35.8 g of water, followed by centrifugation at 10,000 rpm for 5 min and decantation to remove solid precipitates. The product is denoted M-Centrifuged. M-Centrifuged was filtrated with a polyether sulfone membrane with 0.45 μm pores (ADVANTEC 25AS045AN) because the liquid part of molasses smoothly passed through this filter, and the product was named M-Filtrated. Besides, M-Centrifuged was stirred with 2.1 g of an adsorbent, montmorillonite K10 (denoted MK10) or activated carbon Norit SX Ultra (denoted AC), at 298 K for 1 h. Subsequently, the solid part was removed by centrifugation and decantation. MK10 and AC are often used for the adsorption of proteins in food industries.[7] This adsorption treatment was repeated once more. Finally, the obtained liquid was filtrated with the polyether sulfone membrane filter. The sample was named based on the adsorbent used, M-MK10 and M-AC.

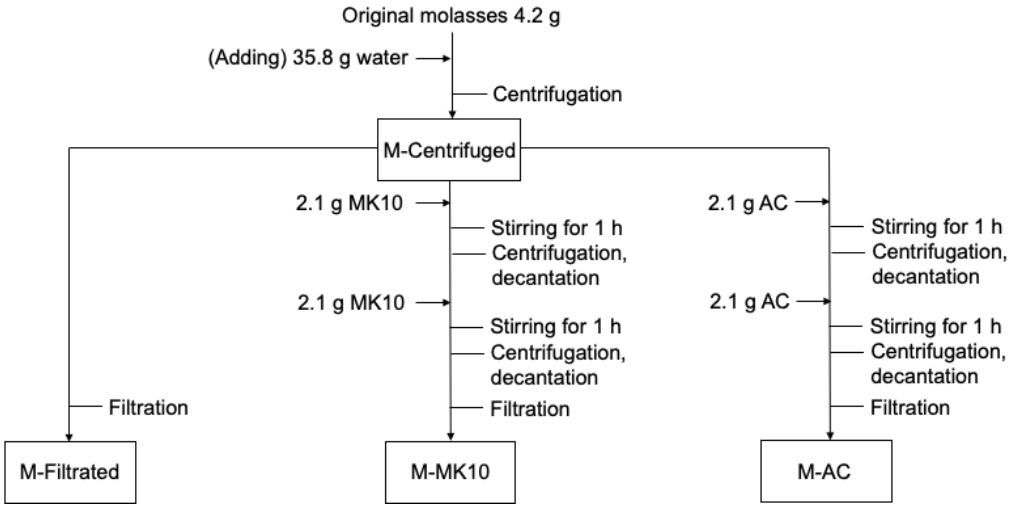

Scheme 4.2 Pretreatment of molasses samples.

4.2.3 Composition analysis of molasses

4.2.3.1 Sugar composition

For the analysis of sugar composition, the pretreated molasses solutions (M-Centrifuged, M-Filtrated, M-MK10, and M-AC) after the dilution by five times were put into a Mini-UniPrep (PVDF, 0.2 μm) for the analysis with an high performance liquid chromatograph (HPLC; LC-10ATVP, Shimadzu; detector: refractive index detector and UV detector) equipped with a Rezex RPM-Monosaccharide Pb++ column (ø 7.8 × 300 mm, Phenomenex; 70 °C; mobile phase: water 0.6 mL min^{-1}). Typical HPLC analysis data are shown in Table 4.1 and Fig. 4.1. Total content of sugars in the solution was calculated using eq. 4.1. The quantity in the pristine molasses was calculated by eq. 4.2 based on the analysis data of M-Centrifuged sample.

$$W_s\ (\text{wt\%}) = \frac{\sum(M_x \times A_x \times f_x \times V)}{M_s} \times 100 \quad (4.1)$$

where W_s is the total content of sugars in the sample, M_x is the molecular weight of sugar (sucrose, glucose and fructose) (g/mol), A_x is peak area of the sugar, f_x is a calibration factor for the sugar (mol/L), V is the volume of the sample (L), M_s is mass of the sample (g).

$$W\ (\text{wt\%}) = W_{s-\text{Centrifuged}} \times \frac{40}{4.2} \times 100 \quad (4.2)$$

where W is the total content of sugars in pristine molasses, $W_{s-\text{Centrifuged}}$ is the total content of sugars in M-Centrifuged calculated in eq. 4.1.

Table 4.2 Retention time of sugar components (RPM Monosaccharide Pb++).

Sugar	Retention time /min
Sucrose	11.7
Glucose	13.9
Fructose	18.8

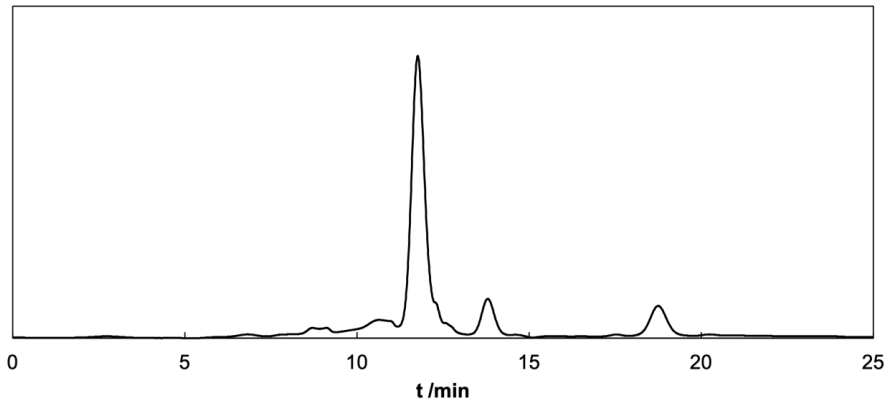

Figure 4.1 HPLC chromatogram of M-Centrifuged.

4.2.3.2 Elemental analysis

A molasses sample of 10 g was dried in an egg-plant flask at 40 °C using a rotary evaporator under vacuum. The N content in the dried sample was analyzed by a CE-440 elemental analyzer. The analysis of S content used the oxygen flask combustion method. The dried sample (2 mg) was wrapped in a piece of filter-paper and inserted into a platinum gauze. The wrapped sample was combusted in an oxygen-filled flask containing water for absorbing sulfur compounds. After cooling down, the liquid was analyzed by ICS-1600 ion chromatography. The conditions for the N and S analyses are shown below. The atomic composition of samples was calculated using eq. 4.3.

N analysis

Equipment: CE-440 elemental analyzer

Atmosphere: oxygen

Temperature of combustion chamber: 980 °C

Temperature of reduction furnace: 620 °C

Detector: differential thermal conductivity detector

S analysis

Equipment: Dionex ICS-1600 ion chromatography

Column: IonPac AS-12A

Eluent: 2.8 mM Na_2CO_3 with 0.3 mM $NaHCO_3$, 1.5 mL/min

Column temperature: 30 °C

Detector: electrical conduct

$$E\ (\text{wt}\%) = \frac{M_d}{M \times w} \times 100\% \quad (4.3)$$

where E is the content of each element in the molasses sample (wt%), w is the content of element in the dried sample (g), M_d is the mass of dried sample (g), M is the mass of molasses sample before drying (g).

4.2.3.3 Ion chromatography analysis

Inorganic anions in molasses samples were analyzed by ion chromatography (IC). A 0.5 g of molasses sample was diluted to 100 g with water, which was analyzed by a Shimadzu ICS-3000 system. The IC conditions are shown below. The content of element in each sample was calculated by eq. 4.4.

Column: IonPac AS-12A

Moving phase: 2.8 mM Na_2CO_3 with 0.3 mM $NaHCO_3$, 1.5 mL/min

Column temperature: 30 °C

Detector: electrical conductivity detector (ELCD)

$$E_i\ (\text{wt}\%) = \frac{A \times f \times V \times M_e}{M} \quad (4.4)$$

where E_i is the concentration of the element in inorganic ion form in the molasses sample; A is area count of the ion in IC analysis; f is the calibration factor of the ion (mol/L); V is the volume of the molasses sample (L); M is the mass of molasses sample (g); M_e is the atomic weight of the element (g/mol).

To know the organic S and N content, ion chromatography analysis and elemental analysis were combined by eq. 4.5.

$$E_o = E - E_i \quad (4.5)$$

where E_o is the content of element in an organic form in the samples, E is the total element content provided by eq. 4.3, E_i is the inorganic element content given by eq. 4.4.

4.2.3.4 Amino acid analysis

Amino acids in molasses samples were analyzed by the following method. For the analysis of all kinds of amino acids (denoted as total AA), the analysis sample was prepared by the method shown in section 2.2.2. The sample of 10 g was subsequently dried by rotary evaporator at 40 °C. The dried sample was hydrolyzed by 50 mL of 6 M HCl at 110 °C for 24 h. After removing HCl, the solution was diluted and analyzed by L-8900 amino acid analyzer using the ninhydrin reaction. [8] S-containing amino acids (denoted as S-AA, containing cysteine, cystine and methionine) were analyzed by a different method. The dried molasses sample described above (0.5 g) was treated with 25 mL performic acid, which is a mixture of formic acid and hydrogen peroxide aq. (30-35%) in a ratio of 9:1 (v/v), to oxidize the sulfur-containing functional groups to detectable groups before the hydrolysis.[9] The content of amino acids was calculated by eq. 4.6.

$$C_{AA}\ (\text{wt}\%) = \frac{M \times A \times f \times V}{M_s} \times 100 \quad (4.6)$$

where C_{AA} is the content of amino acids, M is the molecular weight of amino acid (g/mol), A is the peak area of amino acid, f is the calibration factor of amino acid (mol/L), V is the volume of the molasses sample (L), M_s is the mass of molasses sample (g).

4.2.4 DFT calculations

DFT calculations were performed to elucidate the interaction between organosulfur

compounds and Ni metal. Seven Ni atoms were located at the same positions as Ni(111) surface, and they were fixed except for the center one. The chemical structure was optimized after putting an adsorbate on the top of central Ni atom at the unrestricted B3LYP/LanL2DZ (Ni)/aug-cc-pVDZ (S)/cc-pVDZ (C, H) level of theory with spherical harmonics and an ultrafine grid using the Gaussian 16 software.[10–13] Septet was chosen for the spin state because of the low energy and low spin contamination.

4.2.5 Hydrolytic hydrogenation of molasses

As the concentration of sugar varied from 2.9 to 4.5 wt% in the samples prepared in section 2.2.2, I diluted the samples with water to make the sugar concentration 1 wt%. The diluted solution of 40 g was made, and the pH was adjusted to 3 using H_2SO_4. The solution and Raney Ni (280 mg) were charged into a Teflon-lined high-pressure reactor (MMJ-100; OM Lab-Tech) with H_2 (5 MPa). Raney Ni is a practical catalyst for the hydrogenation of sugars.[14] The reactor was heated to 140 ℃ in 6 min and kept for determined time for the reaction. Afterward, the reactor was cooled down to ambient temperature by immersing the reactor in water. The reaction mixture was separated by centrifugation and decantation. The products in the aqueous phase were analyzed by HPLC. The used Raney Ni was moved to a bottle filled with water to prevent it from drying. The retention time of each product is shown in Table 4.3 and the typical HPLC chart is shown in Fig. 4.2. For calculation of product yields, an absolute calibration method was used (eq. 4.7).

Table 4.3 Retention time of products

Component	Retention time /min
Sucrose	11.7
Glucose	13.9
Fructose	18.8
Sorbitol	39.8
Mannitol	27.5

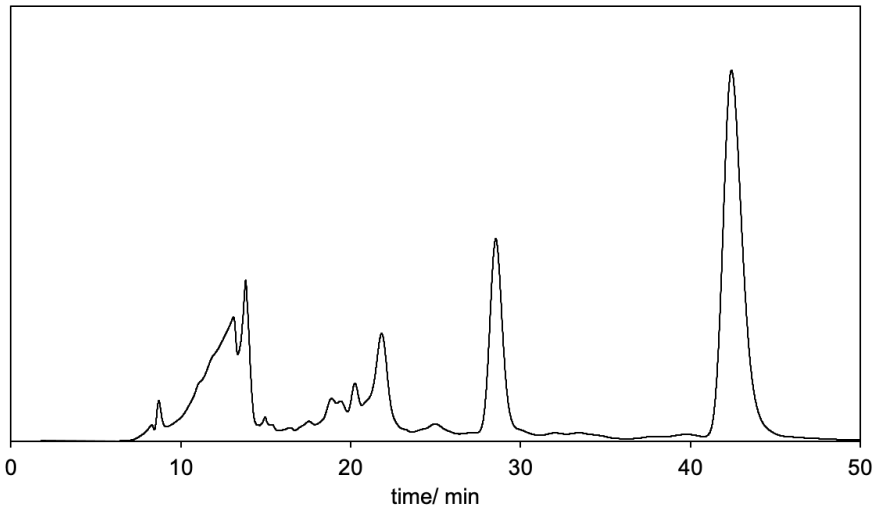

Figure 4.2 Typical HPLC chromatogram of the product solution of molasses hydrolytic hydrogenation.

$$\text{Yield (\%C)} = \frac{A \times f \times V}{2n_{Suc} + n_{Glu} + n_{Fru}} \times 100 \quad (4.7)$$

where A is the area of each compound in the HPLC analysis; f is a calibration factor of the compound (mol/L); V is volume of the reaction solution (L); n_{Suc} , n_{Glu}, and n_{Fru} are the amount of sucrose, glucose, and fructose in the substrate (mol), respectively.

4.3 Results and discussion

4.3.1 Influence of molasses pretreatments on product yield

The pretreatment of molasses was performed to remove potential catalyst poisons such as proteins and complicated organic S and organic N compounds which are similar to humins.[15] Three kinds of pretreatments were conducted for the molasses after the dilution and centrifugation treatments (M-Centrifuged): filtration only (M-Filtrated) and the adsorption treatment with MK10 or AC followed by filtration (M-MK10 and M-AC).

I determined the sugar content in the molasses samples to clarify whether sugars were lost by the pretreatments (Table 4.4). Filtration and adsorption using MK10 barely changed the sugar content compared with M-Centrifuged. On the contrary, AC

significantly decreased the sugar amount from 4.4% to 2.8% (2.0 wt% sucrose, 0.38 wt% glucose, and 0.42 wt% fructose). In addition, due to the adsorption of liquid into the powder adsorbents, the pretreatments with MK10 and AC decreased the amount of solution from 40 mL to 32–25 mL.

Table 4.4 Composition of molasses samples.

Sample	Recovered solution mass[a] /g	Sugars /wt%				Organic S /wt%	Inorganic S /wt%	Organic N /wt%	Inorganic N /wt%
		Total	Sucrose	Glucose	Fructose				
M-Centrifuged	40	4.4	3.3	0.44	0.69	0.041	0.048	0.049	<0.001
M-Filtrated	38	4.4	3.3	0.44	0.69	0.036	0.055	0.045	<0.001
M-MK10	32	4.4	3.3	0.44	0.69	0.031	0.077	0.037	<0.001
M-AC	25	2.8	2.0	0.38	0.42	0.009	0.083	0.021	<0.001

[a]Starting from 40 g.

The amounts of organic S and N in samples were determined by subtracting inorganic forms of S and N (SO_4^{2-}, NO_2^-, NO_3^-, NH_4^+) from the total amount (see section 2.2.3.3). M-Centrifuged contained 0.041 wt% organic S and 0.049 wt% organic N. After the filtration pretreatment (M-Filtration), the amounts decreased marginally (S 0.036 wt%, N 0.045 wt%). I speculate that the cellulosic membrane filter (0.45 μm pores) removed fine particles including a part of humins containing S and N.[16]

Compared to the simple filtration, the pretreatment using MK10 removed more organic S (0.031 wt%) and N (0.037 wt%). This is due to the cation exchange property of MK10.[17-18] A typical structure of a montmorillonite crystal includes an AlO_6 octahedral sheet sandwiched by two SiO_4 tetrahedral sheets (Fig. 4.3). Al^{3+} ions in the octahedral sheet are partly substituted by other low-valent metal cations such as Mg^{2+}; the difference of electric charge (−1) between Mg^{2+} and Al^{3+} makes the three-layer unit charged negatively. In molasses (pH 5–6), nitrogen-containing organic molecules such as proteins are positively charged, because amino groups are protonated.[19] Those charged protein molecules can be adsorbed by MK10 via electrostatic interactions.[20,21]

Besides, small protein molecules with positive charge can be intercalated into the interlayer of MK10 through cation exchange.[18] In addition to electrostatic forces, the hydrophilicity/hydrophobicity interactions are also responsible for adsorption of protein molecules by clay minerals.[22,23] AlO_6 and SiO_4 sheets are basically hydrophobic, however, the negative charge induced by the ion substitution can attract of metal cations (such as Na^+, Ca^{2+}) into the interlayer spacing, thus leading to a partial hydrophilic character of MK10.[24,25] The hydrophilic/hydrophobic portion of montmorillonite interact with the hydrophilic/hydrophobic surface of protein formed by polar/non-polar amino acids.[26,27] For summary, montmorillonite can absorb proteins by electrostatic forces, and hydrophilicity/hydrophobicity interactions.

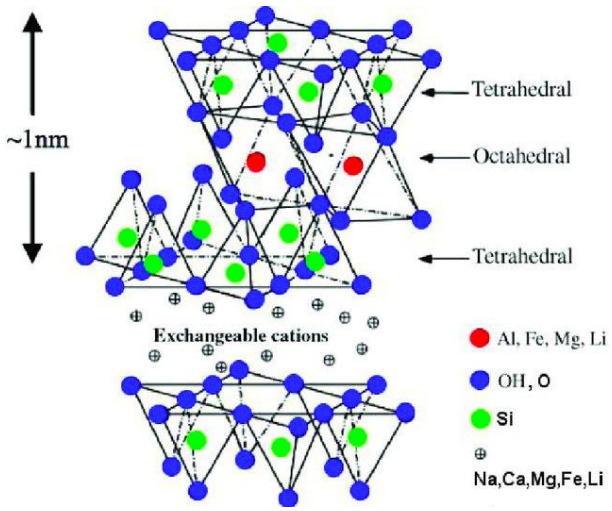

Figure 4.3 Crystal structure of montmorillonite (common structural formula: $Na_x(Al_{2-x}Mg_x)Si_4O_{10}(OH)_2 \cdot nH_2O$). Adapted from the reference.[28]

AC showed the highest performance for the adsorptive removal of organic S (0.009 wt%) and N (0.021 wt%). This is supposed to be driven by the CH-π interactions between CH groups of proteins and π conjugation systems of the polycyclic aromatic structures of the carbon, or electrostatic interactions with oxygenated functional groups on the surface of AC (Fig. 4.4).[29,30] Since AC has only a small amount of weak acid sites (carboxylic groups 0.08 mmol g^{-1}), the polycyclic aromatics may predominantly drive the adsorption by CH-π dispersion interactions.[31–33] I conclude that MK10 and

AC can partly remove S and N compounds in molasses.

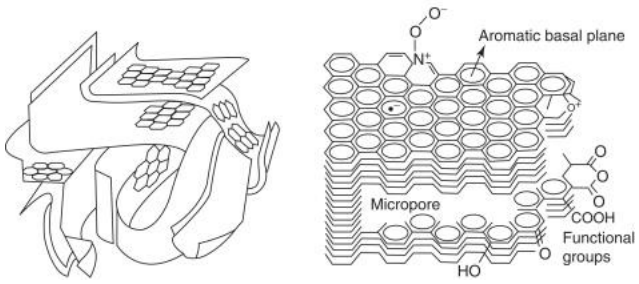

Figure 4.4 A typical structure of activated carbon. Adapted from the reference.[34]

Proteins contained in the molasses samples were analyzed after hydrolyzing them into amino acids. M-Centrifuged contained 0.13 wt% of amino acids in total, in which aspartic acid was the major constituent (0.064 wt%). The concentration of aspartic acid corresponds to the organic N content of 0.021 wt%, which accounts for 43% of the total organic N in the sample (0.049 wt%). After pretreatment using absorbents, the total amount of amino acids was decreased to 0.11 wt% by MK10 and to 0.069 wt% by AC. Focusing on sulfur-containing amino acids, the total content of cysteine (including cystine) and methionine decreased from 0.0026 wt% to 0.0023 wt% for M-Filtrated, 0.0016 wt% for M-MK10, and 0.0003 wt% for M-AC. These amounts correspond to organic S contents of 0.0007–0.00008 wt%, which was much lower than the total organic S content of the samples (0.041–0.009 wt%). I conclude that the amino acids are the major source of organic N compounds, and these compounds can be partly removed by pretreatment with AC and MK10. However, we should remind that different types of pretreatments resulted in different sugar concentration. To normalize the contents of organic S and N at the same sugar concentration, Table 4.5 shows the composition at a total sugar concentration of 1 wt%.

Table 4.5 Composition of diluted molasses samples at a total sugar concentration of 1 wt%.

Sample	Concentration /wt%							
	Sugar in total	Sucrose	Glucose	Fructose	Organic S	Organic N	Amino acids in total	S-containing amino acids
M-Centrifuged	1	0.75	0.1	0.16	0.0093	0.0111	0.13	0.0026
M-Filtrated	1	0.75	0.1	0.16	0.0082	0.0102	0.13	0.0023
M-MK10	1	0.75	0.1	0.16	0.0070	0.0084	0.11	0.0016
M-AC	1	0.71	0.14	0.15	0.0032	0.0075	0.07	0.0003

4.3.2 Hydrolytic hydrogenation of real molasses

I studied the hydrolytic hydrogenation reaction of molasses samples at a total sugar concentration of 1 wt% at 140 °C for 4 h. Accordingly, the composition is the same as that shown in Table 4.6. The reaction contains the hydrolysis of sucrose and the hydrogenation of glucose and fructose (Scheme 4.1). To accelerate hydrolysis, I decreased pH of the solution to 3.0. The lower pH is, the faster the reaction rate is. However, a low pH may also accelerate side-reactions. Therefore, the mild acidic condition was chosen. To facilitate hydrogenation, Raney Ni was selected because it is a practical commercial catalyst used for the hydrogenation of glucose.[35]

As discussed above, molasses contains many impurities which may affect the reaction. Therefore, first, I used a mixture of pure sugars with the same sugar ratio as M-Centrifuged (total 1 wt%; sucrose 0.75 wt%, glucose 0.10 wt%, fructose 0.16 wt%) to evaluate the original catalytic performance. This reaction produced sugar alcohols in 95%C yield (sorbitol 71%C, mannitol 25%C) (Fig. 4.5). Accordingly, the activity of Raney Ni and 1 mM H_3O^+ is sufficient for the conversion of sugars to sugar alcohols. Then, M-Centrifuged, a real molasses sample, was used for reaction, but the yield of sugar alcohols was only 33%C in total (sorbitol 24%C, mannitol 8.7%C). Sucrose was mostly consumed, but large amounts of glucose (21%C) and fructose (19%C) remained after the reaction. In addition, a significant amount of sugars was converted to unidentified compounds (21%C). This result indicates that Raney Ni is deactivated by the impurities in molasses.

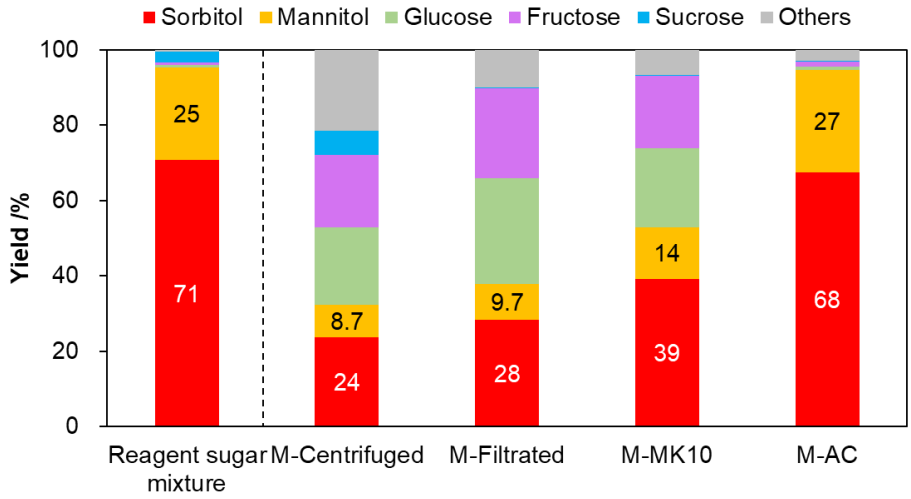

Figure 4.5 Product analysis of the hydrolytic hydrogenation using M-Centrifuged sample and reagent sugar mixture (Reaction condition: reagent sugar solution 40 g (sugar 1 wt%); Raney Ni 280 mg; $p(H_2)$ 5 MPa; 4 h; pH 3; 140 °C).

Therefore, pretreated molasses samples were used for the hydrolytic hydrogenation under the same reaction condition (Fig. 4.5). Compared to M-Centrifuged (33%C), M-Filtrated only slightly improved the yield of sugar alcohols (total 38 %C; sorbitol 28%C, mannitol 10%C). In contrast, the pretreatment using absorbents effectively increased product yield. M-MK10 increased the yield of sugar alcohols to 53%C (sorbitol 39%C, mannitol 14%C), and AC elevated the yield to 95%C (sorbitol 68%C, mannitol 27%C). The result for M-AC is similar to that with reagent sugar mixture (95%C).

To study the relationship between the content of impurities in molasses with the product yield, correlation plots of yield of sugar alcohols in the catalytic reactions against the concentration of organic N (Fig. 4.6a), organic S (Fig. 4.6b), sulfur-containing amino acids (Fig. 4.6c), and total amino acids (Fig. 4.6d) were made. The concentration of organic N and organic S in these figures are that of the diluted samples used for the reaction (Table 4.5). All the plots show inverse correlations with the concentration of the impurities. This result suggests that they are poisons for Raney Ni catalyst, but is it unclear which is the predominant factor.

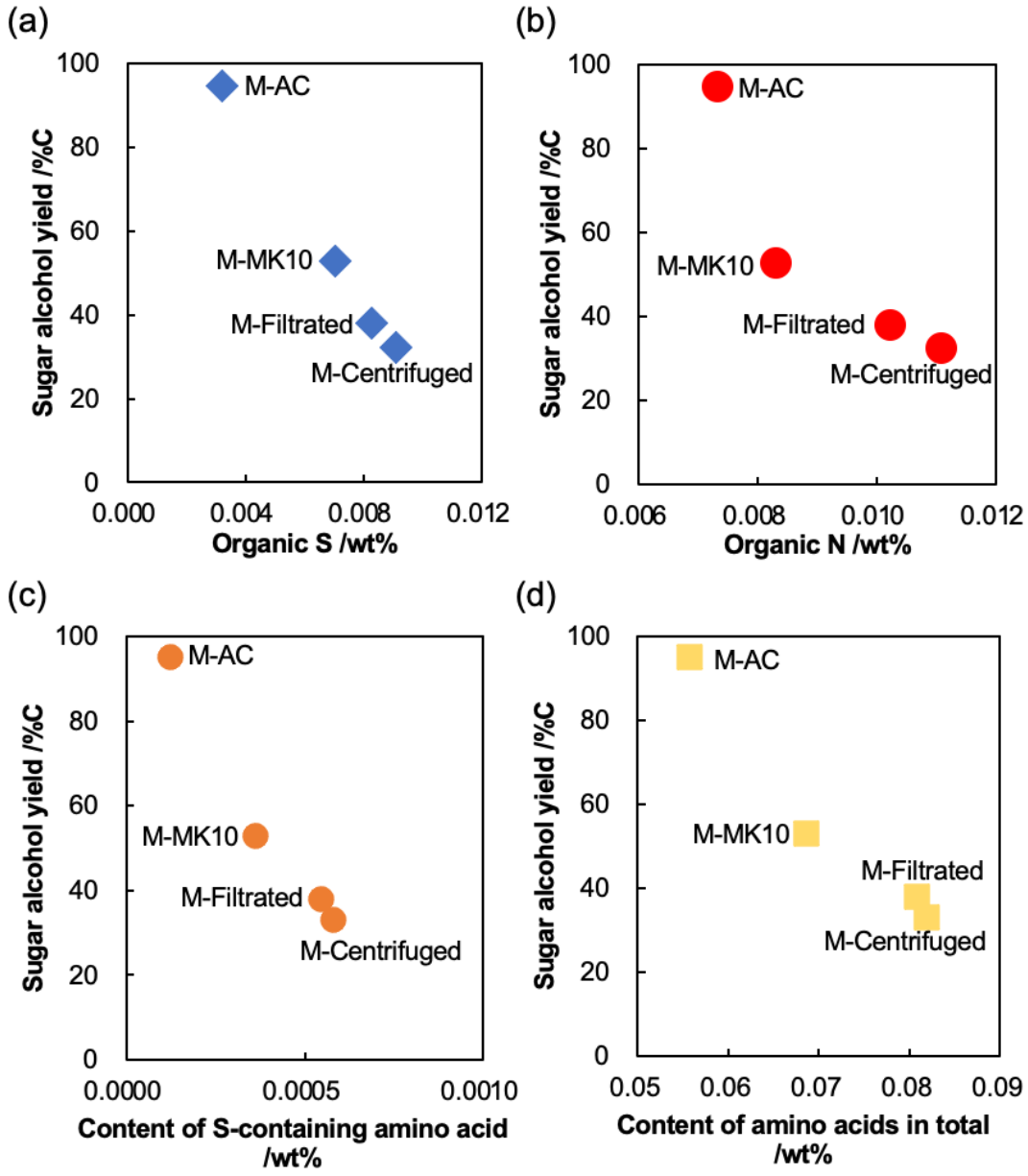

Figure 4.6 (a) The correlation plot of sugar alcohols yield against the concentration of organic S compounds; (b) organic N compounds; (c) S-containing amino acids; (d) amino acids in total.

To evaluate the poisoning effect of organic S and N compounds, I added model catalyst poisons in the hydrolytic hydrogenation of reagent sugars (Fig. 4.7). The concentration of additives was modified to match the levels of organic S or N compounds found in M-Centrifuged. L-aspartic acid was added as a model of organic N compounds because it was the predominant amino acid found in molasses. The

concentration of L-aspartic acid in the reaction mixture was set at 0.10 wt% to make the concentration of organic N the same as that in M-Centrifuged (0.011 wt%). In this case, only slight inhibition (sorbitol 64 %C, mannitol 24 %C) was observed compared with the reaction in the absence of inhibitors (sorbitol 71 %C, mannitol **25** %C). Therefore, organic nitrogen compounds provide minor influence on the catalytic activity at the concentration. Then, I tested L-cysteine, which contains both S and N atoms. L-cysteine is the predominant amino acid found in my molasses samples. This compound decreased the yield of sorbitol (43 %C) and mannitol (16 %C) and increased by-products (13 %C). To verify the influence of organic S compound excluding the effect of organic N, a model sulfur compound that is obtained by the removal of amino group from cysteine, namely 3-mercaptopropionic acid, was applied as an additive. It led to a very low yield of sugar alcohols (sorbitol 4.8 %C, mannitol 2.4 %C). Organic S compounds are the predominant poisons for Raney Ni catalyst.

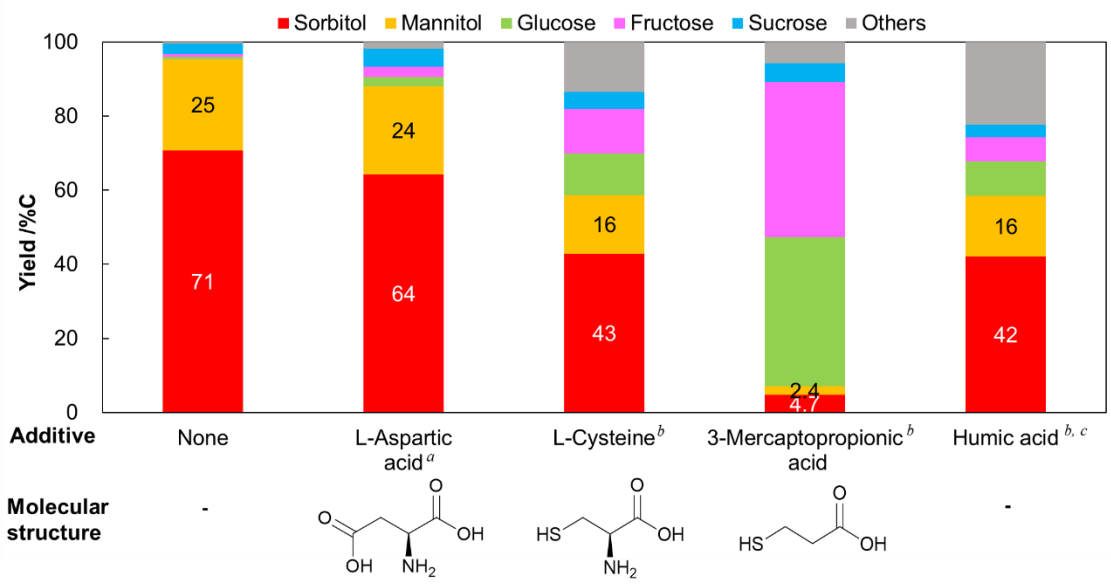

Figure 4.7 Effect of amino acids on organic S and organic N on the hydrolytic hydrogenation of reagent sugars. Reaction condition: reaction solution 40 g (sugar concentration 1 wt% in total); Raney Ni 280 mg; p(H_2) 5 MPa; 4 h; pH 3; 140 °C.
[a] To be 0.011 wt% N, the same as that in the diluted M-Centrifuged to be 1 wt% sugar.

[b] 0.009 wt% S to be the same as that in the diluted M-Centrifuged in 1 wt% sugar.

[c] Humic acid contained 0.72 wt% S.

I consider why sulfur is very harmful for the Ni catalyst. Sulfur-containing functional groups with lone pairs such as thiol strongly chemisorb on metal surface.[36] Previous DFT calculations showed that organic S adsorbs on Ni(111) surface with the interaction of p orbitals of S and d band of Ni in the band theory.[37] To improve the clarity of the interaction at the local structural level, a more accurate hybrid functional (B3LYP) with the Gaussian-based linear combination of atomic orbitals (LCAO) approximation was applied in this work, to model a Ni(111) surface subjected to the adsorption of the simplest sulfur-containing organic compounds, methanethiol and dimethylsulfide. Methanethiolate adsorbed on a bridge site with an adsorption energy of −185 kJ mol^{-1}, while dimethylsulfide bound on the top of a Ni atom with the energy of −35 kJ mol^{-1}. The adsorption of methanethiolate is more stable, and thus it was focused in the calculation. The natural bond orbital analysis [38] shows that the electron donation from occupied hybrid orbitals of S including 3s and 3p in a methanethiolate molecule to unoccupied Ni 4p orbital predominantly contributes to the adsorption on Ni(111) surface (Fig. 4.8).[39] Additionally, it is known that organic S compounds sometimes produce atomic S on metal surfaces. The S atom can strongly adsorbs on plural Ni atoms.[37,40] A typical manner is that a S atom binds with three Ni atoms on Ni(111) surface (Fig. 4.9). A typical mechanism of hydrogenation on Ni surface requires multi Ni atoms for dissociation of a single H_2 molecule;[41] for hydrogenation of monosaccharides, more Ni atoms are necessary to absorb those sugar molecules. The binding of S on Ni surface will make the surface too occupied to provide multi-atom adsorption sites for H_2 and monosaccharide, thus even a small amount of organic S can poison plenty of Ni atoms. The adsorption of S decelerates the hydrogenation by inhibiting the adsorption of H_2 molecules on metal surface.[42] Additionally, organic S compounds are possibly decomposed to form atomic sulfur on metal, which also contributes to the deactivation of catalyst.[40] Therefore, the removal of organic S compounds by adsorbents is effective for the production of sugar alcohols.

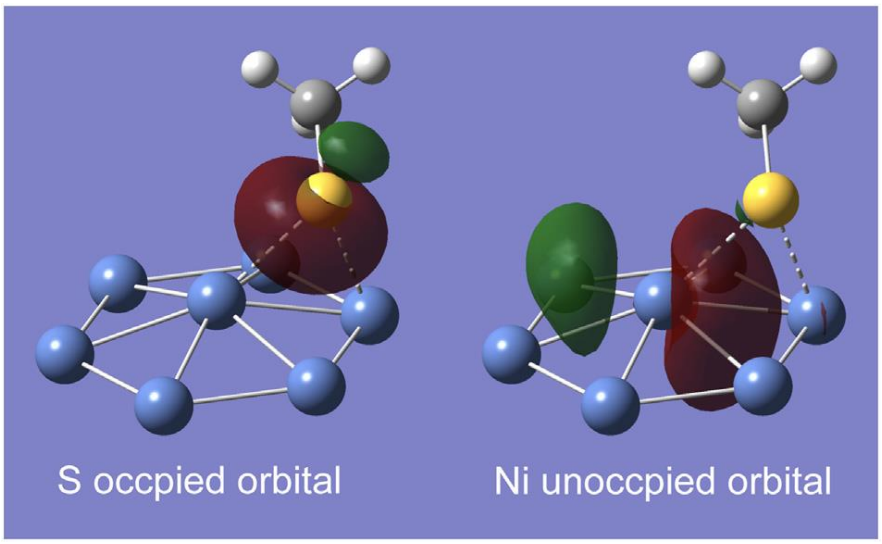

Figure 4.8 A donor-acceptor interaction pair to show the contribution of Ni 4p in the adsorption of methanethiolate. Isovalue 0.05.

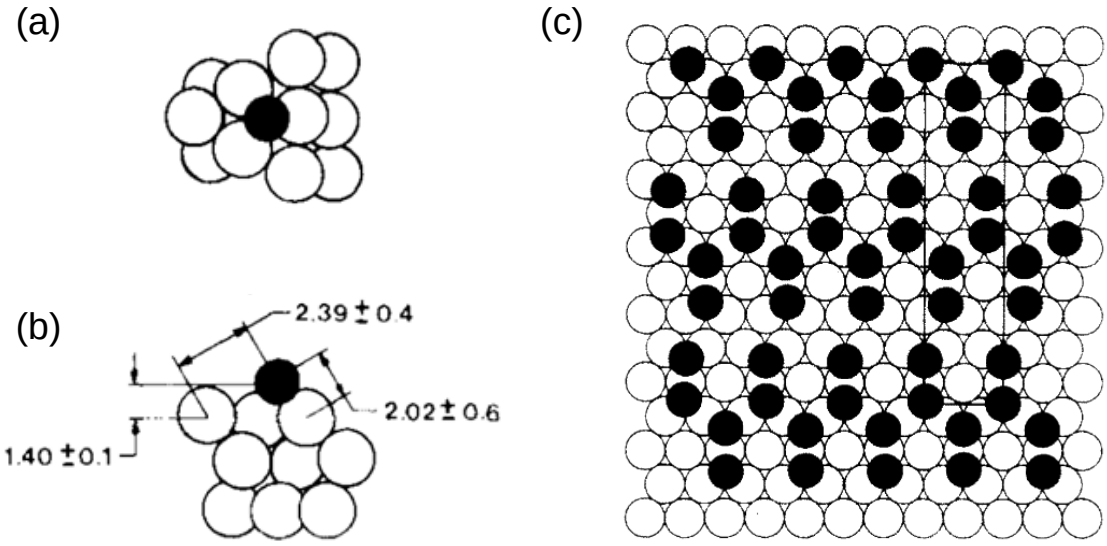

Figure 4.9 Location of adsorbed atomic sulfur on the (111) planes of Ni: (a) top view, (b) side view (unit: Å). (c) structure of sulfur-adsorbed Ni(111) surface at a coverage (θ) = 0.40. Black circles represent sulfur atoms; white circles represent nickel atoms. Adapted from the reference.[43]

In addition, I also tested a humin-type compound (humic acid, Fig. 4.7), which decreased the yield of sugar alcohols (sorbitol 42 %C, mannitol 16 %C) and increased that of by-products (22 %C). Humin has reactive functional groups such as furanics and aldehydes in addition to sulfur-containing groups. They react with reducing sugars to

further promote the formation of humins.[44]

I conclude that organic S compounds significantly decrease the catalytic activity. They are likely major inhibitors for the Ni catalyst in the hydrolytic hydrogenation of molasses. Additionally, the formation of humins can further promote side-reactions.

4.3.3 Detailed study to enhance the yield using M-MK10

4.3.3.1 Influence of pretreatment methods on overall yield of sugar alcohol

The pretreatment using AC the most effectively removed poisonous impurities for metal catalyst, thus M-AC gave the highest yield of sugar alcohols. However, the solution volume decreased obviously after pretreatment with absorbents (Table 4.4). Thus, the loss of sugar influences the overall yield of sugar alcohols, starting from the same amount of molasses. Herein, with taking the loss of sugars into account, I calculated the overall yield of sugar alcohol to reveal how much sugar alcohol can be produced using different pretreatment methods with a particular amount of molasses (Table 4.6). The calculation uses eq. 4.8–4.11. Among MK10 gave 42%C yield of sugar alcohol, which was the highest among the samples. Although M-AC achieved the highest yield of sugar alcohol on the basis of 1 wt% sugar solution (95%C), the loss of sugars in the pretreatment decreased the overall yield of sugar alcohol to 37%C. Moreover, the price of montmorillonite (about $200–300 /ton) makes it more affordable as absorbent than activated carbon (about $900–1,300 /ton). Therefore, M-MK10 was applied as substrate for further optimization.

Table 4.6 Overall yield of sugar alcohols

Sample	Overall yield /%C
M-Centrifuged[a]	33
M-Filtrated	36
M-MK10	43
M-AC	38

[a] Since all pretreated samples (M-Filtrated, M-MK10, and M-AC) were derived from

M-Centrifuged, and sugars almost not lost during the preparation of M-Centrifuged, the amount of sugars in M-Centrifuged was set as 100 %C.

$$\text{Overall yield of sugar alcohol of a sample} = \frac{n_{sugar\ alcohol}}{n_{sugar}} \times 100\% = \frac{\alpha_{sugar\ alcohol} \times n\prime_{sugar} \div \sigma_{dilution}}{n_{sugar}} \times 100\% \quad (4.8)$$

in which n_{sugar} is the molar amount of sugars contained in M-Centrifuged sample, obtained by eq. 4.9; $\alpha_{sugar\ alcohol}$ is the total yield of sugar alcohols, obtained from Fig. 4.5; n'_{sugar} is the amount of sugars in diluted sugar solution (total sugar 1 wt%), obtained by eq. 4.10; $\sigma_{dilution}$ is the dilution ratio from a pretreated solution to make a diluted sugar solution (total sugar 1 wt%), obtained by eq. 4.11.

$$n_{sugar} = 2 \times n_{sucrose} + n_{glucose} + n_{fructose} = 2 \times \frac{m_{sucrose}}{M_{sucrose}} + \frac{m_{glucose}}{M_{glucose}} + \frac{m_{fructose}}{M_{fructose}} = 2 \times \frac{m\prime \times c_{sucrose}}{M_{sucrose}} + \frac{m' \times c_{glucose}}{M_{glucose}} + \frac{m\prime \times c_{fructose}}{M_{fructose}} \quad (4.9)$$

in which n_x is the molar amount of each sugar (sucrose, glucose, fructose), m_x is the mass of each sugar, M_x is the molecular weight of each sugar molecule, c_x is the weight concentration (wt%) of each sugar in M-Centrifuged; m' is the recovered solution mass of M-Centrifuged; all those data above can be found in Table 4.4.

Likely, n'_{sugar} of each pretreated sample (M-Filtrated, M-MK10, and M-AC) is calculated by the following formula:

$$n'_{sugar} = 2 \times \frac{m\prime \times c\prime_{sucrose}}{M_{sucrose}} + \frac{m\prime \times c\prime_{glucose}}{M_{glucose}} + \frac{m\prime \times c\prime_{fructose}}{M_{fructose}} \quad (4.10)$$

in which m' is the recovered solution mass of each pretreated sample; c_x is the weight concentration (wt%) of each sugar in each pretreated sample; m' is the mass of each pretreated sample; all those data above can be found in Table 4.4.

$$\sigma_{dilution} = \frac{m'_{reaction}}{\frac{m' \times c_{total}}{c_{reaction}}} = \frac{40}{m' \times c_{total}} \quad (4.11)$$

in which $m'_{reaction}$ is the mass of diluted sugar solution used for reaction (40 g), c_{total} is the total weight concentration (wt%) of sugars (sucrose, glucose, fructose) in each pretreated sample (M-Filtrated, M-MK10, and M-AC); $c_{reaction}$ is the total weight concentration (wt%) of sugars in reaction solution (1 wt%); those data above can be found in Table 4.4 and Table. 4.5.

4.3.3.2 Comparison of metal catalysts

For the benchmark, I tested other metal catalysts without catalyst supports in the hydrolytic hydrogenation of M-MK10 (Fig. 4.10). Pt black and Ru powder catalysts afforded about 1 %C yield of sugar alcohols, which was significantly lower than that given by Raney Ni (53 %C). The specific surface areas of these catalysts are not very different (Raney Ni 80–100 m^2 g^{-1},[45] Pt powder < 25 m^2 g^{-1},[46] and Ru powder 30 m^2 g^{-1}).[47] Therefore, the difference in catalytic activity may be due to varied influence of catalyst poisons to the particular metal. Sulfur, the most important catalyst poison, is a soft base, and it prefers soft acids. In this context, Pt and Ru are softer acids than Ni, thus indicating that Ni is less poisoned by sulfur. I speculate that this is the reason why Ni shows high activity.

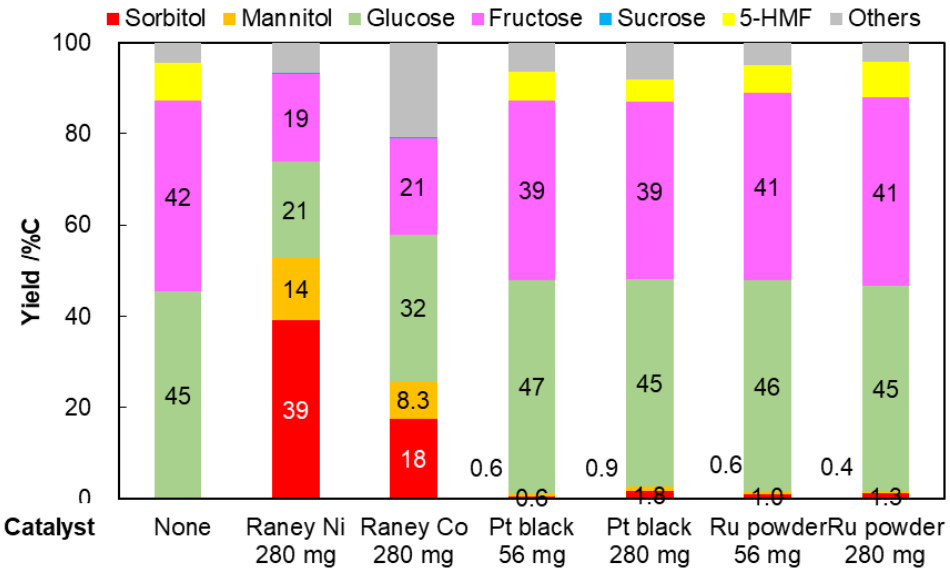

Figure 4.10 Result of catalyst screening for M-MK10 (Reaction condition: reaction solution 40 g (sugar concentration 1 wt% in total); Catalyst 280 mg; $p(H_2)$ 5 MPa; 4 h; pH 3; 140 ℃)

4.3.3.3 Influence of pH on the activity and selectivity

As aforementioned, in this reaction, oxonium ions catalyze the hydrolysis of sucrose. However, Ni may leach out under acidic environment ($Ni + 2H^+ \rightarrow Ni^{2+} + H_2$). Furthermore, a high concentration of oxonium ions often decompose sugars and sugar alcohols.[48] Thus, the optimization of pH is needed to balance the hydrolytic activity and inhibition of side-reactions.

Changing the initial pH by 1 from 2 to 5 significantly influenced the yield of sugar alcohols (Fig. 4.11). At pH 2, the yield of sugar alcohols was only 21 %C (sorbitol 14 %C, mannitol 6.6 %C), while by-products were produced in 34 %C yield. The large amount of by-products is attributed to the formation of humins by the catalysis of Brønsted acid.[49]

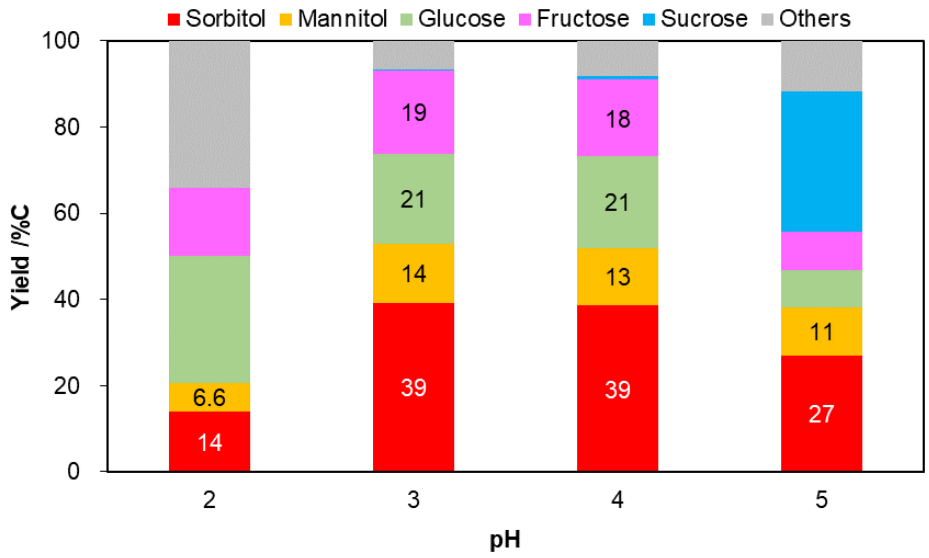

Figure 4.11 Effect of pH on hydrolytic hydrogenation of reagent sugar solution (Reaction condition: reaction solution 40 g (sugar concentration 1 wt% in total); Raney Ni 280 mg; $p(H_2)$ 5 MPa; 4 h; 140 °C)

Increase in pH to 3 gained the yield of sugar alcohols to 53 %C (sorbitol 39%C, mannitol 14%C). The reaction at pH 4 gave almost the same result. However, further increase in pH to 5 decreased the yield to 38%C. This is due to the slow hydrolysis of sucrose, as a large amount of sucrose remained after the reaction (33%C).

To evaluate the influence of pH on Ni leaching, the reaction solutions were analyzed with ICP (Fig. 4.12). The leaching amounts were 361, 198, 91, and 34 ppm at pH 3.0, 3.6, 4.2, and 5.0, respectively. The logarithm of Ni leaching amount was proportional to pH, which can be described by eq. 4.12. With increasing pH, the leaching amount of Ni can be exponentially decreased. At pH 3.6, the leaching amount (198 ppm) is similar to the equilibrium concentration of Ni^{2+} theoretically estimated with the Nernst equation (eqs. 4.13–4.17, 234 ppm). However, the actual leaching amount of Ni is higher than the theoretical values at pH 3.6–5.0. This phenomenon suggests that other Ni species such as $Ni(OH)_2$ are also involved in the leaching at a pH > 3.6 to increase the concentration of Ni.[50] Indeed, the presence of $Ni(OH)_2$ on Ni catalyst has been detected by X-ray diffraction analysis after hydrolytic hydrogenation in another system.[50]

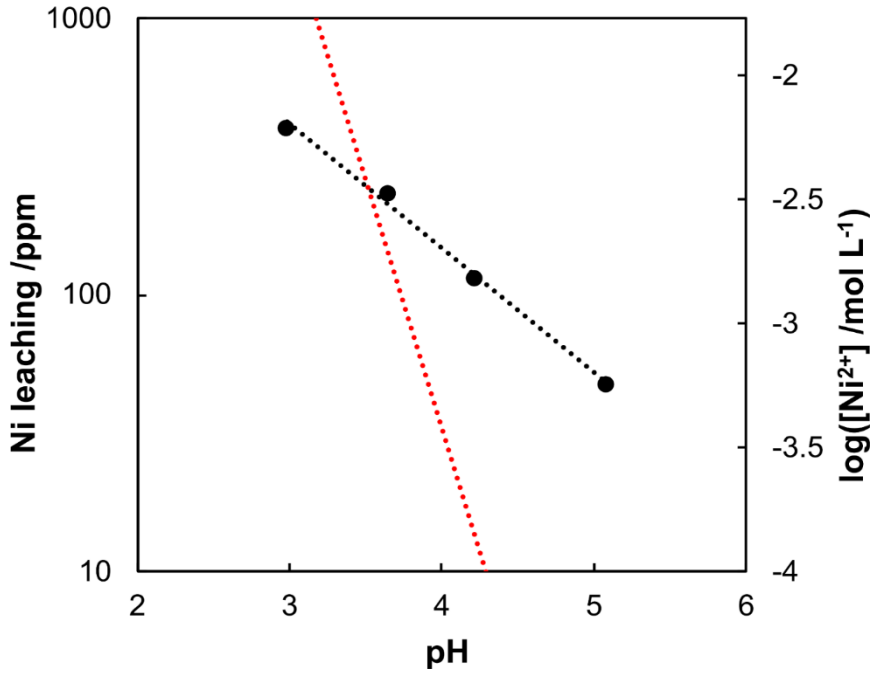

Figure 4.12 Effect of pH on Ni leaching amount (Black points: the actual leaching amount; Black dash line: the trendline of actual leaching amount, eq. 4.12; Red dash line: the theoretical line of leaching amount, eq. 4.17).

$\log([Ni^{2+}]) = 0.70 - 0.50pH$ (4.12)

$$E = 0 = E_0 - \frac{RT}{nF}\ln\frac{a_{Ni^{2+}}a_{H_2}}{a_{Ni}a_{H^+}^2} \quad (4.13)$$

$$\approx E_0 - \frac{RT}{nF}\ln\left(\frac{[Ni^{2+}]p_{H_2}}{10^{-2pH}}\right) \quad (4.14)$$

where E_0 =0.257 V, R = 8.314 J·K^{-1}·mol^{-1}, T = 413.15 K, n = 2, F = 96485 C mol^{-1}, p_{H_2} = 50 atm, a_{Ni} = 1.

$$\Leftrightarrow 0.257 = 0.0178 \times \left[\ln\frac{[Ni^{2+}]}{10^{-2pH}} + \ln 50\right) - \ln(10^{-2pH})] \quad (4.15)$$

$\Leftrightarrow \log([Ni^{2+}]) = \log e^{14.43} - \log 50 - 2pH$ (4.16)

$\Leftrightarrow \log([Ni^{2+}]) \approx 4.57 - 2pH$ (4.17)

To summarize, pH 4 is the best to nicely balance hydrolysis activity, selectivity, and Ni leaching.

4.3.3.4 Influence of temperature

Time course was measured for the conversion of molasses at pH 4 at different temperatures ranging from 140 to 180 °C (Fig. 4.13). At 140 °C, sucrose was consumed over 4 h, and the amounts of glucose and fructose were maximized at 1–2 h. Yield of sorbitol and mannitol increased in parallel over 16 h by consuming the sugars. The yields of sorbitol and mannitol reached 63 %C and 21 %C, respectively, (in total 84 %C; overall yield 68 %C) at 16 h. Increasing temperature gradually decreased the maximum yield of sugar alcohols (68 %C at 150 °C; 63 %C at 160 °C; 45 %C at 180 °C), while the reaction time was shortened from 16 h to 2 h. The decrease in the sugar alcohol yield indicates the significant acceleration of side-reactions by elevating the temperature.

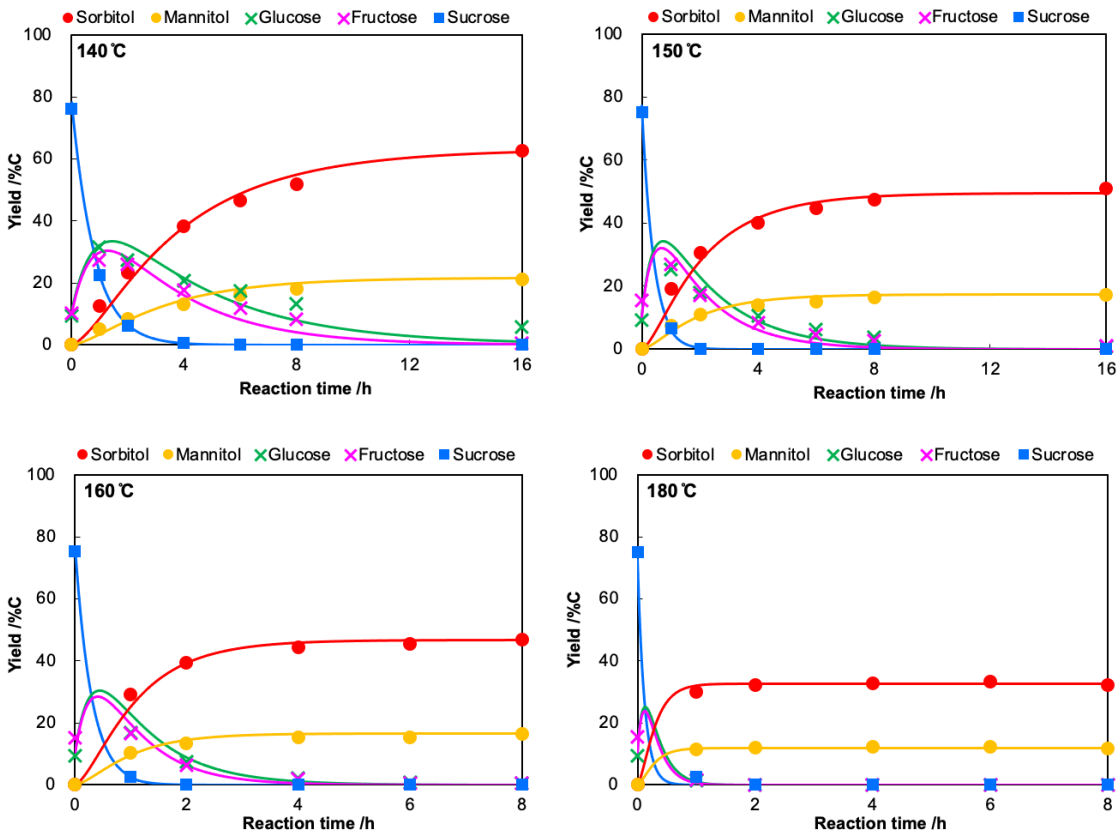

Figure 4.13 Time course of hydrolytic hydrogenation of M-MK10 at 140 °C, 150 °C. 160 °C, 180 °C. Reaction condition: 1 wt% reagent sugar solution 40 g; Raney Ni 280 mg; $p(H_2)$ 5 MPa; pH 4.

To quantitatively understand the kinetic characteristics of this reaction, a pseudo first-order analysis was conducted, which is often employed for the dehydration of sugar alcohols[51–53]. The hydrolysis of sucrose is a typical first-order reaction because the concentration of water can be approximated as constant since its concentration almost not change during the reaction (40 mL). As for hydrogenation, at the low concentration of sugars (1 wt%), the coverage of sugar substrate on metal surface is approximately proportional to their concentration,[54,55] and the concentration of H_2 can be considered as constant during the reaction (5 MPa). Thus, the hydrogenation reaction can be approximated as a pseudo first-order reaction on the sugar concentration as shown in Scheme 4.3. Sucrose is hydrolyzed to glucose and fructose by k_1, glucose is hydrogenated to sorbitol by k_2, and fructose is converted to sorbitol (k_3) and mannitol (k_4). The decomposition of glucose and fructose, having reactive hemiacetal groups, to by-products are also involved by assuming the first-order kinetics (k_5 and k_6).

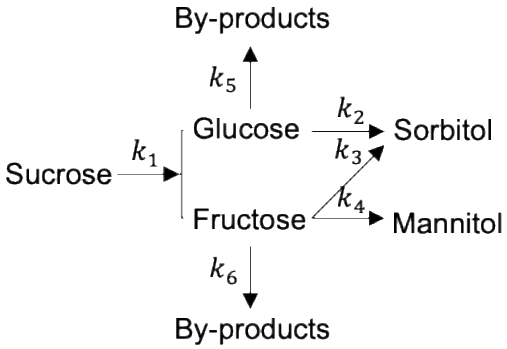

Scheme 4.3 Kinetic parameters in the hydrolytic hydrogenation (where k_1, k_2, k_3, k_4, k_5, k_6 (unit: h^{-1}) are pseudo first-order rate constants of respective steps)

Numerical simulations shown as solid lines in Fig. 4.13 nicely reproduced the actual experimental data depicted as circles. The obtained rate constants are summarized in Table 4.7. At 140 °C, the rate constant for the hydrolysis (1.2 h^{-1}) was several times larger than those for the hydrogenation of glucose (0.21 h^{-1}) and fructose (0.30 h^{-1} as sum of k_3 and k_4), showing that the rate-determining step is the hydrogenation. Therefore, the poisoning of Ni remarkably slows down the reaction. The formation of by-products was relatively slow (0.045 h^{-1}). By elevating the temperature to 150 °C, the rate constant for the side reactions of monosaccharides) increased from 0.045 to

0.17 h^{-1}, but that of hydrogenation was gained only slightly (from 0.21 to 0.30 h^{-1} for glucose). This trend was similar at higher temperatures. Therefore, the increase in the reaction temperature promotes the side-reactions rather than the hydrogenation, which decreases the yield of the sugar alcohols.

Table 4.7 Calculated rate constants of the hydrolytic hydrogenation of molasses

Temp. /°C	Rate constants /h^{-1}					
	k_1	k_2	k_3	k_4	k_5	k_6
140	1.2	0.21	0.15	0.15	0.045	0.045
150	2.4	0.30	0.20	0.20	0.17	0.17
160	3.3	0.60	0.40	0.40	0.40	0.40
180	8.0	1.8	1.2	1.2	2.6	2.6

Based on the kinetics analysis at different temperature, Arrhenius plots were depicted to determine the apparent activation energy (E_a) of each reaction step (Fig. 4.14). The E_a values of hydrogenation steps (86 kJ mol^{-1}; (b) and (c)) were higher than that of the hydrolysis step (72 kJ mol^{-1}). More importantly, E_a for the by-product formation is as high as 160 kJ mol^{-1}, and therefore a low temperature is preferable for the selective synthesis of sugar alcohols.

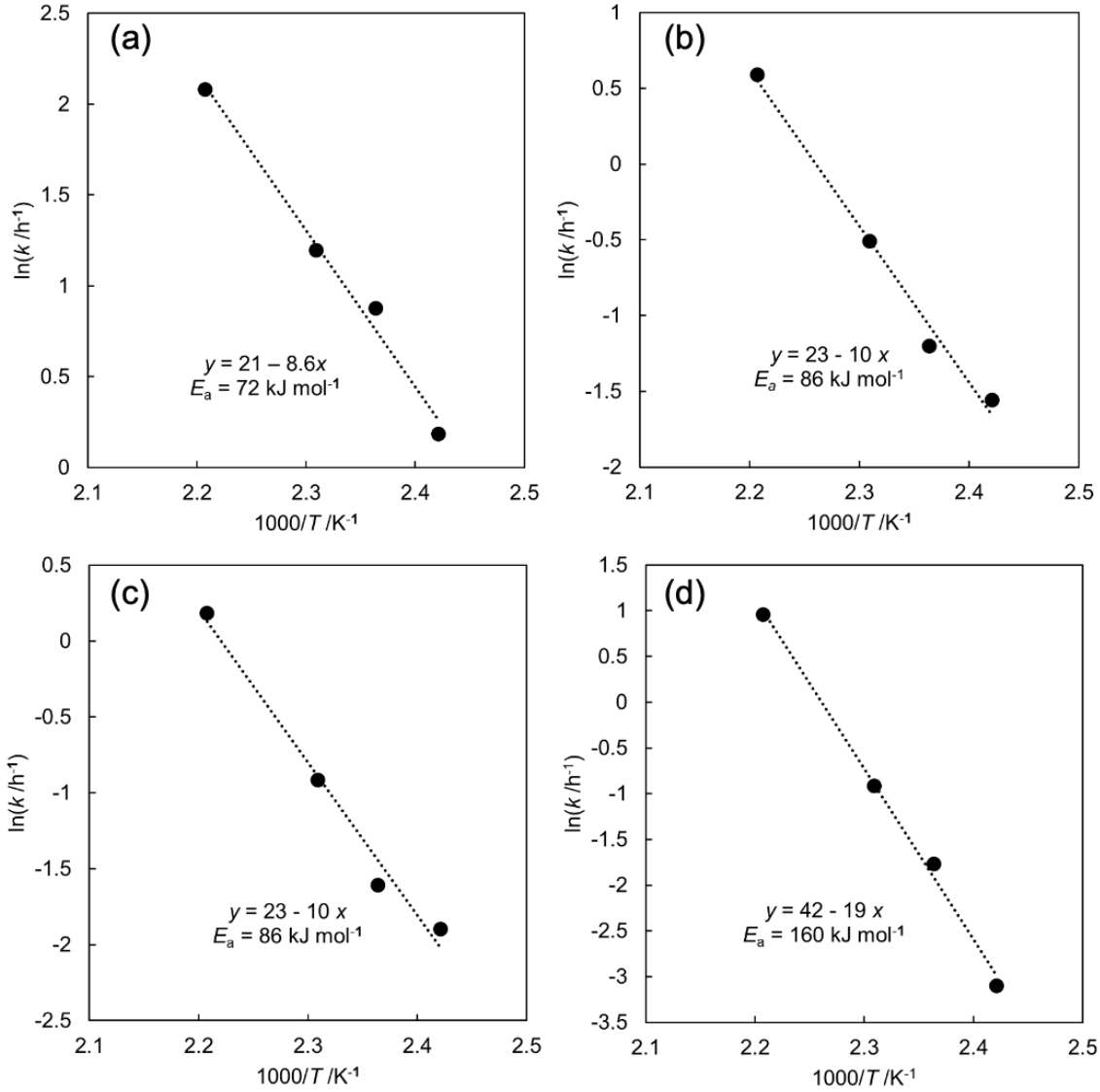

Figure 4.14 Arrhenius plot for the hydrolysis of sucrose (a), hydrogenation of glucose (b), hydrogenation of fructose (c), and side-reaction steps (d) in the conversion of molasses.

4.4 Recyclability test of Raney Ni

Raney Ni catalyst was reused in the hydrolytic hydrogenation of M-MK10 under the optimum reaction conditions ($p(H_2)$ 5 MPa; pH 4; 140 °C; 16 h). After a reaction, the catalyst was recovered by centrifugation and decantation, and the recovered catalyst was used for the next run. The first run gave 84%C yield of sugar alcohols. At the second run, the yield of sugar alcohols decreased significantly to 34 %C, and the third run only gave sugar alcohols in 17 %C yield; as the number of run increased, the yield of glucose and fructose also increased. Those phenomenon implies Raney Ni was

seriously deactivated during the reaction with molasses. In contrast, Raney Ni is a practical catalyst for the hydrogenation of glucose with a long lifetime. Moreover, we have confirmed that Ni leaching is very small under the reaction conditions at pH 4. Accordingly, the deactivation strongly suggests the catalyst poisoning by the impurities in the molasses. I conclude that Raney Ni can be hardly reused without regeneration.

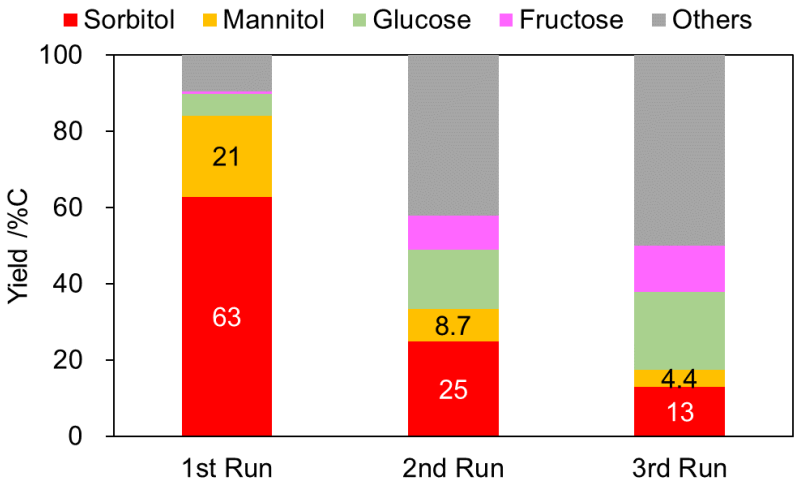

Figure 4.15 Recyclability test of Raney Ni catalyst for the hydrolytic hydrogenation of M-MK10. Reaction condition: 1 wt% reagent sugar solution 40 g; Raney Ni 280 mg; $p(H_2)$ 5 MPa; 140 °C; pH 4; 16 h.

4.5 Conclusion

In this Chapter, the author studied the pretreatment and catalytic conversion of molasses derived from sugarcane, a waste in the food industry, to synthesize sugar alcohols using Raney Ni catalyst. Molasses treated with simple filtration can barely produce sugar alcohols, due to the existence of organic S compounds that are poisonous to the Raney Ni catalyst. To maintain the activity of catalyst, a pretreatment using an adsorbent is needed. Pretreatment using Montmorillonite K10 can enhance the yield of sugar alcohols with retaining lots of sugars, thus it is considered as a suitable absorbent. A further optimization of reaction conditions for M-MK10 increased the yield of sugar alcohols up to 84 %C yield (overall yield at 68 %C) at 140 °C and pH 4 with a small amount of Ni leaching. A kinetic study of M-MK10 shows that the rate-determining

step is the hydrogenation of monomeric sugars. A lower temperature more selectively produces sugar alcohols due to the high activation energy for by-product formation.

4.6 References

1 H. Olbrich, *The Molasses*, Biotechnologie-Kempe GmbH, Berlin, 2006.

2 沖縄県農林水産部糖業農産課, 砂糖類・でん粉情報, 2020, 41–47.

3 F. W. Lichtenthaler, *Acc. Chem. Res.*, 2002, **35**, 728–737.

4 H. Kobayashi and A. Fukuoka, *Green Chem.*, 2013, **15**, 1740–1763.

5 M. D. Argyle and C. H. Bartholomew, *Catalysts*, 2015, **5**, 145–269.

6 M. Paterson-Beedle, J. F. Kennedy, F. A. D. Melo, L. L. Lloyd and V. Medeiros, *Carbohydr. Polym.*, 2000, **42**, 375–383.

7 T. Kondo, N. Ishihara, T. Fukuhara, M. Kojima, T. Kato, T. Itoh and K. Terao, *J. Brew. Soc. JAPAN*, 2013, **108**, 707–715.

8 H. Rosen, *Arch. Biochem. Biophys.*, 1957, **67**, 10–15.

9 R. McGillivray and S. C. Woodger, *Analyst*, 1966, **91**, 611–620.

10 A. D. Becke, *J. Chem. Phys.*, 1993, **98**, 5648–5652.

11 P. J. Hay and W. R. Wadt, *J. Chem. Phys.*, 1985, **82**, 270–283.

12 D. E. Woon and T. H. Dunning, *J. Chem. Phys.*, 1993, **98**, 1358–1371.

13 T. H. Dunning, *J. Chem. Phys.*, 1989, **90**, 1007–1023.

14 P. Gallezot, P. J. Cerino, B. Blanc, G. Flèche and P. Fuertes, *J. Catal.*, 1994, **146**, 93–102.

15 M. H. B. Hayes, R. Mylotte and R. S. Swift, *Humin: Its Composition and Importance in Soil Organic Matter*, Elsevier Inc., 1st edn., 2017, vol. 143.

16 J. A. Rice and P. MacCarthy, *Org. Geochem.*, 1991, **17**, 635–648.

17 M. Fujimaki and T. Kurata, *KAGAKU TO SEIBUTSU*, 1971, **9**, 85–95.

18 W. H. Yu, N. Li, D. S. Tong, C. H. Zhou, C. X. Lin and C. Y. Xu, *Appl. Clay Sci.*, 2013, **80**–**81**, 443–452.

19 I. Gitlin, J. D. Carbeck and G. M. Whitesides, *Angew. Chemie - Int. Ed.*, 2006, **45**, 3022–3060.

20 L. O. B. Benetoli, C. M. D. De Souza, K. L. Da Silva, I. G. De Souza, H. De Santana, A. Paesano, A. C. S. Da Costa, C. T. B. V. Zaia and D. A. M. Zaia, *Orig. Life Evol. Biosph.*, 2007, **37**, 479–493.

21 X. C. Wang and C. Lee, *Mar. Chem.*, 1993, **44**, 1–23.

22 M. Fernandes De Oliveira, C. T. Johnston, G. S. Premachandra, B. J. Teppen, H. Li, D. A. Laird, D. Zhu and S. A. Boyd, *Environ. Sci. Technol.*, 2005, **39**, 9123–9129.

23 H. Quiquampoix, S. Staunton, M. H. Baron and R. G. Ratcliffe, *Colloids Surfaces A Physicochem. Eng. Asp.*, 1993, **75**, 85–93.

24 I. Derungs, M. Rico, J. López, L. Barral, B. Montero and R. Bouza, *Polym. Adv. Technol.*, 2021, **32**, 4479–4489.

25 C. J. Van Oss and R. F. Giese, *Clays Clay Miner.*, 1995, **43**, 474–477.

26 A. K. Bajpai and R. Sachdeva, *Colloid Polym. Sci.*, 2002, **280**, 892–899.

27 S. Servagent-Noinville, M. Revault, H. Quiquampoix and M. H. Baron, *J. Colloid Interface Sci.*, 2000, **221**, 273–283.

28 D. Mondal, M. M. R. Mollick, B. Bhowmick, D. Maity, M. K. Bain, D. Rana, A. Mukhopadhyay, K. Dana and D. Chattopadhyay, *Prog. Nat. Sci. Mater. Int.*, 2013, **23**, 579–587.

29 M. J. Plevin, D. L. Bryce and J. Boisbouvier, *Nat. Chem.*, 2010, **2**, 466–471.

30 S. C. Smith, F. Ahmed, K. M. Gutierrez and D. Frigi Rodrigues, *Chem. Eng. J.*, 2014, **240**, 147–154.

31 M. Yabushita, H. Kobayashi, J. Hasegawa, K. Hara and A. Fukuoka, *ChemSusChem*, 2014, **7**, 1443–1450.

32 H. Kobayashi and A. Fukuoka, *Bull. Chem. Soc. Jpn.*, 2018, **91**, 29–43.

33 P. W. Chung, A. Charmot, O. M. Gazit and A. Katz, *Langmuir*, 2012, **28**, 15222–15232.

34 P. T. Moseley, D. A. J. Rand, A. Davidson and B. Monahov, *J. Energy Storage*, 2018, **19**, 272–290.

35 H. Li, W. Wang and J. F. Deng, *J. Catal.*, 2000, **191**, 257–260.

36 M. Cohen-Atiya and D. Mandler, *J. Electroanal. Chem.*, 2003, **550**–**551**, 267–

276.

37 D. Karhánek, T. Bučcko and J. Hafner, *J. Phys. Condens. Matter*, 2010, **22**, 265005.

38 A. E. Reed, R. B. Weinstock and F. Weinhold, *J. Chem. Phys.*, 1985, **83**, 735–746.

39 C. Yang, H. Kobayashi and A. Fukuoka, *Fuel Process. Technol.*, 2019, **196**, 106155.

40 C. H. Bartholomew, P. K. Agrawal and J. R. Katzer, *Adv. Catal.*, 1982, **31**, 135–242.

41 J. D. Roberts and M. C. Caserio, *Basic Principles of Organic Chemistry, second edition*, W. A. Benjamin, Inc., Menlo Park, 2020, vol. 84.

42 R. June, W. Hzs, H. Kong and H. Kong, 1978, **396**, 384–396.

43 P. Delescluse and A. Masson, *Surf. Sci.*, 1980, **100**, 423–438.

44 I. Van Zandvoort, Y. Wang, C. B. Rasrendra, E. R. H. Van Eck, P. C. A. Bruijnincx, H. J. Heeres and B. M. Weckhuysen, *ChemSusChem*, 2013, **6**, 1745–1758.

45 Sigma-Aldrich, Raney® Nickel, https://www.sigmaaldrich.com/JP/ja/product/aldrich/221678, (accessed 13 October 2021).

46 Sigma-Aldrich, Platinum powder, https://www.sigmaaldrich.com/JP/ja/product/aldrich/205915, (accessed 13 October 2021).

47 Sigma-Aldrich, Ruthium powder, https://www.sigmaaldrich.com/JP/ja/product/aldrich/545023, (accessed 13 October 2021).

48 H. Kobayashi, K. Techikawara and A. Fukuoka, *Green Chem.*, 2017, **19**, 3350–3356.

49 G. Tsilomelekis, M. J. Orella, Z. Lin, Z. Cheng, W. Zheng, V. Nikolakis and D. G. Vlachos, *Green Chem.*, 2016, **18**, 1983–1993.

50 H. Kobayashi, Y. Hosaka, K. Hara, B. Feng, Y. Hirosaki and A. Fukuoka,

Green Chem., 2014, **16**, 637–644.

51 H. Yokoyama, H. Kobayashi, J. Hasegawa and A. Fukuoka, *ACS Catal.*, 2017, **7**, 4828–4834.

52 A. Yamaguchi, N. Muramatsu, N. Mimura, M. Shirai and O. Sato, *Phys. Chem. Chem. Phys.*, 2017, **19**, 2714–2722.

53 M. Yabushita, H. Kobayashi, A. Shrotri, K. Hara, S. Ito and A. Fukuoka, *Bull. Chem. Soc. Jpn.*, 2015, **88**, 996–1002.

54 E. Crezee, B. W. Hoffer, R. J. Berger, M. Makkee, F. Kapteijn and J. A. Moulijn, *Appl. Catal. A Gen.*, 2003, **251**, 1–17.

55 H. Kobayashi, Y. Ito, T. Komanoya, Y. Hosaka, P. L. Dhepe, K. Kasai, K. Hara and A. Fukuoka, *Green Chem.*, 2011, **13**, 326–333.

Chapter 5

General conclusion

Chapter 1 “Introduction” described the background and objective of this study. The current human society strongly relies on fossil fuel resources, which need hundred centuries for regeneration while they are consumed at a quicker rate. Thus, to find alternative non-depleting and renewable resources is necessary for the sustainable development of human civilization. Biomass-derived sugars have been focused on as an attractive feedstock of biorefinery due to the abundance, specific stereochemistry, and potential as versatile platform chemicals. However, the conventional methods of sugar production from biomass are time-consuming and costly. Therefore, I decided to develop a more efficient method to produce sugars from biomass. Wastes released from food industry often contains a large amount of sugar or sugar compounds, and they are abundant. Herein, the author proposed using artificial catalytic reactions to convert food waste to value-added chemicals. We can design various catalysts suited for the efficient conversion of sugars to chemicals. For the product, the author is particularly interested in plastics, because they are value-added and can be used for a long time different from fuels. In this area, it is notable that the five-membered ring compound named isosorbide, derived from glucose, is a precursor to engineering plastics such as polycarbonate and polyester. The rigid framework provides outstanding physicochemical properties to the plastics, which is a clear advantage of the biomass utilization. The author also considered as follows: if we can use N-containing sugars in the same manner, we can expand the chemistry and the diversity of plastics. Based on the background, the author decided to focus on the catalytic conversion of both typical and N-containing sugars to five-membered ring compounds as the precursors to plastics.

In Chapter 2 “Dehydration condensation of a chitin-derived sugar alcohol using a weak acid catalyst”, the author studied the dehydration condensation of an N-containing sugar alcohol (ADS) derived from chitin via NAG. My major finding is that H_3PO_3

catalyst shows characteristic high activity among the weak acids tested, and it is due to the different reaction mechanism. In addition, the reducing ability of H_3PO_3 suppresses the coloring of the product likely by reducing unsaturated bonds to saturated ones. SEC analysis indicates that H_3PO_3 may decrease the formation of humins, because the formed unsaturated structures lead to intermolecular condensation.

Regarding the scientific details of the reaction, a kinetic study for the H_3PO_3-catalyzed reaction showed that the rate constants for the dehydration of AHADS to ADI are larger than those of ADS to AHADS. This kinetics is characteristic of H_3PO_3, as the conversion of AHADS to ADI is the slowest step for other acids. LC-MS and ^{31}P NMR analyses showed that the reaction pathway using H_3PO_3 may contain phosphite esters of ADS and AHADS. DFT calculations of the reaction mechanism supported the hypothesis: (i) ADS produces phosphite esters, (ii) the esters convert to AHADS by S_N2 reactions, and (iii) AHADS are likely transformed into ADI by the same mechanism via phosphite esters. In this mechanism, the activation energy is significantly lower than that of conventional acid-catalyzed mechanism. This is because P=O groups in the esters can easily capture proton due to high basicity, which leads to the cyclization reaction. In contrast, in the conventional acid systems hydroxy groups need to be protonated for the reaction, but protons are readily caught by amide groups due to higher basicity than the hydroxy groups. This chapter showed that the new reaction pathway opened by H_3PO_3 is energetically favorable and hopefully to be an alternative of the conventional super strong acid catalyst for ADI synthesis.

In Chapter 3 “Application of H_3PO_3 in the dehydration condensation of sorbitol”, the author applied H_3PO_3 catalyst for the dehydration condensation of sorbitol. In this case also, H_3PO_3 showed the highest activity among weak acids. Similar to the case of ADS dehydration, LC-MS and ^{31}P NMR analysis confirmed the existence of phosphite ester in the reaction system, suggesting the reaction mechanism via phosphite esters. The reaction gave phosphite esters of sorbitan and isosorbide to some extent as final products, but they can be easily hydrolyzed by hot water, which increased the product yield and enabled the recovery of H_3PO_3.

In Chapter 4 “Hydrolytic hydrogenation of molasses to sugar alcohols”, the author studied the pretreatment and catalytic conversion of molasses as an inedible food waste to supply sorbitol efficiently. I found that S-containing organic compounds contained in molasses strongly suppresses the hydrogenation of sugars to sorbitol. I found that an adsorption pretreatment with montmorillonite K10 (MK10) selectively reduces the catalyst poisons. Using the pretreated molasses sample, the optimization of hydrogenation with Raney Ni catalyst provided up to a 68% overall yield of sorbitol and mannitol in total. A kinetic analysis of the reaction showed that the hydrogenation of sugars is the rate-determining step, and a lower temperature is favored to produce sugar alcohols due to the high activation energy for by-product formation.

This dissertation explores the catalytic conversion of biomass-derived sugars to synthesize value-added chemicals. Conversion of biomass-derived sugar alcohols to plastic precursors is also studied, in which a weak acid (H_3PO_3) showed high activity for dehydration condensation of biomass-derived sugar alcohols via a special phosphite ester mechanism. Due to its low-cost and low-environmental-load advantages, H_3PO_3 is hopefully to replace the corrosive conventional acid catalysts. On the other hand, the author achieved the conversion of sugar alcohols from an inedible food waste at a high yield, which contributes to avoid consumption of food crop for biorefinery and is beneficial for supporting food supply. I hope that the insights revealed in this work assist in the utilization of biomass-derived sugars and further contribute to the sustainable development of human society.

List of publications

Journal publications

Cheng Yang, Hirokazu Kobayashi, Atsushi Fukuoka, Removal of catalyst poisons for the production of sugar alcohols from a real biomass molasses using a heterogeneous Ni catalyst. *Fuel Processing Technology*, **2019**, 196, 106155.

Cheng Yang, Takuya Sagawa, Atsushi Fukuoka, Hirokazu Kobayashi, Characteristic activity of phosphorous acid in the dehydration condensation of a chitin-derived nitrogen-containing sugar alcohol. *Green Chemistry*, **2021**, 23 (18), 7228-7234.

Conference contributions

Cheng Yang, Hirokazu Kobayashi, Atsushi Fukuoka, Production of sugar alcohols from molasses using a heterogeneous Ni catalyst. *2019 Winter Research Meeting of the Hokkaido Branch of Joint Chemistry Societies*, Sapporo, January **2019** (Oral)

Cheng Yang, Hirokazu Kobayashi, Atsushi Fukuoka, Conversion of molasses to sugar alcohols using a sponge nickel catalyst. *The 8th Asia Pacific Congress on Catalysis*, Bangkok, August **2019** (Oral)

Cheng Yang, Hirokazu Kobayashi, Atsushi Fukuoka, Production of hexitols from a real biomass molasses using a sponge Ni catalyst. *IRCCS the 3rd Joint International Symposium*, Nagoya, January **2020** (Poster)

楊程，小林広和，佐川拓矢，福岡淳．キチン由来糖アルコールの脱水反応における亜リン酸の触媒作用．第126回触媒討論会，静岡，2020（口頭発表）

Cheng Yang, Takuya Sagawa, Hirokazu Kobayashi, Atsushi Fukuoka, Synthesis of a potential precursor to nitrogen-containing polymers from a chitin-derived sugar

alcohol using weak acid catalysts. *The 18th Japan-Korea Symposium on Catalysis*, Online, November **2021** (Oral)

Acknowledgement

As my PhD course is coming to end, I would like to express my great gratitude to those people who helped me during this period.

First, I would like to thank my supervisor, Prof. Atsushi Fukuoka, for offering me the opportunity to conduct academic research in his team. Your broad experience and knowledge helped me a lot. Your constructive advice helped me to enhance the quality of my work. Your class helped me to gather knowledge about catalysis. It is very appreciative that you spent time on checking my papers, presentations, and thesis during your busy schedule. I am thankful to you for providing me the chances to attend conferences and symposiums, which makes me able to meet broader communities of science. Your maintenance of this laboratory provided all necessary equipment and reagents for my research. Your patience allowed me to grow up in a new country. Thank you very much.

I would like to thank Dr. Kiyotaka Nakajima. When I first came to Sapporo, you took time in your busy schedule for helping me to settle down. Your comments and suggestions were always very sharp and valuable, which enlightened me to look my work at another perspective and further increase its quality. Your beneficial advice about my daily performance helped me to adapt myself to Japanese manner. I am thankful to you for checking my thesis and giving valuable comments and questions during the preparation of my defense.

I am grateful to my daily supervisor, Dr. Hirokazu Kobayashi. You always enlightened me when I was stuck in my research. You taught me how to think and behave in Japanese way, which enhanced my performance in job-hunting. You inspired me about learning computational chemistry, which improved the quality of my research. Thank you for spending your time for revising my papers and presentations. I especially appreciate your assistance for finishing my PhD thesis. Your profound erudition impressed me. Thank you so much.

I would like to thank Dr. Abhijit Shrotri. Every discussion with you helped me to find the blind spots of my research. Your suggestions in group meetings always helped me

to understand the science in detail. Your comments and questions during my practice for PhD defense helped me a lot.

I am thankful to the committee members, Prof. Ken-ichi Shimizu, Prof. Shin Mukai and Prof. Jun-ya Hasegawa for reviewing my thesis and attending my defense.

I would like to thank the former and present members of Fukuoka laboratory. They were always beside whenever I need help. Ms. Hiromi Matsushima, thank you for helping me deal with the daily documents. Dr. Hirayama, Dr. Sagawa, and Dr. Techikawara, thank you very much for the kind assistance in experiments. The daily discussion in Japanese with you helped me to realize Japanese culture. Dr. Shazia Sharmin Satter, Dr. Nazmul, Dr. Palai, your optimism always inspired me to deal with the difficulties in research, thank you. Dr. Wiesfeld, it was great pleasure to discuss with you. Your ideas and comments made me believe that the universal values of western and eastern world are similar. Dr. Eunhyeok Yang, Dr. Etty, Dr. Padovan, Dr. Li, Mr. Boonyakarn, Mr. Kato, Mr. Yakuwa, Mr. Endo, Mr. Suzuki, Mr. Osanai, Ms. Fukuma, Ms. Shibayama, and Ms. Asakawa, thank you very much for the daily help in laboratory. Time with you were memorable.

I would like to express thankfulness to Dr. Yoshihara at S-Cubic and Dr. Matsuo at ICaS. Without your assistance, my job-hunting in Japan cannot went smoothly. I am also grateful to AGS office for providing the financial support for studying.

I am highly grateful to my wife, Xi Zhao. You abandoned your job offer in France and came to Japan to stay with me. The delicious cuisine you cooked every day supplied the energies I needed to work at lab. I cannot imagine how my PhD period would be without your accompanying.

At last, I would like to acknowledge the continuous support from my family and friends in China. I would like to end this by showing great gratitude to my parents, Xia Cheng and Lianchen Yang, who devoted their most for my study in Japan.